LAMINAR FLOW AND HEAT TRANSFER IN CURVED TUBES FILLED WITH SATURATED POROUS MEDIA

By

Omar Mohammed Jdaitawi

Supervisor

Professor Nasri J. Rabadi

Submitted in Partial Fulfillment of the Requirements of the Degree of Doctor of Philosophy in Mechanical Engineering

Faculty of Graduate Studies

University of Jordan

September 2002

This thesis was successfully defended and approved on: 26/9/2002.

Examination Committee	**Signature**
Prof. Nasri J. Rabadi, Chairman **Dean of Faculty of Engineering and Technlogy** **University of Jordan**	.....
Dr. Mohhammed Al-saad, Member **Professor, Mechanical Engineering Department** **University of Jordan**	.....
Dr. Ali Badran, Member **Assoc. Prof., Mechanical Engineering Department** **University of Jordan**	.....
Dr. Mahmood Abu Zaid, Member **Assoc. Prof., Mechanical Engineering Department** **Muta University**	.....

نوقشت هذه الرسالة واجيزت بتاريخ 2002/9/26

LAMINAR FLOW AND HEAT TRANSFER IN CURVED TUBES FILLED WITH SATURATED POROUS MEDIA

By

Omar Mohammed Jdaitawi

Supervisor

Professor Nasri J. Rabadi

Submitted in Partial Fulfillment of the Requirements of the Degree of Doctor of Philosophy in Mechanical Engineering

Faculty of Graduate Studies

University of Jordan

September 2002

This thesis was successfully defended and approved on: 26/9/2002.

Examination Committee	**Signature**
Prof. Nasri J. Rabadi, Chairman **Dean of Faculty of Engineering and Technology** **University of Jordan**	.....
Dr. Mohhammed Al-saad, Member **Professor, Mechanical Engineering Department** **University of Jordan**	.....
Dr. Ali Badran, Member **Assoc. Prof., Mechanical Engineering Department** **University of Jordan**	.....
Dr. Mahmood Abu Zaid, Member **Assoc. Prof., Mechanical Engineering Department** **Muta University**	.....

نوقشت هذه الرسالة واجيزت بتاريخ **2002/9/26**

Dedication

To my father and mother;

Brothers and sisters;

For their love and endless support.

Acknowledgment

I would like to express my thanks and deep appreciation to my supervisor Professor Nasri Rabadi for his continuous help and encouragement, for his patience and endless support.

Also, I would like to extend my special thanks to the committee members, Prof. Mohammed Al-saad, Dr. Ali Badran and Dr. Mahmood Abu Zaid, for their valuable time in reading and making comments on this thesis.

Finally, I am very grateful to all my lovely family, for their support and encouragement.

Table of Contents

List of Tables

List of Figures

Nomenclature

A Coefficient defined in equation (3.16)

a Channel width, m

b Channel height, m

B Coefficient defined in equation (3.17)

C Coefficient defined in equation (3.18)

C_w Coefficient defined in equation (3.19)

Da, Da', Modified Darcy number and Darcy number, $Da = Da'/\epsilon = K/\epsilon D_h^2$

De Dean number = $(Re\sqrt{D_h/R})$

D_h Hydraulic dimeter = (4 x cross-sectional area / witted perimeter)

f Friction factor

F Porous media inertia coefficient

K Permeability of the porous structure, m^2

k_e Effective thermal conductivity, W/m. °C

k_f Fluid thermal conductivity, W/m. °C

Nu Local Nusselt number

$\overline{Nu}$ Average Nusselt number

P Pressure, Pa

p Dimensionless pressure = $(D_h^2 P/\rho \nu^2)$

q any quantity of dependent variables

Pr, Pr' Modified Prandtl number and Prandtl number, $Pr = \epsilon Pr'$

r Curvature ratio = (R/D_h)

R Radius of coiled tube, m

Re Reynolds number ($\frac{\rho \overline{W} D_h}{\mu}$)

t Dimensionless temperature

t_m Dimensionless bulk mean temperature

T Temperature, K

T_w Temperature of tube wall, K

U, V, W Velocity components in the X, Y, and Z directions , m/s

u, v, w Dimensionless velocity components, = $(U, V, W)D_h/v$

V Volume occupied by fluid and solid matrix, m^3

$\overline{w}$ Dimensionless average axial velocity

X, Y, Z Cartesian coordinates

x, y, z Dimensionless coordinates, = $(X, Y, Z)/D_h$

Greek symbols

α thermal diffusivity =$(k_e/ \epsilon\rho_f c_f)$

ϵ Porosity = (V_f/V)

ε Convergence criterion used in the numerical procedure

λ Aspect ratio = (b/a)

μ Dynamic viscosity, kg/ms

ν Kinematic viscosity, m^2/s

ξ Dimensionless axial component of vorticity

ρ Density, kg/m^3

$\bar{\tau}$ Average wall shear stress defined in equation (5.3), N/m^2

ψ Dimensionless stream function

φ Any quantity associated with the fluid(V,T, P, ...)

Subscripts

c Curved channel

D Darcian

e Effective quantity for the fluid and solid matrix

f Fluid

p Particle of porous media

s Straight channel

v Viscous

w Wall

Laminar Flow and Heat Transfer in Curved Tubes Filled with Saturated Porous Media

By
Omar M. Jdaitawi

Supervisor

Prof. Nasri J. Rabadi

Abstract

This study presents a numerical solution based on the finite element method, for a fully developed laminar flow and heat transfer in curved rectangular channels, filled with saturated porous media.

It is found that Darcy number has a significant effect on the average Nusselt number and friction factor. The effect of aspect ratio is also studied. It is shown that the average Nusselt number is weakly affected by decreasing the aspect ratio. Solutions for Prandtl numbers ranging from 0.05 to 5 are obtained. It is found that the average Nusselt number is greatly affected by Prandtl number in porous media. Stream function contours and temperature contours are presented to show their strong dependence on Dean number. Solutions for Dean number as high as 800 are obtained, and Darcy number ranging from $1x10^{-6}$ to one is also studied.

The wall average Nusselt number and boundary viscous friction are presented as a function of Dean number De, Prandtl number Pr, and Darcy number Da, and a correlation equations based on the least square method are developed.

1. INTRODUCTION

Fluid flow and heat transfer in curved pipes or ducts is of importance in several engineering applications, such as pipe bends, cooling and heating systems, blade passages of turbo machinery, aircraft intakes, heat exchangers, chemical reactors, helical and spiral coils and many others.

Curved tube flows have been extensively studied both theoretically and experimentally. The flow in curved tube is characterized by a secondary flow in a cross sectional plane normal to the main flow, Truesdell et al.(1970) and Patankar et al.(1974). The nature of which depends upon the Dean number $De = Re(D_h/R)^{1/2}$ (D_h being the radius of the tube or width of the channel, R its radius of curvature and Re is the Reynolds number).

Centrifugal forces, which are proportional to the square of the axial velocity, tend to push fluid in the central region towards the outer bend of the coiled tube. This induces a pressure gradient directed toward the inner bend. The induced pressure gradient is almost uniform throughout the cross section of the tube. The axial velocity, however, varies widely throughout the cross-section. As a result, the centrifugal force acting on the flow varies throughout the cross section.

In the central region, the centrifugal force assumes its maximum value and is roughly in balance with pressure gradient. The net effect is a smooth movement of fluid axially down the tube.

Near the tube wall, the axial velocity is slowed by viscous forces, hence the pressure gradient is stronger than the centrifugal force and forces fluid inward along the top and bottom of the tube wall. This inward movement along the walls begins at the outer bend, where fluid from the core encounters the wall. It ends at the inner bend

where the two streams meet and then separate from the wall, and more into the central region. The net effect is to produce two vortices of equal magnitude but of opposite direction, with a horizontal line of symmetry separating them.

It has been made clear that the secondary flow resulting from the centrifugal force causes the heat transfer coefficient, to be significantly higher than that in straight tube.

Useful characteristics include, in addition to compactness, flow in curved tubes, gives high rates of heat and mass transfer, enhances cross-sectional mixing, low axial dispersion and extended laminar flow regime, and the transition from laminar to turbulent flow occurs at higher Reynolds number than in straight tubes. Furthermore, the secondary flows present in curved tube cause a marked variation in local heat transfer coefficients around the periphery of tube. A knowledge of this variation may suggest advantages in instances where only a portion of the peripheral boundary is available for transport processes.

On the other hand, heat transfer in porous media has been the subject of numerous investigations due to increasing interest in chemical catalytic reactors, building thermal insulation, heat exchangers, petroleum reservoirs, geothermal operations, packed sphere beds and many others. This increased use of porous media has made it essential to have a better understanding of the associated transport processes.

Laminar flow and heat transfer through porous media in straight pipes, annuli and channels, has been widely investigated theoretically and experimentally, covering wide ranges of flow conditions, and porous matrix characteristics.

The importance of this study arises from the presence of a solid matrix in the passage of a fluid flow in curved tube, which has less attention from investigators.

Therefore, laminar flow and heat transfer in curved rectangular channels filled with saturated porous medium is solved numerically using finite element method. The effect of curvature ratio, aspect ratio, and porous parameters on axial velocity profile and secondary flow patterns is presented. The effect of Prandlt number on the axial temperature profile, temperature contours and local Nusselt number is also studied.

2. LITERATURE REVIEW

2.1 Introduction

Flow in curved tubes differs from that in straight tubes, principally through exhibiting a secondary flow in planes normal to the main flow. Centrifugal forces act at right angles to the main direction of flow, so that the profile of axial velocity is distorted, and the point at which the velocity has its peak is shifted to the outside. The flow is three dimensional where as that in straight tube is two dimensional. In this chapter, some of the previous work, which is conducted on flow and heat transfer in nonporous curved tubes, as well as straight porous tubes is presented.

2.2 Flow and Heat Transfer in Curved Tubes

Truesdell and Adler (1970) studied numerically the fully developed laminar flow in helically coiled tubes. In this study, finite difference approximation solutions were obtained for different cases of axial pressure gradient and curvature ratio from10 to 100. Dean numbers less than 200 were found to be accurate to within 0.02, higher Dean number solutions were approximate. It was inferred that as the Dean number increases, the secondary flow patterns shift back toward x = 0 and more upward and downward in the y-direction.

Austin and Seader (1973) solved numerically the Navier-Stokes equations in stream function vorticity form. Solutions were obtained for circular pipes using curvature ratios ranging from 5 to 100. The cross sectional pressure distribution was calculated and a correlation equation is presented for a diametral pressure drop in terms of the Dean number.

Prediction of laminar flow and heat transfer in helically coiled pipes was presented by Patankar et al (1974). The effect of Dean number on the friction factor and heat transfer is presented. Axial velocity profiles for developing and fully developed regions were compared with experimental data. It is found that the velocity profile at the horizontal centerline is distorted from the parabolic shape with increasing Dean number. It was also found that the local Nusselt number is increased with increase in Dean number.

Kalb and Seader (1974) studied numerically fully developed flow in curved pipes with uniform wall temperature. Solutions were obtained over a wide range of Prandtl numbers and Dean numbers as large as 1200. A correlation equation for the average Nusselt number over Prandtl number range from 0.7 to 5 was presented in the following formula:

$$\overline{Nu} = 0.836\, De^{0.5}\, Pr^{0.1} \qquad De \geq 80 \qquad (2.1)$$

Joseph et al. (1975) studied numerically laminar flow in helically coiled tubes of square cross-section. In this work it is seen that up to Dean numbers of 100, the expected secondary flow pattern appears with twin counter rotating vortices. Above Dean number of 100, a new secondary flow regime, reported for the first time, appears with four vortices. The numerical results were experimentally confirmed at Dean number of 100. Flow visualization and pressure drop experiments were performed, and a helically coiled tube of square cross section was constructed from clear acrylic plastic.

Fully developed laminar flow in curved rectangular channels was studied by Cheng et al. (1976). This work was recognized by solving the equations for different aspect ratios (length to width ratio) of 0.5, 1, 2, and 5, Dean number ranges from 5 to 715, and the appearance of an additional counter-rotating pair of vortices near the

central outer region of the channel, in addition to the familiar secondary flow at a certain higher Dean number depending on the aspect ratio. Friction factor correlation equations were also developed. It takes the following shape:

$$f_c/f_s = 0.0.1278\ K^{1/2}\ (\ 1\text{-}0.257\ K^{-1/2} + 0.669\ K^{-1} - \quad 187.7\ K^{-3/2} - \ 512.2\ K^{-2}\ ) \qquad (2.2)$$

where the subscript c denotes for curved tube and s for straight one. The coefficients in the above equation were correlated for the case of square ducts. Coefficients for other channel configurations were reported.

The influence of both centrifugal and buoyancy forces was studied analytically by Yao and Berger (1977). Both horizontal and vertical flow in curved pipes is considered. Solutions for these two cases are obtained by regular perturbations in the Dean number, and the product of the Reynolds and Rayleigh numbers. It was noticed that the combination of the centrifugal and buoyancy forces generates two vortices whose line of symmetry intersects the direction of gravity at a finite angle. Also, the line of symmetry is no longer a straight line when both body forces act on the fluid particles.

Humphrey et al. (1977) gave both theoretical and experimental results for laminar flow in a 90^{o} bend duct. The calculated results were obtained by solving Navier-Stokes equations in cylindrical coordinates. Flow visualization was used to identify qualitatively the characteristics of the flow and laser Doppler anemometry to quantify the velocity field. Secondary velocities up to 65% of the bulk longitudinal velocity were calculated and small regions of recirculation close to the other corners of the duct and in the upstream region, were also observed. The region of recirculation was confirmed by the calculations. Measured and computed velocity contours were reported for different planes with respect to the center of the bend.

Rabadi (1980) investigated numerically pulsating flow and heat transfer in curved tubes. In this study, the effects of pulsation on the transport rates are discussed. Results for the shear stresses at different Dean numbers from 12 to 294, pulsation parameter from 1 to 15 are presented. Temperature contours for different pulsation parameters and time positions were reported. A considerable interest was also devoted to the effect of pressure amplitude on the variation of Nusselt number, axial velocity, temperature contours and axial shear stress.

Prusa and Yao (1982) investigated fully developed flow in heated curved tubes numerically. In this work, the effect of buoyancy forces was considered, besides centrifugal forces. Results for a Prandtl number of one are presented for moderate range of Dean numbers, and the product of Reynolds and Raleigh numbers. It was also reported that the mass flow rate is drastically reduced owing to the secondary flow for a given axial pressure gradient, and the total heat transfer rate decreases for a more curved tube and larger axial temperature gradient.

Hille et al. (1985) provide an experimental procedure, to discuss the development flow in a 180° section of a curved square duct. A numerical solution was obtained to compare with measured values. The streamwise flow velocity component and the secondary flow component were measured as a function of Dean number and azimuth angle (φ), where $\varphi = 0$ represents the angle at the onset of curvature. A second vortex with opposing sense of circulation was found to develop near the outer wall only for Dean numbers between 150 and 300 ($R/d = 6.45$), in agreement with numerical calculations.

Buoyancy effects on developed laminar curved tube flows, with axially uniform heat flux, and peripherally uniform wall temperature were investigated by Lee et al. (1985). The solution covers a wide range of Prandtl, Dean and Grashof numbers and

includes the curvature ratio as an explicit parameter. It is found that buoyancy acts to increase the average Nusselt number distribution around the periphery. The curvature ratio in the range 4-50 has a negligible explicit influence on the average Nusselt number and skin friction factor, though it has a fairly large effect on the location of the maxima.

Futagami and Aoyama (1988) investigated the laminar heat transfer in a helically curved tube. In this work, numerical analysis was made taking into account both centrifugal and buoyancy forces. The solutions cover a wide range of Prandtl number, 1 to 100. The Velocity and temperature profiles, the friction factor, and heat transfer coefficient are obtained. The effects of the secondary flow on heat transfer are divided into three types: those in the centrifugal, the buoyant and the composite range. Correlation equations for Nusselt number were obtained:

$$\left(\frac{Nu_c}{Nu_o}\right)^6 = 1 + \left[0.195(De Pr^{0.5})\right]^6 \qquad (2.3)$$

where Nu_c denotes the Nusselt number for Rayleigh number Ra = 0, and Nu_o is the Nusselt number for straight tube. Experimental results using water, in a helically coiled tube of curvature ratio 101, were obtained to compare with calculated values. The effect of the inclination of the tube was also discussed.

Yang and Chang (1993) gave a numerical study of fully developed laminar flow and heat transfer in a curved pipe. The range of the parameters are the curvature ratio ($\delta = D_h/R$), varying from 0.01 to 0.9, the Reynolds number varying from 1 to 2000 and the Prandtl number varying from 0.7 to 300. The results indicate except for $Re_s<10$, that the friction ratio increases with increasing pressure gradient and increasing curvature ratio. On the other hand, the heat transfer ratio increases with increasing δ until at a certain value of δ, the heat transfer rate no longer varies significantly. Correlation

equations for friction ratio and heat transfer ratio were developed. For $\delta < 0.9$ the friction ratio is

$$\frac{F_c}{F_s} = 1 \qquad De \le 500 \qquad (2.4)$$

$$\frac{F_c}{F_s} = 0.397 De^{0.149} \qquad De \ge 500 \qquad (2.5)$$

The heat transfer ratio for $0.01 < \delta < 0.9$, $0.7 < Pr < 5$, and $0.01 < De < 10^6$ is:

$$\frac{\overline{Nu_c}}{\overline{Nu_s}} = 0.722 De^{0.098} \delta^{-0.015} Pr^{0.181} \qquad (2.6)$$

Gyves et al. (1998) investigated gravitational and centrifugal boundary effects in curved square channels, with conjugated boundary conditions. Numerical solutions were presented for 4.4<De<210.9, 0.01<Pr<7.2, and $0.01 < \phi < 20$, where $\phi = k_w t/k_s D_h$ is dimensionless wall conduction parameter, defining the thermal boundary condition. An increase in the curved channel forced convection average Nusselt number ($\overline{Nu}$) over the straight $\overline{Nu}$ was documented for all values of ϕ. This increase in $\overline{Nu}$ can be attributed to the presence of secondary flow vortices in the channel. Fluid density variations in both the radial and vertical directions have been examined. Changes in gravitational buoyancy (Gr_g) have been shown to have a negligible effect on $\overline{Nu}$, when the influence of centrifugal boundary (Gr_c) is included.

Gyves and Irvine (2000), studied fully developed laminar flow, and conjugated forced convection heat transfer in curved rectangular channels. The wall average Nusselt number $\overline{Nu}$, is presented as a function of the wall conduction parameter ϕ, the Dean number De, and the channel aspect ratio λ (channel height/channel width). It is

noted that $\overline{Nu}$ is increased with increasing De for all values of ϕ. It has been shown that the curvature effect is less significant as the channel aspect ratio decreases from λ = 1. Solutions for straight channel are also included, and it is found that ϕ_{eff} is independent of λ for $\lambda \leq$ ¼, where ϕ_{eff} is defined as the value of ϕ at which a constant wall temperature boundary condition can be assumed.

2.3 Flow and Heat Transfer in Straight Porous Tubes

Although research on fluid flow and heat transfer in porous media extends to more than 50 years ago, only recent work on this field will be reviewed here. Most analytical studies dealing primarily with the mathematical formulation are based on Darcy's law, which neglects the effects of solid boundaries, and the inertia forces on fluid flow and heat transfer through porous media. These effects are expected to become more significant near the boundary and in high porosity media, thus causing the application of Darcy's law to be invalid. Moreover, recent increase in utilizing high porosity media in contemporary technology provides further need for a thorough understanding of the boundary and inertia effects.

Vafai and Tien (1981), studied boundary and inertia effects on flow and heat transfer in porous media. This is accomplished by, at first formulating the general problem with these effects, and then applying the formulation to the specific case of two-dimensional flow confined by an external boundary. The effect of boundary on heat transfer is found to be quite important, and is more pronounced for the thermal boundary layer. This is expected to happen at high Prandtl numbers, and large pressure differences. The inertia effects increase with the higher permeability and the lower fluid viscosity. Further more, the velocity gradients near the wall are bound to increase,

Kaviany (1985), gives a closed form solution for fully developed laminar flow through a porous channel bounded by isothermal parallel plates. Fully developed fields for a simplified case, in which the inertia term is neglected. It is found that the velocity profile depends strongly on the porous media shape factor, $\gamma = (W^2\varepsilon/K)^{1/2}$ where W is channel width, ε is the porosity, and K is the permeability. As γ increases, the central region containing a uniform velocity distribution spreads further toward the plates. At large γ, the velocity variation is confined to a very thin layer adjacent to the plates. The boundary frictional drag coefficient is proportional to γ, while the bulk frictional drag is proportional to γ^2. Also it is found that Nusselt number increases with an increase in γ, while the temperature profile does not change significantly with γ. Its value at the centre line increases as γ increases.

Cheng and Hsu (1986) performed an analysis for a fully developed, forced convective flow, through a packed sphere bed between concentric cylinders maintained at different temperatures. The variation of the porosity near the wall was considered by an exponential function. Analytical solution based on the method of asymptotic expansions is obtained for the velocity. It is shown that velocity overshoots occur in the variable porosity bed near the inner and outer cylinders.

Fluid flow and heat transfer characteristics of a fully developed forced convective flow in a cylindrical packed tube with symmetric heating, are analyzed by Cheng and Zhu (1987). The Darcy–Brinkman-Ergan model is used as the momentum equation. The radial porosity variation of the packed column approximated by an exponential function. The method of matched asymptotic expansion is applied to construct a composite solution for the axial velocity. The effects of radial thermal dispersion, and variable stagnant thermal conductivity are taken into consideration in the energy equation. It is found that at high Reynolds numbers, the dimensionless radial

temperature profile becomes relatively independent of the thermal boundary conditions at the wall.

Poulikakos and Renkan (1987) investigated numerically, the effects of flow inertia, variable porosity, and Brinkman friction, in a channel filled with porous media. Two channel configurations were used: circular pipe and parallel plate channels. It was found that the channeling phenomenon near the walls of both duct configurations enhanced the thermal communication between the fluid solid matrix and the walls. This fact yielded an overall of 12 percent increase in the value of Nusselt number, in the parallel plate channel compared to the value predicted when the Darcy model was used. Similarly, 22 percent increase in the value of Nusselt number for the circular channel in the fully developed region was observed.

Vafai and Kim (1989), found an exact solution to the problem concerning forced convection in a channel filled with porous medium. Results for velocity and temperature profiles were obtained for two value of the Darcy number, these are $Da^{-1/2}$ = 10 and 30. It is shown that, for a high permeability porous medium the thickness of the momentum boundary layer depends or both the Darcy number and the inertia parameter, while that for a low permeability porous medium depends only on the Darcy number. A significant increase in the rate of heat transfer, as the inertia parameter increases, especially for high to medium permeability porous media was also reported.

Mixed convection flow over vertical cylinder was studied by Chen et al. (1992) taking the non-Darcian effects into consideration. These effects include, in addition to the non-slip boundary condition, flow inertial force, and variable porosity, the transverse thermal dispersion effect. Numerical results show that thermal dispersion tends to enhance the heat transfer rate, while boundary and inertia effects decrease it.

The large enhancement in heat transfer caused by dispersive transport was attributed to the better mixing of convective fluid within the pores.

Hwang and Chao (1992), obtained a numerical solution for the effects of wall conduction and Darcy number on laminar mixed convection flow. The flow and heat transfer characteristics are greatly affected by the peripherally non-uniform wall temperature distribution. Secondary flow patterns, isotherms, wall temperature distributions, the friction factor, and the Nusselt number are presented for a flow in the Darcian porous medium ($Da \to 0$), to a pure fluid flow ($Da \to \infty$), with $Gr = 0 - 10^{10}$, and $Pr = 0.1, 0.73, 7.2$, and 100. It is seen that, the product $f\,Re$ calculated for Darcy's friction and Forchheimer's friction (inertia of porous matrix) are almost negligible when $Da^{-1} \leq 1$, and the flow behaves just like Poiseuille flow.

Kou and Lu (1993), provided a closed form solution for a fully developed mixed convection in a vertical channel. Both the boundary and inertia effects of the porous medium are considered. Different thermal boundary effects on channel wall are investigated. It is found that the temperature distribution depends on the thermal boundary conditions only. As to the velocity profile, it is a function of the pressure gradient, in addition to the no-slip and thermal boundary conditions. The influence of inertia effect is investigated by solving numerically the equations of motion.

Lan and Yhodadadi (1993) studied the effect of permeable walls on fluid flow and heat transfer in porous channel. The transport equations are transformed to ordinary differential equations following White (1991). For a given porous medium shape parameter [$\gamma = 2H/(K/\varepsilon)^{0.5}$], where H is half channel width, it is shown that as the blowing Reynolds number ($B = VH/\nu_f$), V being the permeation velocity at the walls increases, profiles of the axial velocity component, and temperature become flatter near the symmetry axis, and the respective gradients near the wall increase markedly. For a

given shape parameter, as the permeation at the walls is strengthened, frictional drag increases as a result of steep shearing next to the walls. For low Peclet numbers, the enhanced Nusselt number exhibits a dependency on the shape parameter, but for high Peclet numbers, the Nusselt number is independent of the shape parameter.

Hadim (1994) performed a numerical solution for laminar flow in porous channel. Two configurations are considered: a fully porous channel, and a partially porous channel, which contains porous layers above heat sources, and is non-porous elsewhere. Heat transfer rate and pressure drop are evaluated for a wide ranges of Darcy and Reynolds numbers. The results indicate that as the Darcy number decreases, a significant increase in heat transfer is obtained, especially at the leading edge of heat source. In the partially porous channel, it is found that when the width of the heat source and the spacing between the porous layers are of the same magnitude, as the channel height, the heat transfer enhancement is almost the same, as in the fully porous channel, while the pressure drop is significantly lower. These results suggest that the partially porous channel is a potentially attractive heat transfer augmentation technique for electronic equipment cooling.

A numerical study is made to the heat transfer characteristics from forced pulsating flow in a channel by Kim et al. (1994). The walls of the porous channel are assumed to be at uniform temperature. In comparison with the case of no pulsating flow, the presence of flow pulsation brings forth a reduction in heat transfer in the entrance region, and an enhancement of heat transfer at moderate downstream regions. When Darcy number is large, the velocity profiles at low frequency parameter are similar to the quasi-steady flows in a non-porous channel. For high frequency parameter, only a narrow portion very close to the wall is affected. The axial pressure

gradient and skin friction coefficient are little affected by the changes in the frequency parameter.

Sadrul et al. (1995) investigated asymmetric heating of packed channel. The wall effects on the variation of porosity and thermal dispersion have been considered. For same Reynolds number, it was seen that velocity profile is affected markedly by increasing particle diameter. The variation of Nusselt number with Reynolds number is also compared with previous correlations and a good a agreement was observed for three different particle size of the porous medium.

Varahasamy and Fand (1996) determined empirical correlation equations for the average Nusselt number in spheres packed pipes. The equations cover the Darcy, Forchheimer and turbulent regimes of flow. The results of experiments show that, for equal pumping power, the method of packing tubes with spheres can provide heat transfer enhancement two to seven times that of unpacked tubes, for laminar flow and two to two and half times for turbulent flow.

Huang and Liu (1996) presented an analytic solution, for the developing flow in a channel, filled with porous media. The effects of the inlet velocity, and Darcy number on the variation of the velocity distribution were determined. It was also seen that the downstream velocity profile is greatly affected by the Darcy number. Three different inlet velocity profiles are examined, namely, linear, backward- triangle and parabolic shapes. It is noted that for the same Darcy number, the parabolic inlet flow takes the shortest distance to settle into the fully developed flow, whereas the linear inlet flow takes the largest distance.

Nield et al. (1996) studied forced convection flow in porous media. Isothermal and isoflux boundary conditions are applied, and the Brinkman-Forchheimer extension of Darcy's equation is used. For the case of isoflux surfaces, it is found that when Da is

large and F is small, the velocity profile is approximately parabolic, and the Nusselt number is near 70/17. On the contrary, when Da is sufficiently small or F is sufficiently large, the velocity profile is approximately uniform. Similar results are obtained for isothermal surfaces case, but the Nusselt numbers are smaller.

3. THEORITICAL CONSIDERATIONS

In this work laminar flow and heat transfer in curved rectangular channels is studied. The curved tube considered is a part of helical tube with zero pitch. The physical configuration and the system of orthogonal toroidal coordinates (X, Y, Z) and the corresponding velocity components (U, V, W) respectively is shown in Figure (3.1).

3.1 Assumptions

In developing the governing equations, a set of assumptions are imposed thoughout this work. These are:

1. The flow is laminar, hydrodynamically and thermally fully developed.
2. The fluid is viscous, incompressible, Newtonian with constant physical properties.
3. The flow is steady.
4. Buoyancy effects and viscous dissipation are neglected.
5. The porous medium is homogeneous and isotropic and is saturated with a single phase fluid.
6. The fluid and solid matrix are every where in local thermodynamic equilibrium.
7. Negligible coil pitch.

3.2 Governing Equations

The governing equations for forced convection in porous media are developed here using the local volume averaging technique. This is done by associating with each point in the porous medium a small volume, V, bounded by a closed surface A. If the portion of V containing the fluid is denoted by V_f, then the local volume average of

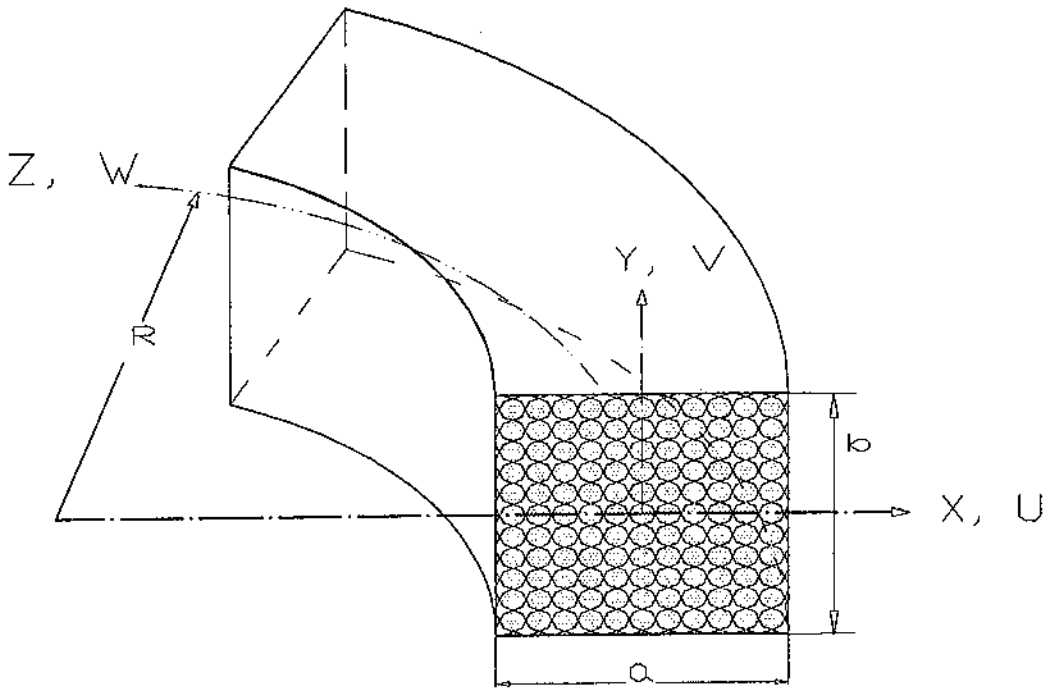

Figure (3.1) System of toroidal coordinates for rectangular channel.

a quantity associated with the fluid is defined as:

$$<\varphi> = \frac{1}{V}\int_{V_f} \varphi dV = \frac{\epsilon}{V_f}\int_{V_f} \varphi \, dV \qquad (3.1)$$

Based on the assumptions stated in the previous section, the mass, momentum and energy equations for an incompressible, steady flow through a porous medium in curved tube are established here as in Vafai and Tien (1981) and Vafai (1984).

For the configuration shown in Figure (3.1), and dropping the averaging sign, the governing equations can be written as follows, Cheng et al. (1976):

Continuity equation:

$$\frac{dU}{dX}+\frac{dV}{dY}+\frac{U}{X+R}=0 \qquad (3.2)$$

X-momentum equation

$$\rho_f\left(U\frac{dU}{dX}+V\frac{dU}{dY}-\frac{W^2}{X+R}\right)=-\frac{dP}{dX}+\mu_f\left(\frac{d^2U}{dX^2}+\frac{1}{X+R}\frac{dU}{dX}+\frac{d^2U}{dY^2}+\frac{U}{(X+R)^2}\right)-\frac{\rho_f \epsilon}{K}U-\frac{\rho_f F \epsilon^2}{K^{1/2}}U^2 \qquad (3.3.a)$$

Y-momentum equation

$$\rho_f\left(U\frac{dV}{dX}+V\frac{dV}{dY}\right)=-\frac{dP}{dY}+\mu_f\left(\frac{d^2V}{dX^2}+\frac{d^2V}{dY^2}+\frac{1}{X+R}\frac{dV}{dX}\right]-\frac{\rho_f \epsilon V}{K}-\frac{\rho_f F \epsilon^2}{K^{1/2}}V^2 \qquad (3.3.b)$$

Z-momentum equation

$$\rho_f\left(U\frac{dW}{dX}+V\frac{dW}{dY}+\frac{UW}{X+R}\right)=-\frac{R}{X+R}\frac{dP}{dZ}+\mu_f\left(\frac{d^2W}{dX^2}+\frac{1}{X+R}\frac{dW}{dX}+\frac{d^2W}{dY^2}-\frac{W}{(X+R)^2}\right)-\frac{\rho_f \in}{K}W-\frac{\rho_f F \in^2}{K^{1/2}}W^2 \qquad (3.3.c)$$

Energy equation

$$U\frac{dT}{dX}+V\frac{dT}{dY}+\frac{WR}{X+R}\frac{dT}{dZ}=\alpha_e\left(\frac{d^2T}{dX^2}+\frac{d^2T}{dY^2}+\frac{1}{X+R}\frac{dT}{dX}\right) \qquad (3.4)$$

It should be noted here that, the first and second derivatives of the quantities in the continuity and momentum equations with respect to the axial coordinate (Z) vanished because the flow is fully developed except for the pressure, since it is the driving force of the flow . Furthermore, the axial conduction term is neglected from the energy equation compared with other terms.

Equations (3.3) represent the Brinkman-Forchhimer extended Darcy model, Vafai and Tien (1981), in which the last two terms account for respectively, the pressure drop caused by the frictional drag ($\frac{\mu_f \in}{K}W$) and the inertia effect which become appreciable at high velocities ($\frac{\rho_f F \in^2}{K^{1/2}}W^2$), where ρ_f denotes the fluid density, μ_f is the fluid dynamic viscosity, ε is the porosity, K is the permeability of the porous structure, F is the inertia coefficient which depends on the permeability and the geometry of the porous medium, and α_e is the effective thermal diffusivity.

A great deal of effort has been spent to develop an expression for K. In the case of beds of particles or fibers, the hydraulic radius theory of Carman-Kozeny leads to the following relationship, Nield et al. (1999);

$$K=\frac{D_p^2 \epsilon^3}{180(1-\varepsilon)^2} \tag{3.5}$$

where D_p is an effective average particle or fiber diameter. The constant 180 was obtained by seeking a best fit with experimental results. This equation gives a satisfactory results for media that consists of particles of approximately spherical shape.

It is relevant at this point to nondimensionalize the above equations here, by introducing the following dimensionless variables:

$$x=\frac{X}{D_h} \qquad y=\frac{Y}{D_h}$$

$$z=\frac{Z}{D_h} \qquad r=\frac{R}{D_h}$$

$$u=\frac{D_h U}{\nu_f} \qquad v=\frac{D_h V}{\nu_f}$$

$$w=\frac{D_h W}{\nu_f} \qquad p=\frac{D_h{}^2 P}{\rho \nu_f{}^2}$$

Where D_h is the hydraulic diameter of the channel, ν_f is kinematic viscosity of the fluid. To nondimensionalize the energy equation, it is important to specify the thermal boundary condition. The heat transfer boundary condition chosen in this work assumes the temperature of the tube wall, T_w, varies linearly in the axial direction only, but it is peripherally uniform, i.e

$$T_w = T_w(Z) \tag{3.6}$$

Accordingly, the dimensionless temperature t is defined in the following form:

$$t=\frac{T_w-T}{D_h(\partial T/\partial Z)} \tag{3.7}$$

where $(\partial T/\partial Z)$ is the temperature gradient in the axial direction and it is constant for thermally fully developed flow.

A further approximation is made here, by neglecting the inertia term in the momentum equations due to porous matrix. Substituting the above dimensionless variables into equations (3.2) through (3.5) yields:

x- momentum Eq.

$$u\frac{\partial u}{\partial x}+v\frac{\partial u}{\partial y}-\frac{w^2}{x+r}=-\frac{\partial p}{\partial x}+\frac{\partial^2 u}{\partial x^2}+\frac{\partial^2 u}{\partial y^2}+\frac{1}{x+r}\frac{\partial u}{\partial x}-\frac{u}{(x+r)^2}-\frac{u}{Da} \tag{3.8.a}$$

y-momentum Eq.

$$u\frac{\partial v}{\partial x}+v\frac{\partial v}{\partial y}=-\frac{\partial p}{\partial y}+\frac{\partial^2 v}{\partial x^2}+\frac{\partial^2 v}{\partial y^2}+\frac{1}{x+r}\frac{\partial v}{\partial x}-\frac{v}{Da} \tag{3.8.b}$$

z- momentum Eq.

$$u\frac{\partial w}{\partial x}+v\frac{\partial w}{\partial y}+\frac{uw}{x+r}=\frac{-r}{x+r}\frac{\partial p}{\partial z}+\frac{\partial^2 w}{\partial x^2}+\frac{\partial^2 w}{\partial y^2}+\frac{1}{x+r}\frac{\partial w}{\partial x}-\frac{w}{(x+r)^2}-\frac{w}{Da} \tag{3.8.c}$$

and the energy equation is :

$$u\frac{\partial t}{\partial x}+v\frac{\partial t}{\partial y}-\frac{rw}{x+r}=\frac{1}{Pr}\left(\frac{\partial^2 t}{\partial x^2}+\frac{\partial^2 t}{\partial y^2}+\frac{1}{x+r}\frac{dt}{dx}\right) \tag{3.9}$$

where Da is the modified Darcy number and Pr is the modified Prandtl number defined as :

$$Da = \frac{K}{\epsilon a^2} = \frac{Da'}{\epsilon}$$

$$Pr = \epsilon \frac{\nu_f}{\alpha_e} = \epsilon Pr'$$

and

$$\alpha_e = \frac{k_e}{\rho_f c_f}$$

$$k_e = \epsilon k_f + (1-\epsilon) k_s$$

where c_f is the fluid specific heat, k_e is the effective thermal conductivity, α_e and the effective thermal expansion coefficient.

One of the main difficulties in solving the flow and heat transfer problems is the unknown pressure field. Fortunately in many cases the pressure field is not of primary interest, and the problem can be made simple if the pressure is eliminated from the solution process. This elimination can be achieved by using the vorticity stream function approach.

At first, the pressure terms can be eliminated by differentiating x-momentum with respect to y and differentiating y-momentum with respect to x and subtracting them, the resulting equation is :

$$\frac{\partial^3 u}{\partial y^3} - \frac{\partial^3 u}{\partial x^3} + \frac{\partial^3 u}{\partial y\, \partial x^2} - \frac{\partial^3 v}{\partial x\, \partial y^2} +$$
$$\left(\frac{1}{x+r} - u\right)\left(\frac{\partial^2 u}{\partial y\, \partial x} - \frac{\partial^2 v}{\partial x^2}\right) - v\left(\frac{\partial^2 u}{\partial y^2} - \frac{\partial^2 v}{\partial y^2}\right) -$$
$$\left(\frac{1}{(x+r)^2} - \frac{\partial u}{\partial x} - \frac{\partial v}{\partial y}\right)\left(\frac{\partial u}{\partial y} - \frac{\partial v}{\partial x}\right) -$$
$$\frac{1}{Da}\left(\frac{\partial u}{\partial y} - \frac{\partial v}{\partial x}\right) + 2w\frac{\partial w}{\partial y} = 0 \qquad (3.10)$$

Now, the stream function ψ is introduced in such away that the continuity equation is identically satisfied i.e.

$$u = \frac{1}{x+r}\frac{\partial \psi}{\partial y} \tag{3.11}$$

$$v = -\frac{1}{x+r}\frac{\partial \psi}{\partial x} \tag{3.12}$$

Substituting for u and v in terms of ψ into the momentum equations results in two differential equations in terms of the axial velocity w and the stream function ψ, but the stream function equation is raised to the fourth order. By introducing the definition of the axial vorticity :

$$\xi = \frac{1}{x+r}\frac{\partial^2 \psi}{\partial y^2} + \frac{1}{x+r}\frac{\partial^2 \psi}{\partial x^2} - \frac{1}{(x+r)^2}\frac{\partial \psi}{\partial x} \tag{3.13}$$

the fourth order equation is reduced to second order as well as the axial momentum equation. The final set of dimensionless equations are :

Axial vorticity equation:

$$\frac{\partial^2 \xi}{dx^2} + \frac{\delta^2 \xi}{dy^2} + A\frac{d\xi}{dx} + B\frac{d\xi}{dy} + C\xi + \frac{2w}{x+r}\frac{\partial w}{\partial y} = 0 \tag{3.14}$$

Axial momentum equation:

$$\frac{\partial^2 w}{\partial x^2} + \frac{\partial^2 w}{\partial y^2} + A\frac{\partial w}{\partial x} + B\frac{\partial w}{\partial y} + C_w w - \frac{r}{x+r}\frac{\partial P}{\partial z} = 0 \tag{3.15}$$

where :

$$A = \frac{1}{x+r}\left(1 - \frac{\partial \psi}{\partial y}\right) \tag{3.16}$$

$$B = \frac{1}{x+r}\left(\frac{\partial \psi}{\partial x}\right) \tag{3.17}$$

$$C = \frac{1}{(x+r)^2}\frac{\partial \psi}{\partial y} - \frac{1}{(x+r)^2} - \frac{1}{Da} \tag{3.18}$$

$$C_W = -\frac{1}{(x+r)^2}\frac{\partial \psi}{\partial y} - \frac{1}{(x+r)^2} - \frac{1}{Da} \tag{3.19}$$

The energy equation is unchanged except for substituting the velocities u and v in terms of the stream function;

$$\frac{1}{x+r}\left(\frac{\partial \psi}{\partial y}\right)\left(\frac{\partial t}{\partial x}\right) - \left(\frac{1}{x+r}\right)\left(\frac{\partial \psi}{\partial x}\right)\frac{\partial t}{\partial y} - \frac{rw}{x+r} = \frac{1}{Pr}\left(\frac{\partial^2 t}{\partial x^2} + \frac{\partial^2 t}{\partial y^2} + \frac{1}{x+r}\frac{\partial t}{\partial x}\right) \tag{3.20}$$

3.3 Boundary Conditions:

Before discussing the boundary conditions, it is worth to note that we have a symmetrical flow about the x-axis. Therefore the solution is obtained in the upper half plane of the channel cross section. In the following, the boundary conditions for the axial velocity, the stream function, the vorticity and the temperature are discussed separately.

3.3.1 The axial velocity

The value of the axial velocity at the solid boundary is naturally zero, which is the no-slip condition. The symmetrical flow along the positive and negative portions of the horizontal centerline requires that the partial derivative of the axial velocity w with respect to y is zero i.e.

$$\left(\frac{\partial w}{\partial y}\right)\Big|_{y=0} = 0 \qquad (3.21)$$

3.3.2 The stream function

It is clear that the tube wall can be considered a streamline, hence the value of the stream function is constant at the wall. Also, because of symmetry, the horizontal tube centerline is a stream line and its value is taken to be as that of the boundary value. There is no unique value of the stream function, in fact the absolute value of the stream function has no important physical significance. This can be noticed in the governing equation where only the stream function derivatives appear. Thus for convenience, the value of the stream function of the entire boundary is taken to be zero. This reasoning is adapted from Rabadi (1980) .

3.3.3 The Vorticity

Recalling the definition of the vorticity, equation(3.13):

$$\xi = \frac{1}{x+r}\frac{\partial^2 \psi}{\partial x^2} + \frac{1}{x+r}\frac{\partial^2 \psi}{\partial y^2} - \frac{1}{(x+r)^2}\frac{\partial \psi}{\partial x}$$

and referring to the solution domain Figure(3.2), we note that for all y equal to zero, each term is identically zero. Since the stream function is constant along this line, all derivatives with respect to x vanish while the second term is zero comes from the definition of the stream function i.e.

$$u = \frac{1}{x+r}\frac{\partial \psi}{\partial y} \qquad (3.22)$$

and since $(\frac{\partial u}{\partial y}) = 0$ along y = 0, this means that $(\frac{\partial^2 \psi}{\partial y^2}) = 0$, hence the vorticity at the centerline is zero.

Now consider the value of the vorticity on the left and right sides of the plane. The second term is zero because the stream function is constant along these lines, while the third term is zero since it is by definition the no slip condition at the wall. Therefore the vorticity on the vertical portions is given by:

$$\xi = \frac{1}{x+r}\frac{\partial^2 \psi}{\partial x^2} \qquad (3.23)$$

The value of the vorticity on the upper line of the region i.e. y = b/2, is simply given by :

$$\xi = \frac{1}{x+r}\frac{\partial^2 \psi}{\partial y^2} \qquad (3.24)$$

since the first and third terms vanish because the stream function is constant along this line.

3.3.4 The Temperature

As mentioned in the part of developing the energy equation section (3.2), the temperature at the periphery of any cross section is assumed to be constant, and it is denoted by T_w. Therefore the dimensionless temperature at the tube boundary is simply zero by substituting for T by T_w in equation (3.6). From symmetry condition, the partial derivative of temperature with respect to y is zero at the centerline or:

$$\left(\frac{\partial t}{\partial y}\right)\Big|_{y=0} = 0 \qquad (3.21)$$

The complete boundary conditions are shown on Figure(3.2).

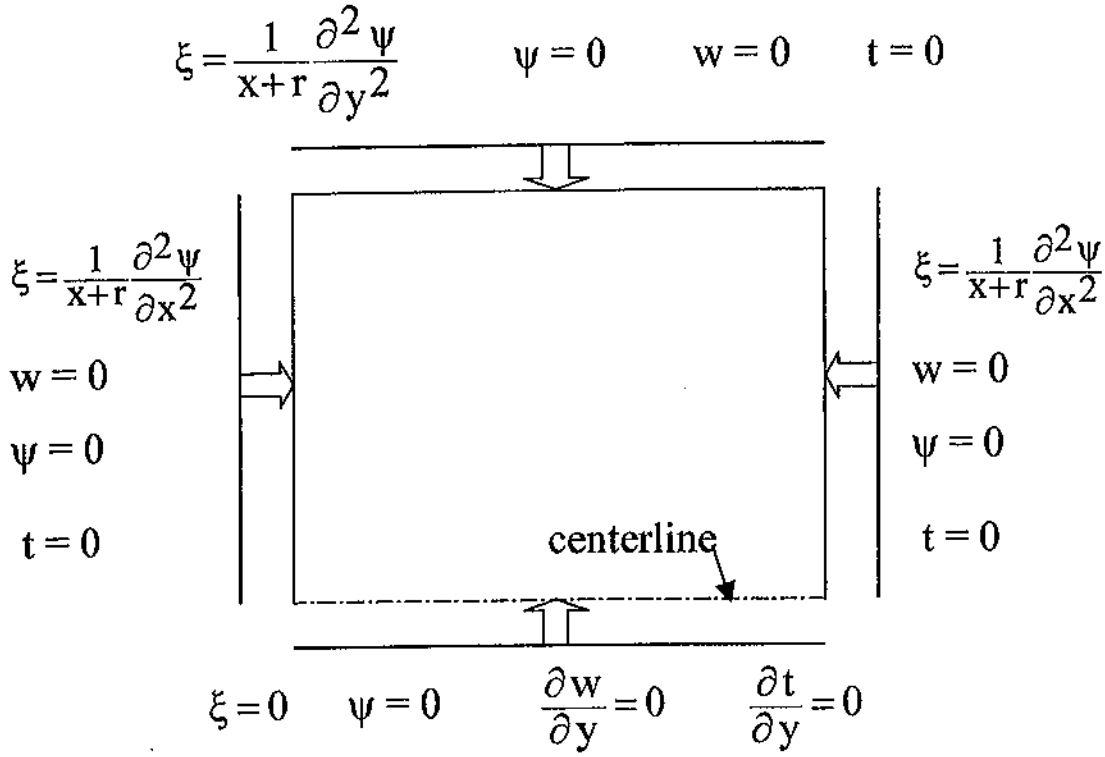

Figure (3.2) Boundary conditions

4. SOLUTION METHOD

4.1 Introduction

As long as the boundary conditions are specified, the dimensionless equations governing laminar flow and heat transfer in rectangular curved porous channel developed in chapter three, Equations (3.13) to (3.15), and (3.20) subject to the boundary conditions shown on Figure(3.2) are ready to be solved.

An inspection of the system of equations reveals that there are three nonlinear, second order partial differential equations, uncoupled with the energy equation of the same characteristics. The only way to solve this system of equations is by choosing one of the available numerical solution methods, excluding any possibility, without further approximations to obtain a closed form analytical solution.

4.2 Finite Element Solution

A well-established numerical procedure, based on the finite element technique, is chosen to solve this problem. At first, this procedure is verified by solving the system of equations for the limit cases of (1) flow in porous, curved tube with large curvature ratio (r), which is similar to straight tube flow, and (2) curved tube flow without porous media. It is found that the results are in a very good agreement with established results. Then, the procedure is extended to solve the system of equations considering the effect of existing porous matrix in curved tube. This computer software is named, Flexible Partial Differential Equations Solution, abbreviated FlexPDE.

4.2.1 Check for convergence

The iterative procedure is terminated whenever the relative error for all dependent variables on each cell is less than a pre-adjusted value. This accuracy control criterion (ε) is defined as follows:

$$\frac{q^{k+1} - q^{k}}{q^{k+1}} < \varepsilon$$

where k+1 refers to the latest iteration. For the solution to be reliable, the procedure is examined if it converges by choosing a smaller convergence criterion (ε) or not. This is done by solving and getting a solution for a certain case using at first a convergence criterion $\varepsilon = 1x10^{-4}$, and then repeating the solution and checking for convergence using $\varepsilon = 5x10^{-5}$, until $\varepsilon = 1x10^{-5}$. The results are shown on Figures (4.1) and (4.2). The starting point of the horizontal axis (abscissa) represents the midpoint of the inner vertical channel side. It is clear from the Figures that the results coincide almost exactly.

The time required for the solution to converge using $\varepsilon = 1x10^{-5}$ is more than four times that required using $\varepsilon = 1x10^{-4}$. Therefore, all solutions reported in this work are considered to be satisfactory taking $\varepsilon = 1x10^{-4}$, since the solution is almost the same, and seeking for more accurate results will be , of course , at the expense of computer time.

4.2.2 Check on the solution

The simple and direct way to check the solution is by comparing the results with previous published ones. The solution to forced convection in a curved rectangular channel, equations (3.13) to (3.16), subjected to the boundary conditions described by Figure (3.2), using a high value for Darcy number, Da, which is the case for flow

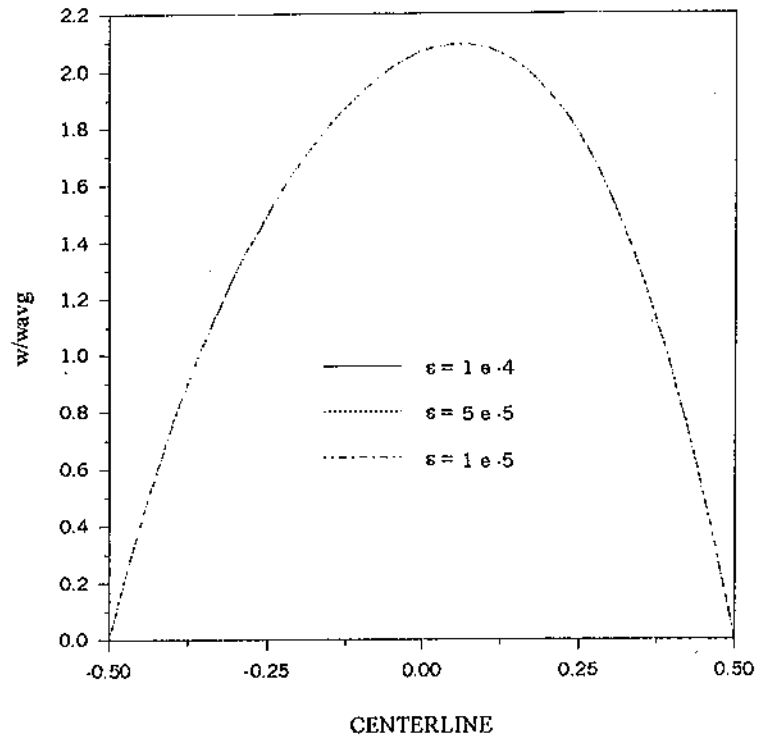

(a)

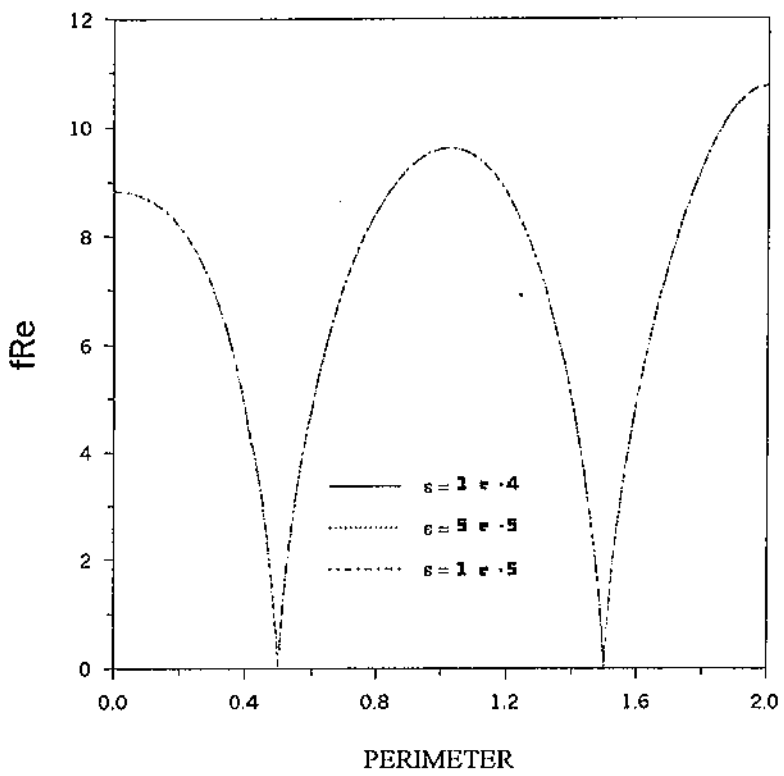

(b)

Figure (4.1) Effect of convergence criterion ε on (a) centerline velocity profile (b) local shear stress, De = 14, r = 100.

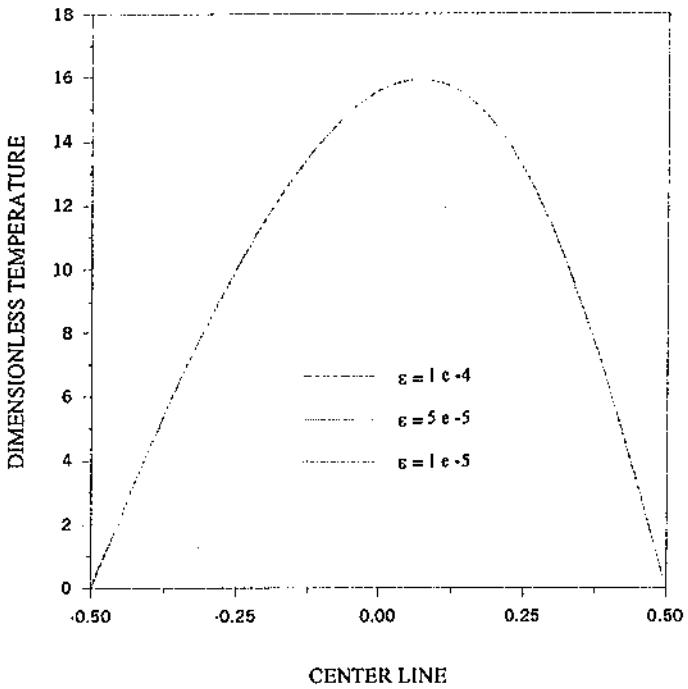

(a)

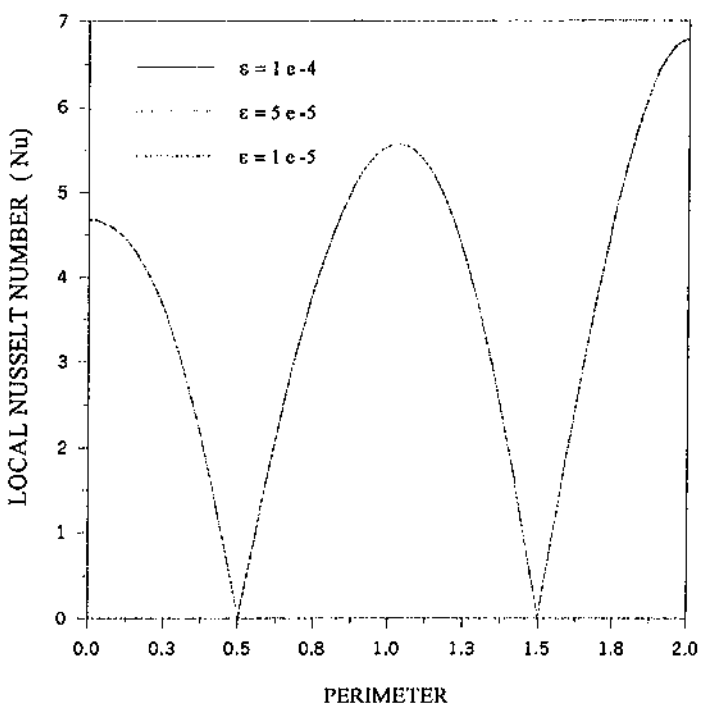

(b)

Figure (4.2) Effect of convergence criterion ε on (a) centerline temperature profile (b) local Nusselt number distribution De = 14, r = 100.

Table (4.1) A comparison between present work and previous work done by Cheng [1976], and Gyves et al. [1998] for different flow parameters without porous media.

-∂p/∂z	r	Re			De			$[(fRe)_o/(fRe)_s]_1$			$[(fRe)_o/(fRe)_s]_2$			$\overline{Nu}$	
		preset	Gyves et al.	Cheng et al.	present	Gyves et al.	Cheng et al.	present	Gyves et al.	Cheng et al.	present	Gyves et al.	Cheng et al.	presen	Gyves et al.
9000	100	290	297	295	29	29.7	29.5	1.087	-	1.06	1.087	1.07	1.07	4.286	4.15
19000	100	524	552	548	52.4	55.2	54.8	1.274	-	1.21	1.274	1.21	1.22	5.617	5.4
40000	100	981	1006	1000	98.1	100.6	100	1.432	-	1.42	1.434	1.38	1.41	6.875	6.9
70000	100	1545	1511	1511	154.5	151.1	151.1	1.596	-	1.67	1.592	1.63	1.63	8.125	-
110000	100	2187	2109	2026	218.7	210.9	202.6	1.766	-	2.18	1.767	1.83	1.91	-	-
60000	100	2909	-	2743	290.9	-	274.3	1.92	-	2.62	1.930	-	2.06	-	-
50000	10	873	-	831	276	-	262.7	1.956	-	2.56	2.013	-	2.11	-	-
80000	10	1259	-	1164	398.2	-	368.1	2.161	-	3.08	2.233	-	2.42	-	-
60000	4	892.3	-	824	446.2	-	411.9	2.217	-	3.09	2.430	-	2.55	-	-
11000	4	1293.7	-	1238	646.8	-	618.8	2.678	-	3.68	2.988	-	3.12	-	-

without porous media, is compared with curved channel solutions published by Cheng et al.(1976), and Gyves et al.(1998), summarized in Table (4.1). The expression (explained in the next chapter) for the product of friction factor and Reynolds number, fRe, is presented in two ways. The first, subscripted by 1 is by considering the velocity gradient along the wall, and the other subscripted by 2, is by considering the overall force balance for the differential axial length. It is clear that there is a good agreement between the present and previous results. It is also appreciable to note here that, the ratio of fRe calculated using both expressions shown in Table (4.1), is almost the same for the present solution, while the difference between the corresponding values obtained by Cheng is somewhat large, and it increases for small curvature ratios. This is another feature for the accuracy of the present results.

4.3 About FLexPDE

4.3.1 Definition

FLexPDE is a scripted finite element model builder and numerical solver. This means that a script written by the user, FLexPDE performs the operations necessary to turn a description of a partial differential equations system into a finite element model, solve the system, and present graphical output of the results. The scripting language allows the user to describe the mathematics of the partial differential equations system and the geometry of his problem domain in a format similar to the way he might describe it to a co-worker. For instance there is an EQUATIONS section in the script, in which Laplace's equation would be presented as Div(grad(N))= 0. Similarly, there is a BOUNDARIES section in the script, where the geometric boundaries of a two-dimensional problem domain are presented merely by walking a round the perimeter.

4.3.2 Scope of FLexPDE

1- FLEXPDE can solve systems of first or second partial differential equations in Cartesian or axi- symmetric two-dimensional geometry.

2- The system may be steady state or time dependent or alternatively, FLexPDE can solve eign value problems. Steady state and time dependent equations can be mixed in a single problem.

3- Any number of simultaneous equations can be solved subject to the limitations of the computer on which FLexPDE is run.

4- The equations can be linear or nonlinear. Nonlinear systems are solved by applying a modified Newton- Raphson iterative process.

5- Any number of regions of different material properties may be defined. Modeled variables are assumed to be continuous across material interfaces. Jump conditions on derivatives follow from the statement of the PDE system.

4.3.3 Main steps of FLexPDE solving

FLexPDE is a fully integrated PDE solver, combining several modules to provide a complete problem solving system.

1- A script-editing module provides a full text editing facility and a graphical domain preview.

2- A symbolic equation analyzer expands defined parameters and relations, perform spatial differentiation, and symbolically apply integration by parts to reduce second order terms to create symbolic Galerkein equations. It then differentiates these equations to term the Jacobian coupling matrix.

3- A mesh generation module controls a triangular finite element mesh over an arbitrary two-dimensional problem domain. In three-dimensional problems, the 2-D

mesh is extruded into a tetrahedral mesh covering an arbitrary number of nonplaner layers in the extrusion dimension.

4- A Finite Element numerical analysis module selects an appropriate solution scheme for steady state, time dependent or eigen-value problems, with separate procedures for linear and nonlinear system. Finite element basis may be either quadratic or cubic.

5- An error estimation procedure measures the adequacy of the mesh and refines the mesh whenever the error is large. The system iterates the mesh refinement and solution until user- defined error tolerance is achieved.

6- A graphical output module accepts arbitrary algebraic functions of the solution and plots contour, surface, vector or elevation plots.

7- A data export module can write reports in many formats, including simple tables, full finite element mesh data, CDF or Tecplot compatible.

$$f_V \, Re = \overline{\left(\frac{\partial w}{\partial n}\right)}\Big|_w \qquad (5.4)$$

where $\left(\frac{\partial w}{\partial n}\right)$ is the axial velocity gradient at the wall, and n is the dimensionless inward-drawn normal.

In addition to the boundary frictional drag, the fully developed flow through a porous duct experiences a bulk frictional drag induced by the solid matrix known as Darcy's pressure drop, and a flow inertia drag induced by the solid matrix, at high flow rate designated as Forchheimers form drag. The latter term is neglected since the flow inertia term in the momentum equation is not included. The bulk friction (Darcy) coefficient is defined as follows; Hwang and Chao (1992) :

$$f_D = \left(\frac{\mu_f \in}{K}\overline{W}\right)\left(\frac{D_h}{4}\right) / \left(\frac{1}{2}\rho_f \overline{W}^2\right) \qquad (5.5)$$

and;

$$f_D \, Re = \frac{1}{2} Da^{-1} \qquad (5.6)$$

c) Nusselt number , Nu : the local Nusselt number distribution is presented to show the strong effect of curved channel flow on heat transfer characteristics.

By definition the local Nusselt number is defined as follows:

$$Nu = \frac{h D_h}{k_f} = \frac{-\left(\frac{\partial t}{\partial n}\right)\Big|_w}{t_m} \qquad (5.7)$$

where h is the local heat transfer coefficient, k_f is the thermal conductivity of the fluid, and t_m is the dimensionless mean fluid bulk temperature defined in a manner similar to that outlined for $\overline{w}$ above, i.e.

$$t_m = \frac{\iint twdxdy}{\iint wdxdy} \tag{5.8}$$

The peripheral average Nusselt number, $\overline{Nu}$, can be obtained by integrating the local Nusselt number over the periphery of the channel cross-section.

$$\overline{Nu} = \frac{1}{p} \oint_p Nu \, d\ell \tag{5.9}$$

where p is the perimeter of the duct, and ℓ is the distance along the perimeter.

d) Darcy number, Da: it is defined as the ratio of the permeability of porous media to the square of the hydraulic diameter of the cross sectional area of the channel.

$$Da = \frac{K}{\in D_h^2} \tag{5.10}$$

5.2 The Effect of Curvature Ratio

It is useful to be noted that, by definition and to be in consistence with existing literature on curved ducts, small curvature ratio represents high curvature ducts, while large curvature ratio represents ducts of low curvature.

The results of laminar incompressible flow of viscous fluid in curved porous square ducts of curvature ratio, r = 5, 10, and 40, are shown in Figures, (5.1) through (5.10), for constant axial pressure gradient and same Darcy number.

At low Dean numbers, the axial velocity profile is essentially parabolic and unaltered from fully developed, straight tube laminar flow. Figure (5.1) shows the effect of curvature ratio on the axial centerline velocity profile. The velocity profile is plotted

as the velocity relative to the average velocity ($w/\overline{w}$), starting from the inner side of the tube to the outer side. As it is clear from the Figure, at higher Dean numbers, the velocity profile is no longer parabolic, and the maximum velocity is shifted outward, away from the vertical axis of the toroid due to the centrifugal force. Also it is noted that increasing the tube curvature (small curvature ratio), results in an increase in Dean number, and the maximum axial velocity is decreased. Although the value of Darcy number taken is 0.01, which means relatively high porosity, the maximum axial velocity is greatly affected, due to the presence of porous medium, i.e. $w/\overline{w}$ is decreased from 2(nonporous case) to about 1.4.

One of the most important results for engineering applications is the estimation of the friction factor for curved ducts. Figure (5.2) shows the results for the boundary viscous friction, $f_V Re$, along the periphery of the tube for r = 5, 10 and 40. It is obvios that the boundary friction increases with increasing curvature since the average velocity decreases for the same axial pressure gradient. The Darcy friction, $f_D Re$, for Da = 0.01 is calculated from equation (5.6) to be 50, which is considerably greater than the average boundary friction.

Curved channel flows are characterized by the development of a secondary cross-stream flow pattern consisting of two counter-rotating vortices. The effect of curvature ratio on secondary flow pattern in the form of stream function contours is shown in Figures (5.3), (5.4) and (5.5). At low Dean numbers a weak secondary flow pattern almost symmetrically located in the center of the tube half planes. It is well to note that the value of the stream function at the eye of the vortices represents the strength of the secondary flow. As the curvature is increased r = 10, Figure (5.4), accordingly an increase in Dean number causing an intensification of the secondary

flow, and the center of the secondary vortices move upward in the positive y-direction and inward in negative x-direction.

At still higher Dean numbers, Figure (5.5), the center of the secondary flow pattern is shifted more back toward x = 0, and furthermore upward. A transition from two vortices to four vortices flow pattern is observed by many researchers, Cheng et al. (1976), Thangam and Hur (1990) and Gyres et al. (1998). An additional counter-rotating pair of vortices appear near the central part of the outer wall, at a certain critical Dean number. Whereas the Dean number at which transition occurs is 202 reported by Cheng, it is 179, 151.1 obtained by Thangam and Gyves, respectively.

The appearance of these vortices was attributed to the unbalance between a pressure gradient inward and the centrifugal force. Since in the region near central outer wall, the pressure gradient across the channel in x-direction is positive, but the centrifugal force decreases from a maximum value to zero at the outer wall. Over the range of parameters concerned in the present work, no such secondary vortices are observed, although it sometimes appear temporarily at some stages of the solution progress.

The effect of curvature ratio on temperature contours (isotherms) for Pr = 1.0 is shown in Figures (5.6), (5.7) and (5.8). It can be seen that the curvature of the tube has a significant effect on temperature. As the curvature is increased from r = 40 to r = 5, the temperature is decreased and the location of maximum temperature is shifted slightly away toward the outer wall due to centrifugal force, this is clearly apparent from the temperature profile at the centerline of the tube, Figure (5.9). The local Nusselt number distribution along the periphery of the tube is shown in Figure (5.10). The results show that as the curvature increases from r = 40 to r = 5, the local Nusselt number increases almost always around the periphery of the tube wall.

5.3 The Effect of Darcy Number

The effect of decreasing Darcy number, Da = 0.008, 0.006 and 0.004, while keeping the curvature ratio at r = 10, and same axial pressure gradient is shown in Figures (5.11) through (5.20). Figure (5.11) shows the effect of Da on the fully developed centerline velocity profile. At Da = 0.008, the velocity profile is still has a point of maxima located away from the vertical axis of the toroid, due to the centrifugal force. As the Darcy number is decreased Da = 0.004, the Dean number decreased and the velocity profile is flattened due to the bulk damping caused by the presence of the porous matrix. But the boundary layer thickness is not the same at inner and outer walls of the tube, as it often appears in straight tube flow. This trend was reported by Hadim (1994) , Vafai and Kim (1989) and many others.

The effect of Darcy Number on stream function contours is readily apparent from Figures (5.13), (5.14) and (5.15). As Darcy number decreases the resistance of the porous matrix against the flow is increased, and therefore the main flow velocity is decreased, hence the secondary flow velocities decrease.

Once again, the situation is repeated here concerning the center of secondary flow pattern. As Darcy number decreases the Dean number decreases and the center of rotation of the secondary flow is moved to the right, toward the center of the tube plane, but still almost at the same horizontal line.

Figure (5.12) shows the effect of Darcy number on boundary friction. Although the Reynolds number is decreased from 1742 (De = 550) to 1062 (De = 336) as Darcy number is decreased from 0.008 to 0.004, a slight change is happened to boundary friction distribution and the average value of f_vRe is almost the same. Also it can be noted that the contribution of Darcy friction is very important as Darcy number is decreased and it becomes the dominant portion of total friction.

The effect of Darcy number on the centerline temperature profile is shown in Figure (5.16), and on temperature isotherms is shown in Figures (5.17), (5.18) and (5.19). It can be seen that, in contrast to velocity profile, as Darcy number decreases, the temperature profile does not change significantly by the introduction of the solid matrix. The results also show that the centerline temperature increases with increasing Darcy number. This trend was reported by Kariany (1985), Vafai and Kim (1989). The variation of Nusselt number with Darcy number is shown in Figure (5.20). It is noted that a considerable reduction in Nusselt number is observed as Darcy number is decreased. This can be attributed to the great reduction in the average axial velocity, due to higher resistance of porous matrix.

5.5 The Effect of Pressure Gradient

The fluid pressure field at any point is often considered to be the sum of a cross-stream average pressure, p(z), which is a function of the streamwise coordinate , and a pressure, $p'(x,y)$, which varies in the cross stream direction. As shown previously, the latter term is eliminated from the governing equations by cross differentiation. For fully developed flow the axial pressure gradient dp/dz is constant, which is the driving force of the flow.

The effect of axial pressure gradient on the flow and temperature fields is shown in Figures (5.21) to (5.28). Figure (5.21) shows the effect of pressure gradient on velocity profile for r = 5, and Da = 0.01. By increasing the pressure gradient, the down stream velocity profile is gradually distorted from a parapoloid, and the region of maximum axial velocity moves toward the outer wall. Unlike changing the curvature ratio or Darcy number, duplicating pressure gradient shifts the maximum velocity outward without any noticeable change in its magnitude.

The axial shear stress distribution with the variation of axial pressure drop is shown in Figure (5.22). It is obvious that more resistance against the flow accompanies the increase in axial pressure drop from the boundaries and porous matrix inserts.

As the pressure gradient is increased, the secondary flow patterns become more intense, and the center of secondary flow vortices move upward in the y-direction, and inward in the negative x-direction as shown in Figures (5.23), (5.4), and (5.24).

The dimensionless temperature, as defined before, represents the difference between the tube wall temperature and fluid temperature. The effect of increasing pressure gradient on temperature isotherms is shown in Figures (5.25), (5.7), and (5.26) for Da = 0.01, r = 5, and Pr = 1, and for $dp/dz = 0.1x10^6$, $0.15x10^6$, and $0.2x10^6$ respectively. These temperature cotours are very useful for visualizing the effects that various parameters have on temperature field. It is noted that increasing the pressure gradient results in an increase in the axial velocity, hence the temperature is increased, and the contours become more dense near the outer and upper right walls. Therefore the maximum temperature is shifted outward, and the temperature profile become steeper in those regions. This is illustrated in Figure (5.27).

Concerning the local Nusselt number distribution, it is noted that increasing the pressure gradient, a considerable increase in Nusselt number is obtained as shown in Figure (5.28). These results compared well with curved channel local Nusselt profiles without porous media, reported by Gyves et al.(1998).

5.4 The Effect of Prandtl Number

Prandtl number is basically defined as the ratio of kinematic viscosity to the thermal diffusivity of a fluid. For Pr = 1, heat and momentum diffuse through the fluid at the same rates, this implies that both the temperature and velocity profiles develop

together. If Pr >1, the velocity profile develops faster than temperature profile, while for Pr < 1 the opposite happens, i.e. the temperature profile leads the velocity profile.

In curved tube flows, the heat transfer characteristics are greatly affected by Prandtl number. This is due to the induced secondary flow pattern. For high Prandtl number, convection dominates over conduction and heat will be carried over by convection from the tube wall to the core of the tube cross-section, and due to centrifugal forces, the temperature profile is shifted toward the outer wall. But for low Prandtl number the conduction dominates over convection and the temperature profile approaches the parabolic shape.

The effect of Prandtl number on temperature isotherms, centerline temperature profile and local Nusselt number distribution is shown in Figures (5.29) to (5.33). By increasing Prandtl number from Pr = 0.05, Figure (5.29), the temperature isotherms deviate from the symmetrical shape with only one maximum located at the centerline to the double maxima above and below the centerline at Pr = 5, Figure (5.31).

The effect of Prandtl number on temperature profile is shown in Figure (5.32). It is clear from the Figure how much the temperature profile is affected by increasing Prandtl number from 0.005 to 1. It is also noted that the maximum temperature is shifted outward from vertical axis by increasing Prandtl number for the same Dean number. The secondary flow present in curved tube cause a marked variation in heat transfer rate around the periphery. This may be advantageous in instances when only a portion of the peripheral boundary is available for energy transport. Figure (5.33) shows the local Nusselt number distribution. It is noted that increasing Prandtl number has a strong effect on Nusselt number.

5.6 The Effect of Dean Number

Of fundamental interest to the development of a complete understanding of viscous flow phenomena in curved tubes is the nature of the velocity and pressure distributions in the fully developed flow region. Previous studies indicate that these profiles have been found to depend strongly on the Dean number. This parameter which characterizes curved tube flow is the ratio of centrifugal forces to viscous forces.

Figure (5.34) shows the effect of Dean number on he ave age Nusselt number, $\overline{Nu}$, at Pr = 1. A wide range of Darcy number is investigated to cover the situations of high porous media, Da = 1, and low porous media, Da = $1x10^{-6}$. The results show that for high porous media, Da = 1, the average Nusselt number is strongly affected by increasing Dean number. It is clear from the Figure that De = 0 corresponds to straight tube solution, where $\overline{Nu}$ = 3.6 is slightly lower than $\overline{Nu}$ = 3.62, the non-porous straight tube solution. As Darcy number is decreased to 0.01, a slight change in $\overline{Nu}$ from straight tube solution until De = 50, but still strongly effected by increasing Dean number. At Da = 0.001, the average Nusselt number is weakly affected by increasing Dean number up to about De = 200, beyond which it starts to increase. A further decrease in Darcy number to $1x10^{-6}$, results in a small increase in $\overline{Nu}$, but has no effect at all with increasing Dean number. The results are compared with tabulated porous straight tube results reported by Hwang and Chao (1992), and a very good agreement is observed.

The ratio of average curved tube Nusselt number to straight tube average Nusselt number ($\overline{Nu}_c / \overline{Nu}_s$) is calculated, and the results are plotted in Figure (5.35). Compared with that for straight tube, the curved tube average Nusselt number is increased dramatically, especially for high porous media, Da = 1. It is interesting to note that for all different Darcy number curves the Nusselt number ratio goes to unity as

Darcy number goes to zero, and for Da≤ $1x10^{-4}$, $\overline{Nu_c}/\overline{Nu_s}$ is unity regardless of Dean number variation.

The effect of Dean Number on boundary viscous friction for Da = $1x10^{-6}$ to 1 is shown in Figure (5.36). It can be noted from the Figure that increasing Dean number has a strong effect on the product of friction factor and Re4ynolds number, for Da = 1. As Darcy number is decreased, Da = 0.1, a slight increase in fRe over Da = 1 curve up to De = 200, then the two curves continue at the same trend. As Darcy number is decreased to 0.01, a considerable increase in fRe is observed at low Dean numbers, then the difference starts to diminish beyond De = 400, approximately. After Darcy number Da = 0.001, no change in the product fRe is observed even at low Dean numbers, and the product fRe is found to be 68, 190, 632 and 1938 for Da = 0.001, $1x10^{-4}$, $1x10^{-5}$ and $1x10^{-6}$, respectively. These results are compared for the limit case as Dean number approaches zero with straight tube results, obtained by Hwang and Chao (1992) and a good agreement is observed.

The Darcy friction, f_DRe, due to the solid matrix is relatively small compared to viscous friction for Da = 0.1 and above, while for low Darcy numbers it is very much greater than f_vRe. For example, at Da = $1x10^{-6}$, f_DRe is as high as 250 f_vRe, since at this low value of Darcy number the flow becomes uniform across the tube due to high resistance from the porous matrix.

The product f_vRe in curved square duct is compared to that in straight tube for Darcy numbers from $1x10^{-6}$ to 1. The ratio $(f\text{Re})_c/(f\text{Re})_s$ is plotted against Dean number as shown in Figure (5.37). It is noted that this ratio is decreased by decreasing Darcy number until Da = 0.001. For Da ≤ 0.001 the ratio $(f\text{Re})_c/(f\text{Re})_s$ is constant and equals to 1. The friction factor ratio at Da = 1 which somewhat represent the case of

high porous media is compared well with the results reported by Thangam and Hur (1990).

The heat transfer performance in curved tubes is superior to that in straight tubes. This is due to the mixing effect caused by the secondary flow. The influence of secondary flow in the heat transfer becomes more apparent at high Prandtl numbers.

The effect of Dean number on the average Nusselt number, for Da = 0.01 and for Pr = 0.05, 0.5, 1 and 5, is shown in Figure (5.38). It is noted that $\overline{Nu}$ is strongly affected by increasing Dean number at Pr = 5, where as at Pr = 0.05, a slight increase in $\overline{Nu}$ is observed even at higher Dean numbers, because convection effects in the cross stream direction are very small.

To clarify the superiority of heat transfer in curve tubes over straight tubes, the variation of $\overline{Nu}_c / \overline{Nu}_s$ is calculated and plotted against Dean number for different Prandtl numbers, these results are shown in Figure (5.39). It is noted that the average Nusselt number reaches about 5 times the straight tube average Nusselt number for Pr = 5.

It is useful to note the effect of Dean number on $\overline{Nu}$ for Pr = 0.7, 1 and 5 as Darcy number is decreased to 0.001. The results show that increasing Prandtl number has a weak effect on $\overline{Nu}$ up to about De = 200, except for Pr = 5, Figure (5.40) illustrates this trend.

An interesting comparison is made to emphasize the effect of Darcy number on $\overline{Nu}$ for Pr = 1 and 5. Figure (5.41) shows the simultaneous effects of Prandtl number and Darcy number on the average Nusselt number as Dean number is increased from zero to 800. The ratio of average Nusselt numbers of curved to straight channels ($\overline{Nu}_c / \overline{Nu}_s$) for Da = 0.01, 0.001 and Pr = 1, 5 is shown in Figure (5.42).

5.7 Correlation Equations

Based on the graphical results obtained in this work, it is useful to combine the effects of Dean number, Prandtl number and Darcy number on the average Nusselt number and friction factor into a correlation equations using the least squares method for the aspect ratio $\lambda = 1$.

1. Average Nusselt number, $\overline{Nu}$:

The correlation equation for $\overline{Nu}$ is found to depend on De, Pr and Da, two correlation equations are obtained depending on the value of Dean number;

For De < 100

$$\overline{Nu} = 3.628 + 0.021De + 0.467Pr - 0.303Da \qquad (5.10)$$

For De > 100

$$\overline{Nu} = 1.335De^{0.388}\, Pr^{0.225}\, Da^{0.0564} \qquad (5.11)$$

2. Friction factor ratio, $(f\mathrm{Re})_c/(f\mathrm{Re})_s$:

The boundary viscous friction ratio is correlated to cover two ranges of Darcy number. For Da $\geq$ 0.01 it is noted that friction factor is increased by increasing Darcy , but for Da $\leq$ 0.001 is independent of Darcy number

For Da $\geq$ 0.01

$$\frac{f_c}{f_s} = 0.712\ De^{0.173}\, Da^{0.097} \qquad (5.12)$$

For Da $\leq$ 0.001

$$\frac{f_c}{f_s} = 1 \qquad (5.13)$$

5.8 The Effect of Aspect Ratio

Curved rectangular channel fluid flow and heat transfer is encountered in many engineering problems of practical interest. So far the aspect ratio considered is $\lambda = 1$, which corresponds to square cross section channel . Aspect ratios other than $\lambda = 1$ are widely investigated, Cheng et al. (1976), Thangam et al. (1990), and Gyves et al. (2000). Previous results show that curved rectangular channels exhibit more stable secondary cross stream flow patterns than do square channels at equal values of De.

In the present study, nonporous curved channel flow solutions are obtained for $\lambda = 1/3, 0.5, 2$, and 5. These results show a good agreement with that obtained by Cheng et al. (1976), and Gyves et al. (2000), Tables (5.1) to (5.5). It is noted that the average Nusselt number is increased by decreasing the aspect ratio, but the trend is reversed for the average Nusselt number ratio, i.e., as λ decreases the $\overline{Nu}_c / \overline{Nu}_s$ is decreased. The effect of aspect ratio on the average Nusselt number in porous media, for $\lambda = 1, 1/2, 1/3$ and 1/4, Da = 0.01 and Pr = 1 is shown in Figure (5.43). It is noted that decreasing the aspect ratio with porous matrix present, has no significant effect on the average Nusselt number as Dean number increases, except for low Dean numbers. Solutions for $\lambda \leq 1/4$ and De > 200 are not stable, therefore the results are not reported.

Table (5.1) Non porous curved channel heat transfer solution ($\lambda = 1/3$, Pr = 1, r = 100).

-dp/dz	De		$\overline{Nu}$		$\overline{Nu}_c/\overline{Nu}_s$	
	Present	Gyves et al. (2000)	Present	Gyves et al. (2000)	Present	Gyves et al. (2000)
5000	14.62	14.72	4.800	4.812	1.00	1.001
8000	23.32	23.49	4.838	4.846	1.008	1.008
10000	29.03	29.24	4.899	4.903	1.02	1.02
14000	39.92	40.25	5.089	5.110	1.061	1.063
20000	54.51	55.17	5.565	5.576	1.16	1.16
30000	75.07	76.71	6.422	6.492	1.342	1.35
40000	93.42	96.01	7.170	7.280	1.495	1.514
50000	110.84	114.09	7.750	7.895	1.642	1.615

Table (5.2) Non porous curved channel flow field solution ($\lambda = 0.5$).

-dp/dz	r	De			$(fRe)_c/(fRe)_s$		
		Present	Cheng et al. (1976)	Gyves et al. (2000)	Present	Cheng et al. (1976)	Gyves et al. (2000)
5000	100	16.0	16.0	16.1	1.003	1.01	1.003
10000	100	31.1	31.1	31.3	1.03	1.04	1.03
26000	100	67.1	68.1	69.3	1.24	1.24	1.22
50000	100	111.7	112.6	115.5	1.44	1.44	1.42
90000	100	178.6	176.6	183.4	1.62	1.65	1.59
11000	100	209.7	200.7	-	1.68	1.77	-
90000	30	280.9	262.0	-	1.88	2.0	-
110000	30	325	312.7	-	1.96	-	-

Table (5.3) Non porous curved channel heat transfer solution ($\lambda = 0.5$, Pr = 1).

-dp/dz	r	De		$\overline{Nu}$		$\overline{Nu}_c/\overline{Nu}_s$	
		Present	Gyves et al. (2000)	Present	Gyves et al. (2000)	Present	Gyves et al. (2000)
5000	100	16.0	16.1	4.15	4.17	1.006	1.01
10000	100	31.1	31.3	4.44	4.46	1.08	1.08
26000	100	67.1	69.1	6.18	6.15	1.5	1.49
50000	100	111.7	115.5	7.66	7.67	1.85	1.85
90000	100	178.6	183.4	9.1	9.34	1.22	2.26
11000	100	209.7	-	9.66	-	-	-
90000	30	280.9	-	10.86	-	-	-
110000	30	325	-	11.64	-	-	-

Table (5.4) Nonporous curved channel flow and heat transfer solution ($\lambda = 2$, Pr = 1).

-dp/dz	r	De		$(f_c/f_s)_1$		$(f_c/f_s)_2$		$\overline{Nu}$
		present	Cheng et al. (1976)	present	Cheng et al. (1976)	present	Cheng et al. (1976)	present
5000	100	15.9	15.9	1.01	1.0	1.01	1.01	4.225
10000	100	29.9	31.5	1.07	1.02	1.07	1.03	4.77
26000	100	69.7	72.2	1.20	1.16	1.20	1.17	5.94
40000	100	101.5	103.5	1.27	1.25	1.27	1.25	6.58
60000	100	144.5	143.8	1.34	1.36	1.33	1.35	7.18
90000	100	189.3	197.3	1.53	1.52	1.53	1.48	8.55
80000	30	279	278.6	1.67	1.81	1.68	1.70	9.73

Table (5.5) Nonporous curved channel flow and heat transfer solution ($\lambda = 5$, Pr = 1).

-dp/dz	r	De		$(f_c/f_s)_1$		$(f_c/f_s)_2$		$\overline{Nu}$
		present	Cheng et al. (1976)	present	Cheng et al. (1976)	present	Cheng et al. (1976)	present
8000	100	20.9	20.8	1.00	1.00	1.00	1.00	5.80
14000	100	36.0	36.0	1.02	1.00	1.02	1.02	5.98
30000	100	74.4	76.9	1.06	1.02	1.06	1.02	6.52
50000	100	119.8	123.1	1.09	1.06	1.09	1.07	6.96
80000	100	184.1	171.8	1.14	1.28	1.14	1.22	7.37
80000	30	312.5	281.8	1.22	1.55	1.22	1.36	8.13

6. CONCLUSIONS

The fully developed laminar flow and heat transfer in curved rectangular porous channels is approached numerically using finite element method. The effects of Dean number, Darcy number, Prandtl number and aspect ratio of the tube on the field and heat transfer characteristics are investigated.

The numerical results show that, Darcy number less than or equal to $1x10^{-4}$ has no effect at all on the average Nusselt number and boundary viscous friction for any Dean number. On the other hand, for Darcy number less than or equal to 0.001, the frictional drag due to the presence of solid matrix is dominated and increases markedly as Darcy number decreases.

It is found that heat transfer in curved rectangular channels is superior to that in straight channels at higher Dean numbers and Prandtl numbers. This is due to the better mixing resulting from the presence of secondary flow vortices in the cross-stream flow.

A comparison with available published theoretical results for the limit cases of porous channels with high curvature ratio, and nonporous curved channels indicates a good agreement. The effect of channel aspect ratio is also studied. The results show that decreasing the aspect ratio in porous rectangular channels has less effect on the average Nusselt number. Correlation equations for the average Nusselt number and friction factor ratios are also developed.

7. RECOMMENDATIONS

This study can be extended to cover more engineering applications. Therefore it is recommended that the following cases can be taken into account:

1- Laminar flow and heat transfer in rectangular curved tubes taking into consideration the variable porosity especially near the boundaries, which results in the channeling effect.

2- Laminar flow and heat transfer in curved tubes of circular cross section with porous media.

3- Laminar flow and heat transfer in curved tubes of circular and rectangular cross section with variable fluid properties such as density.

4- Laminar flow and heat transfer in curved tubes partially filled with porous media.

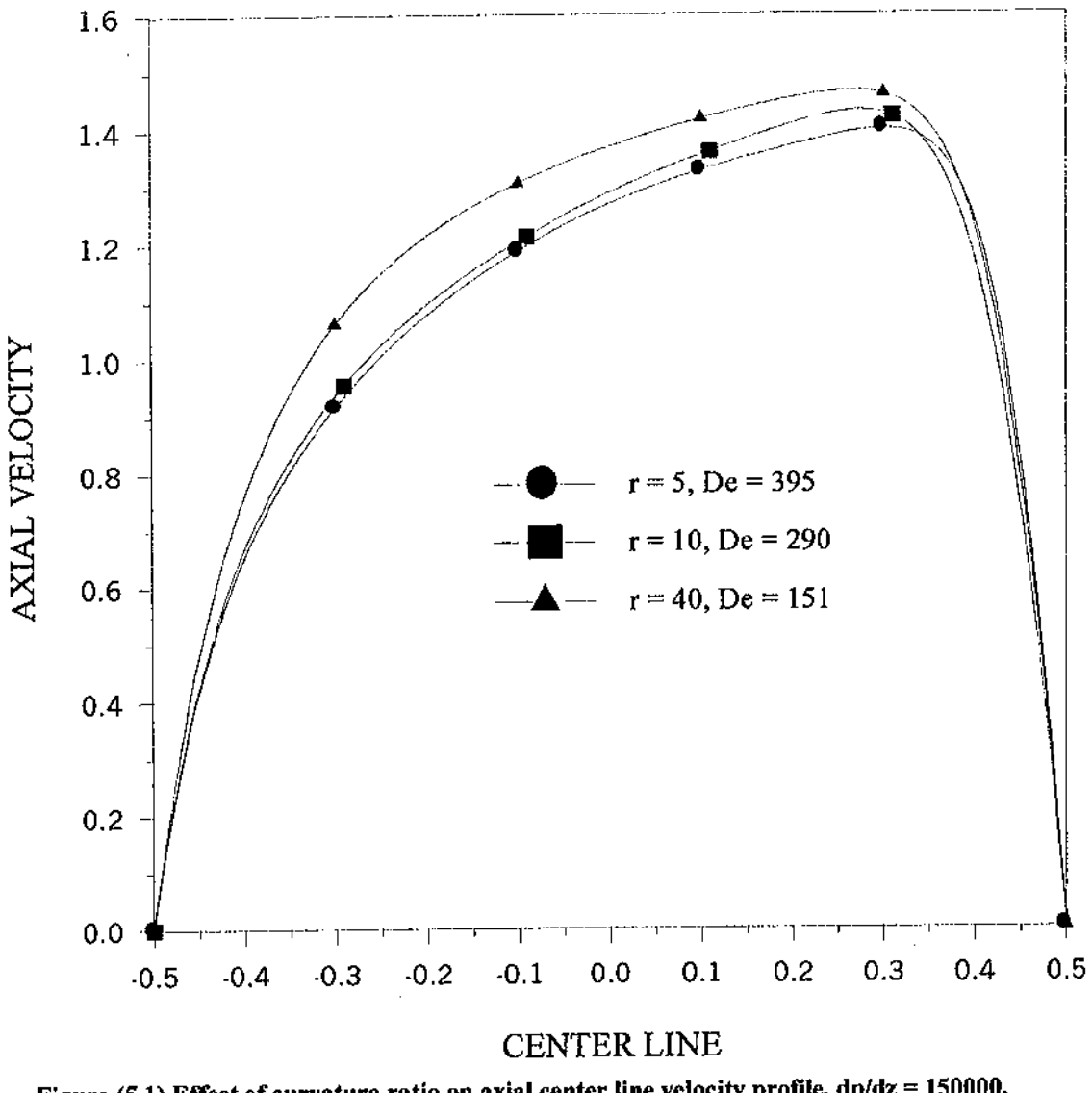

Figure (5.1) Effect of curvature ratio on axial center line velocity profile, dp/dz = 150000, Da = 0.01.

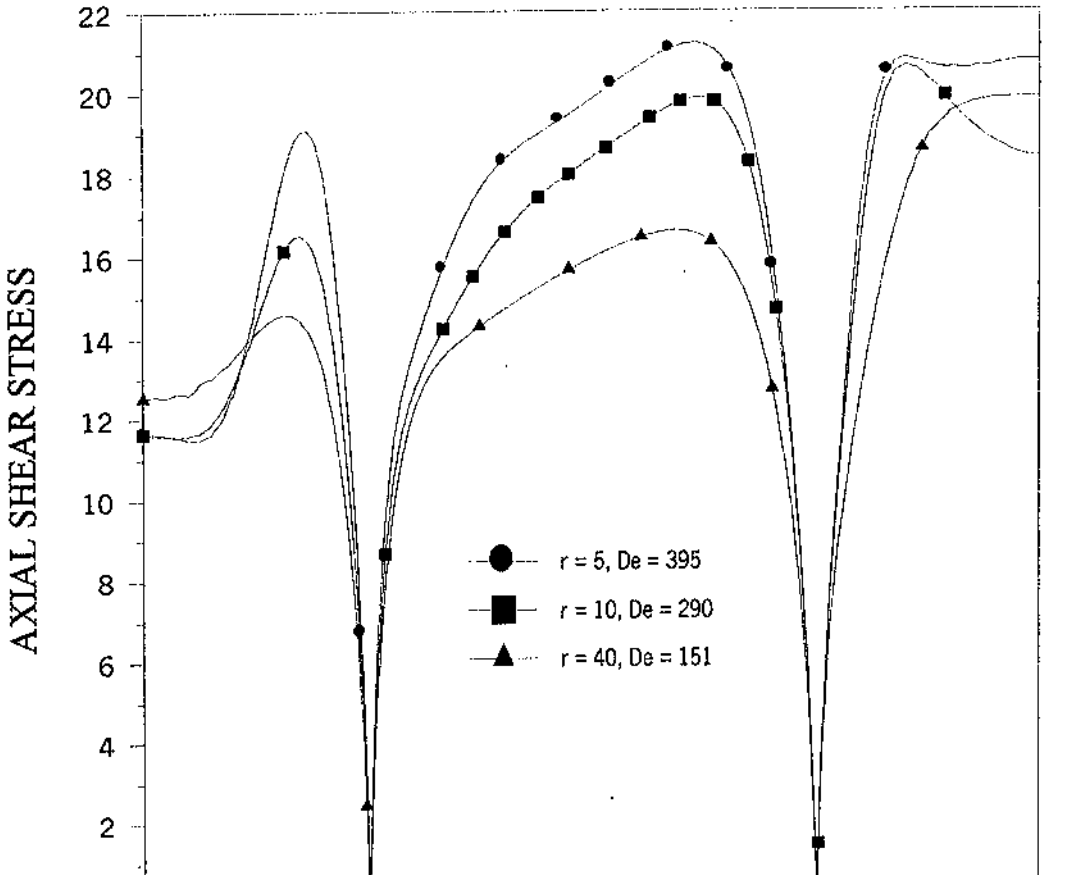

Figure (5.2) Effect of curvature ratio on axial shear stress, dp/dz = 150000, Da = 0.01.

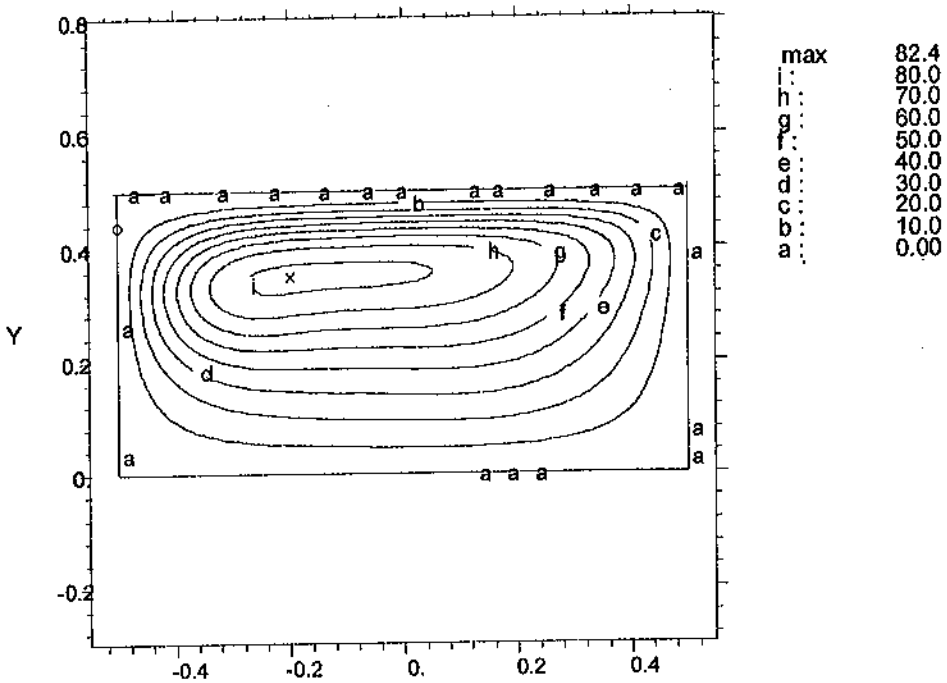

Figure (5.3) Stream function contours (secondary flow), Da = 0.01, De = 395, r = 5.

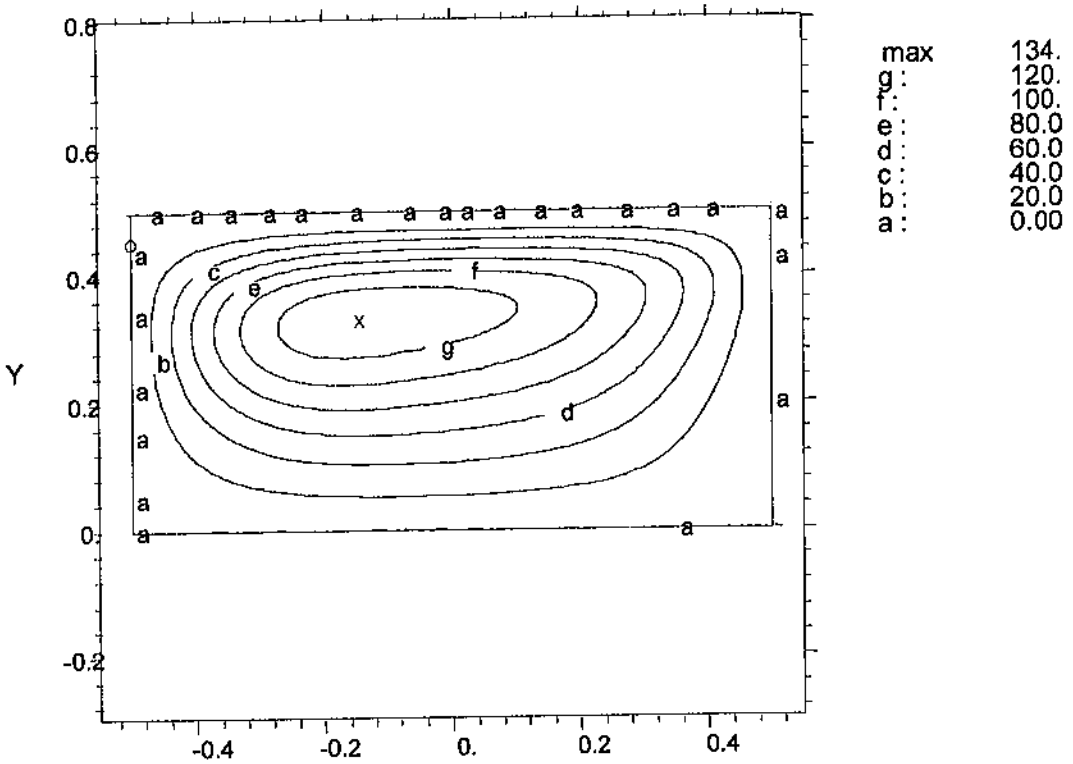

Figure (5.4) Stream function contours (secondary flow), Da = 0.01, De = 291, r = 10.

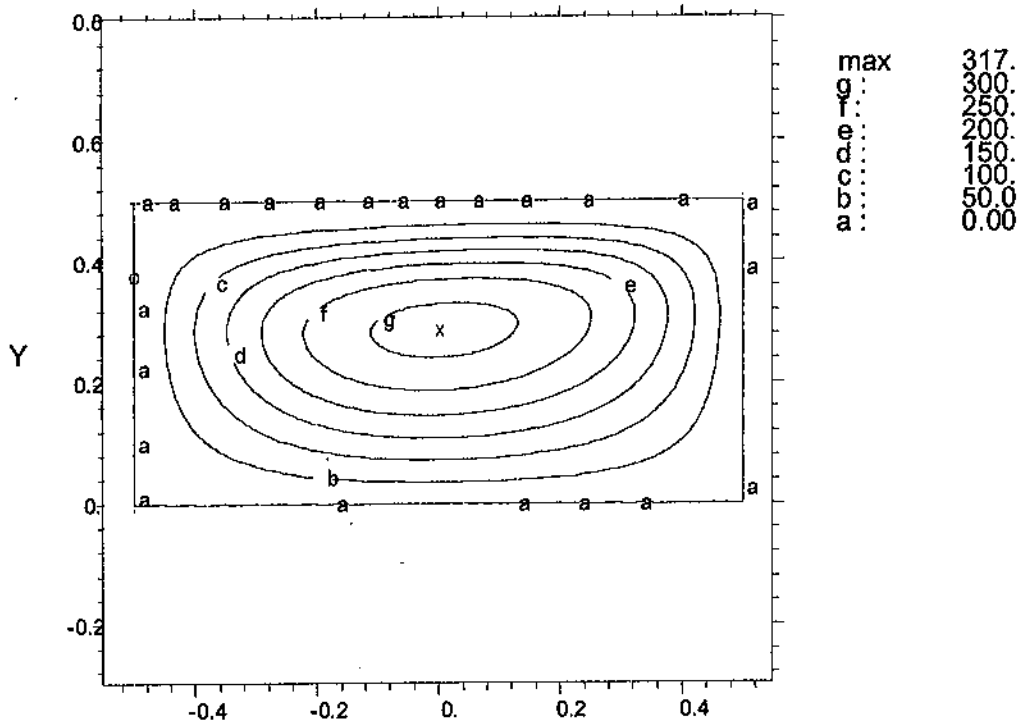

Figure (5.5) Stream function contours (secondary flow), Da = 0.01 , De = 151 , r = 40.

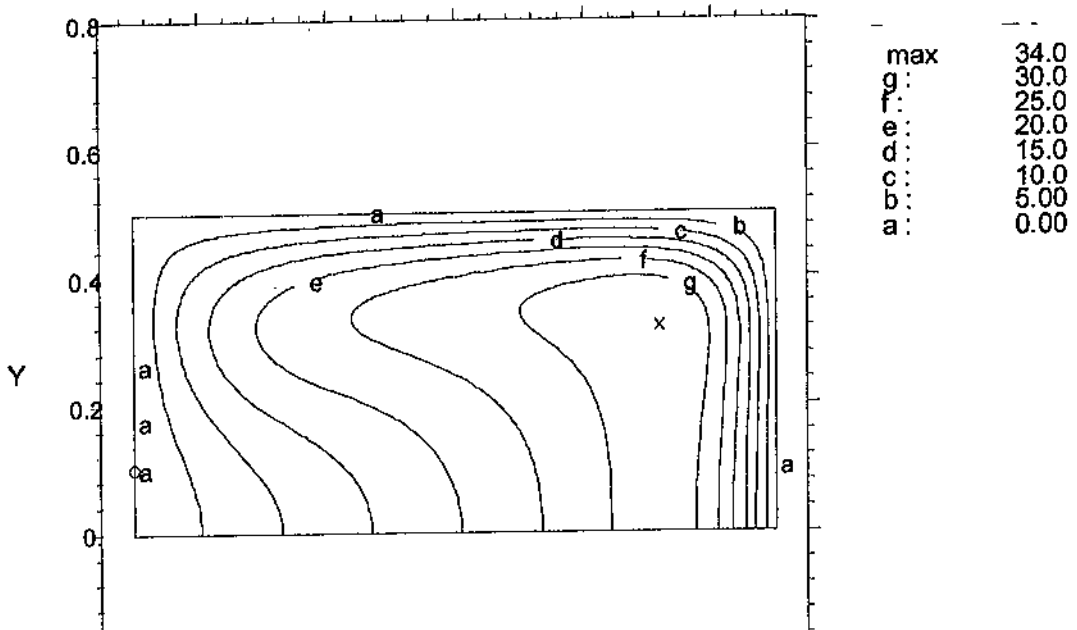

Figure (5.6) Temperature contours, dp/dz = 150000, Da = 0.01, De = 291, r = 10.

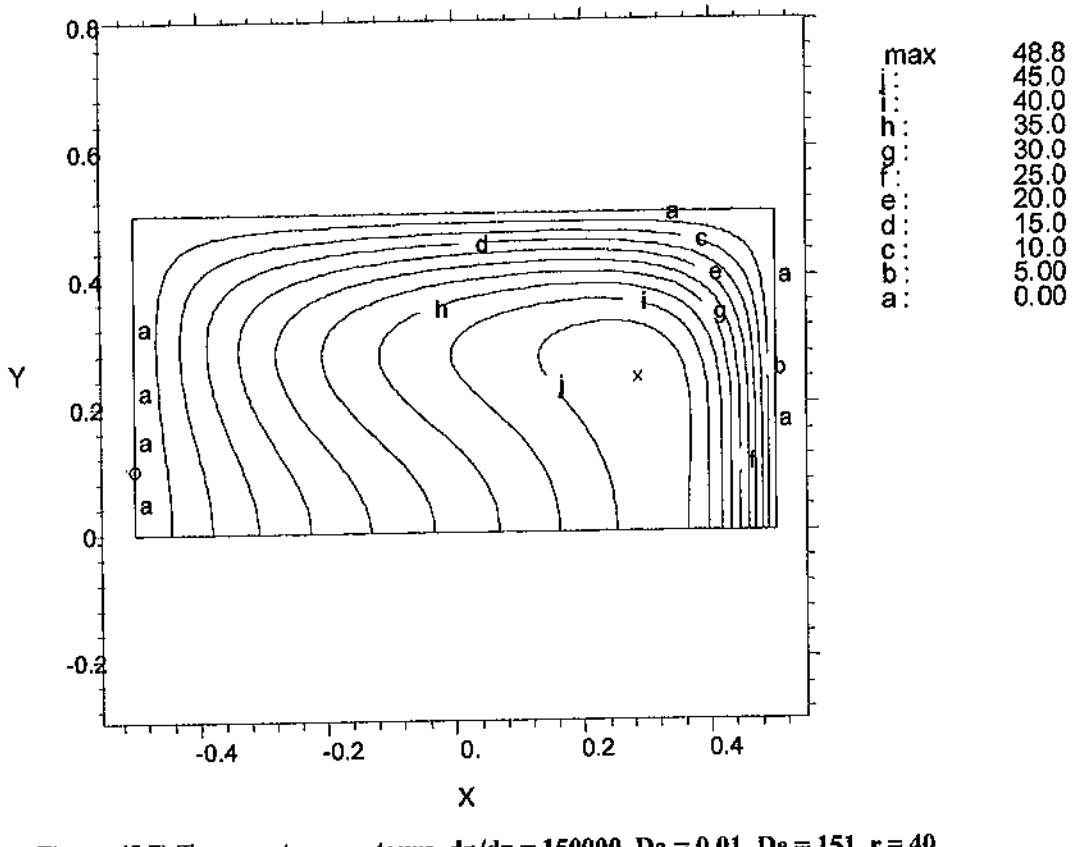

Figure (5.7) Temperature contours, dp/dz = 150000, Da = 0.01, De = 151, r = 40.

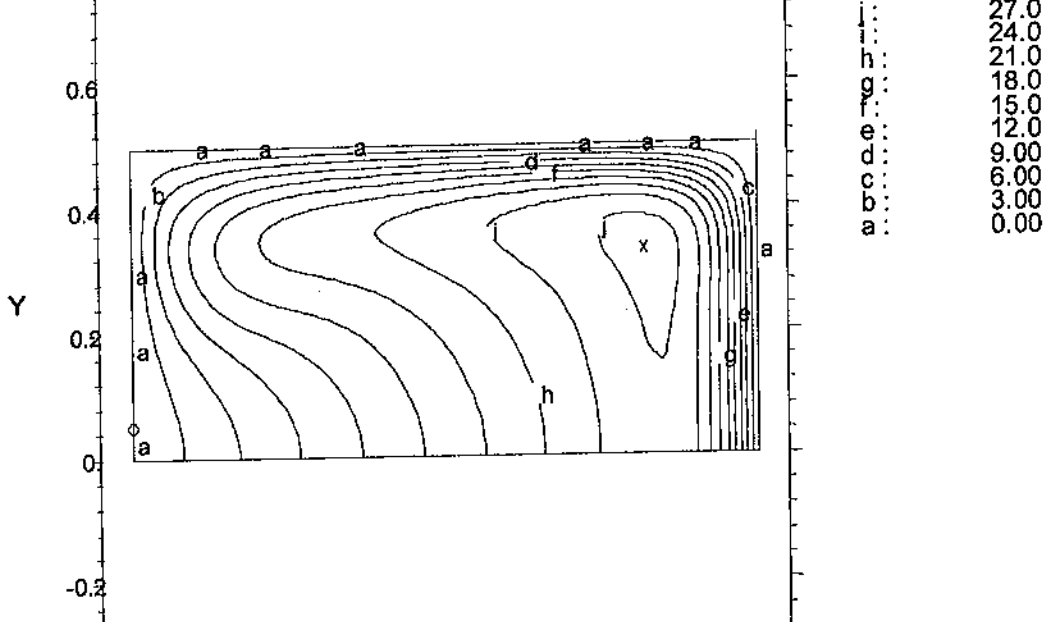

Figure (5.8) Temperature contours, dp/dz = 150000, De = 394, Pr = 1, r = 5.

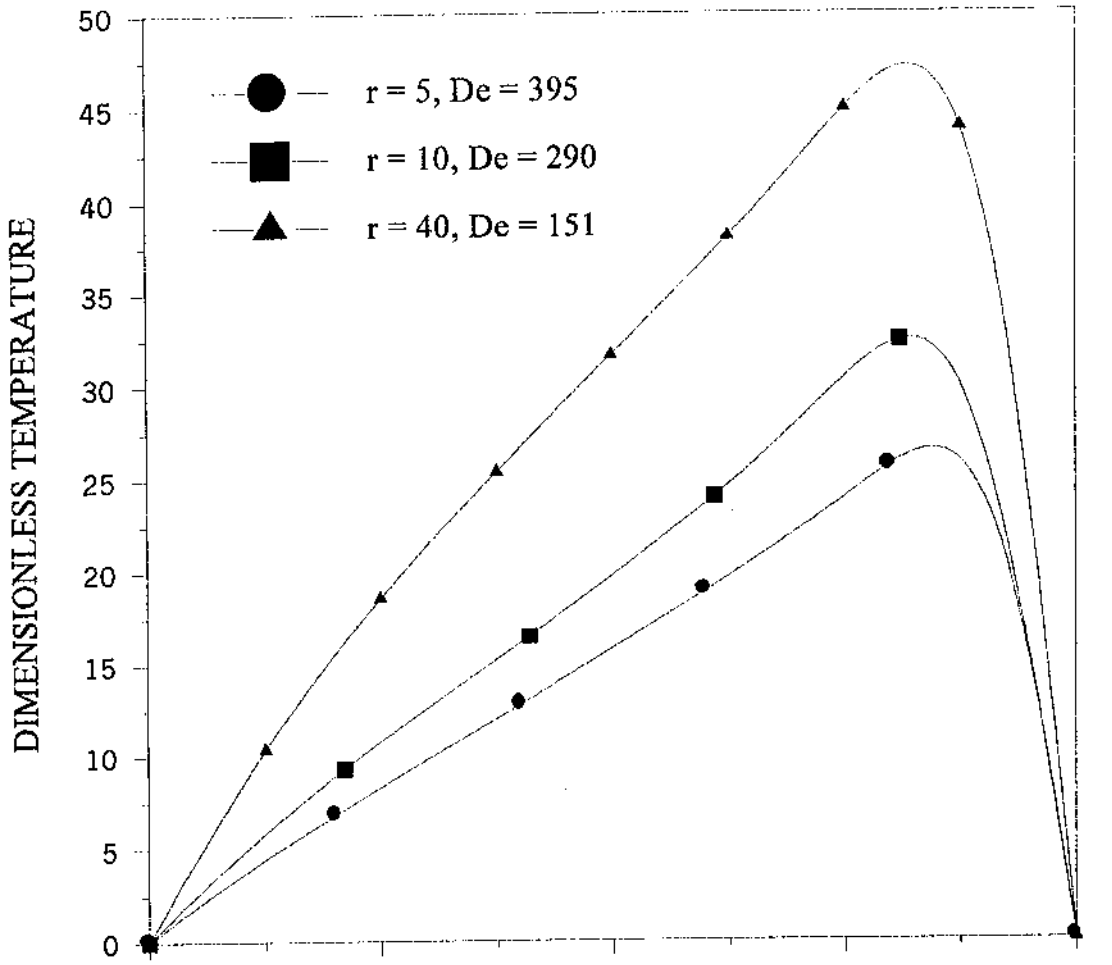

Figure (5. 9) Effect of curvature ratio on centerline temperature profile, dp/dz = 150000, Da = 0.01, Pr = 1.

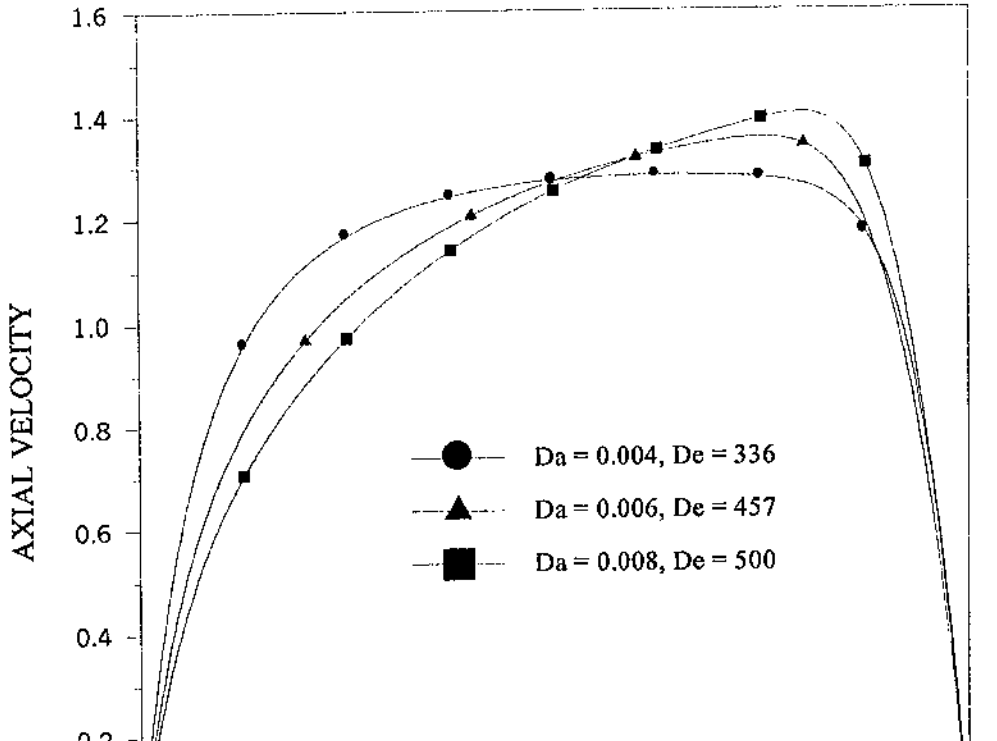

Figure (5.11) Effect of Darcy number on centerline axial velocity , dp/dz = 350000, r = 10.

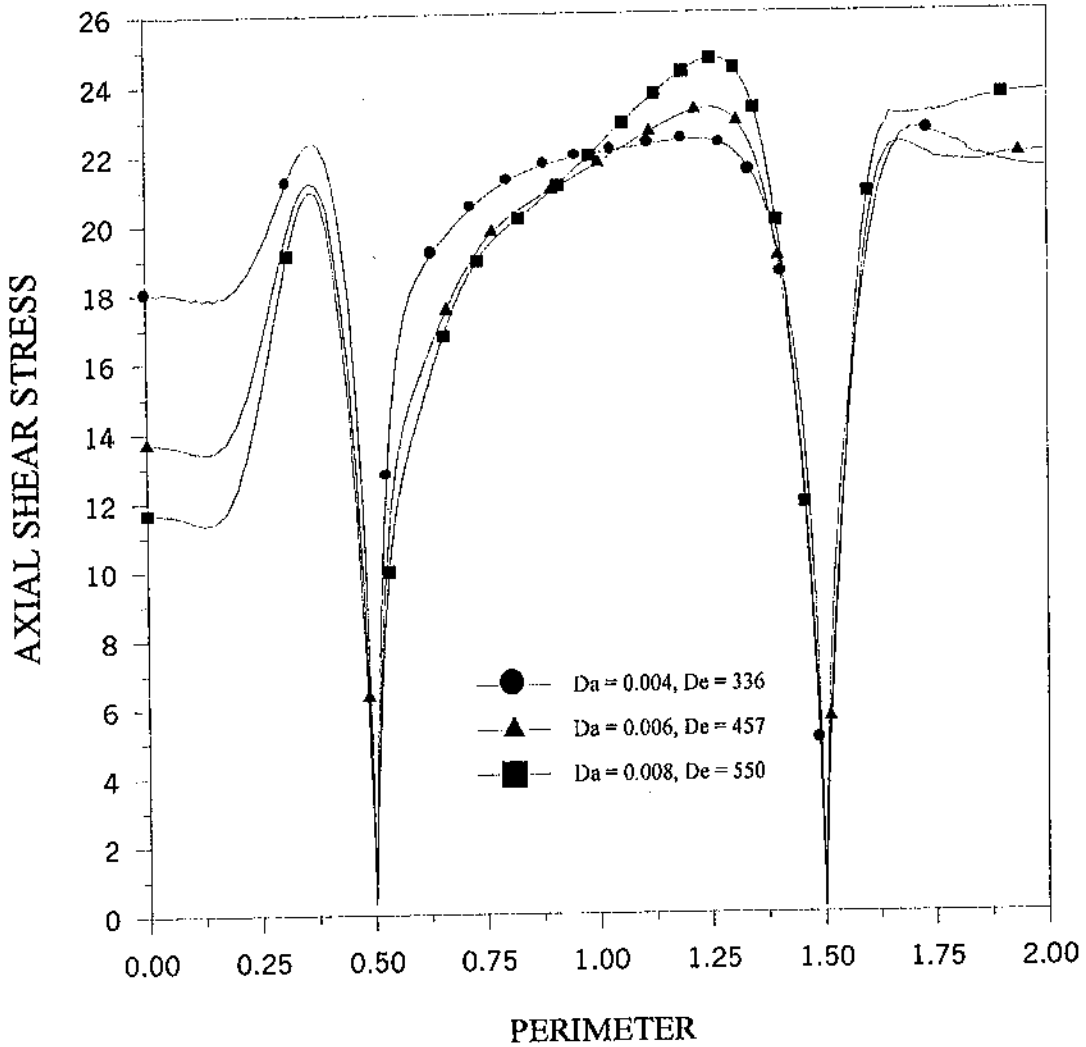

Figure (5.12) Effect of Darcy number on axial shear stress, dp/dz = 350000, r = 10.

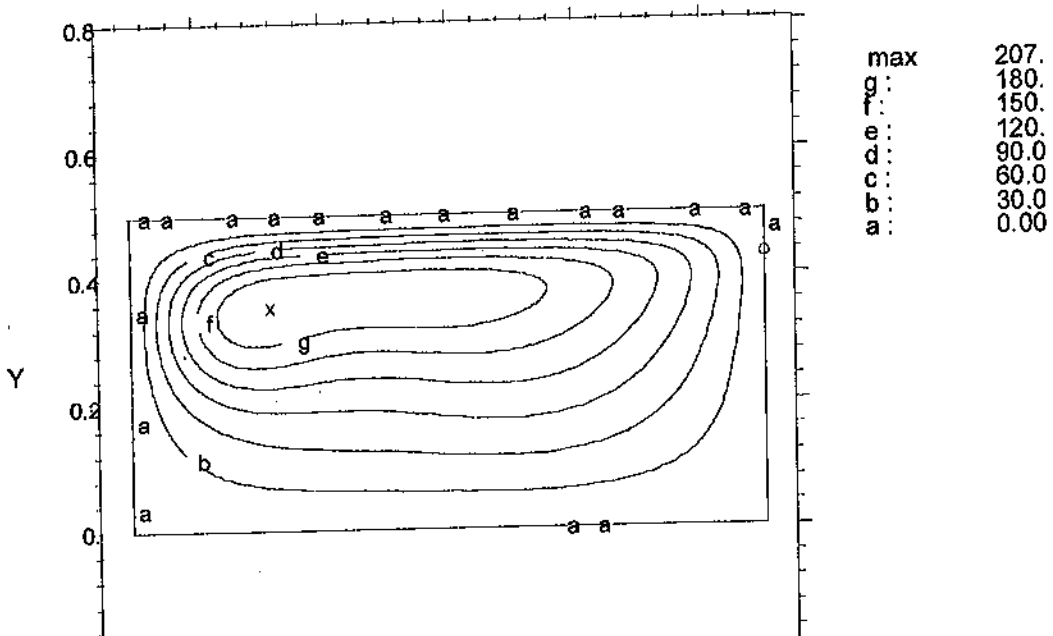

Figure (5.13) Stream function contours (secondary flow), dp/dz = 350000, Da = 0.008, De = 550, r = 10.

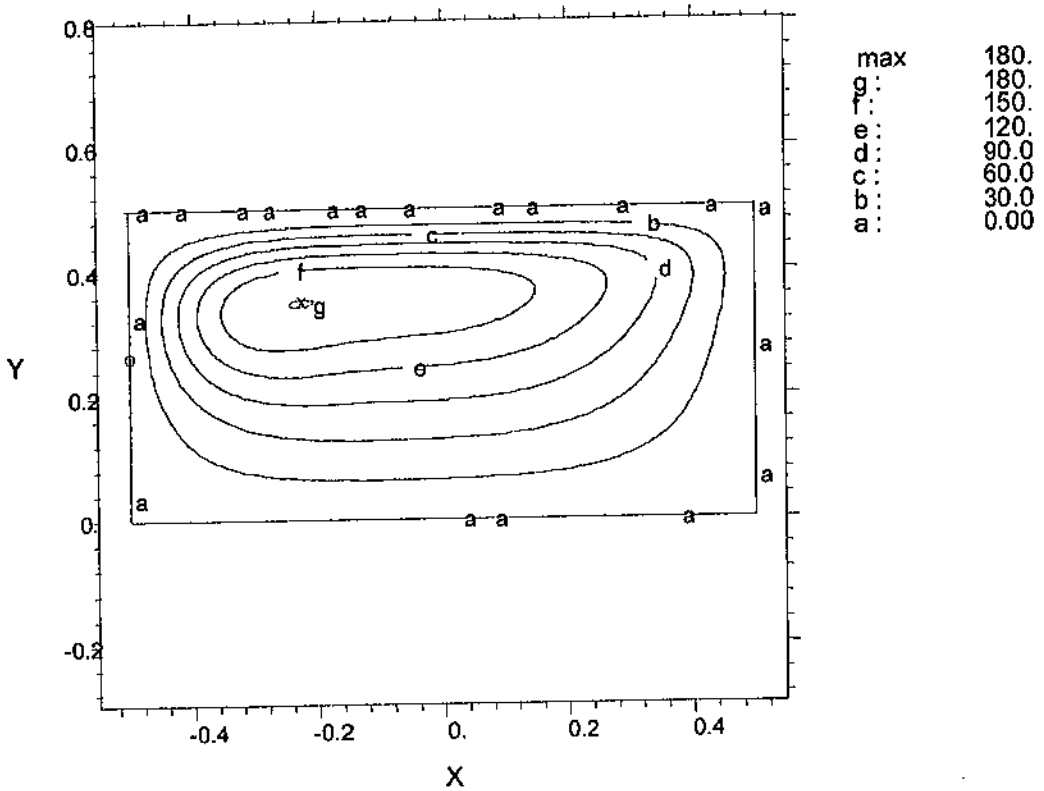

Figure (5.14) Stream function contours (secondary flow), Da = 0.006, De = 457, r = 10.

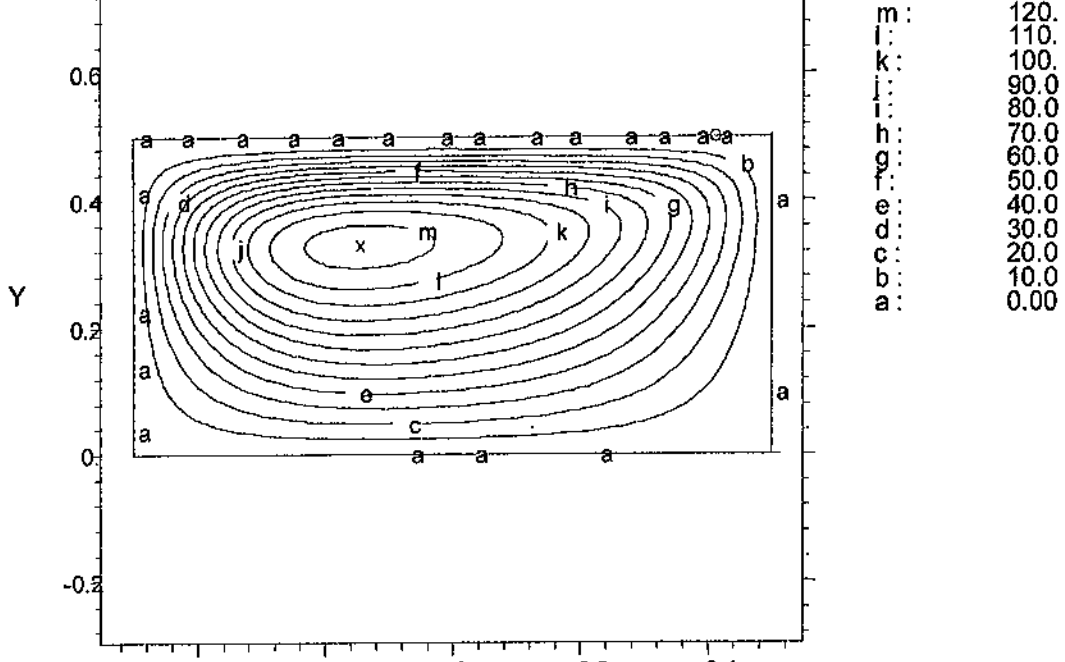

Figure (5.15) Stream function contours (secondary flow), dp/dz = 350000, Da = 0.004, De = 336, r = 10.

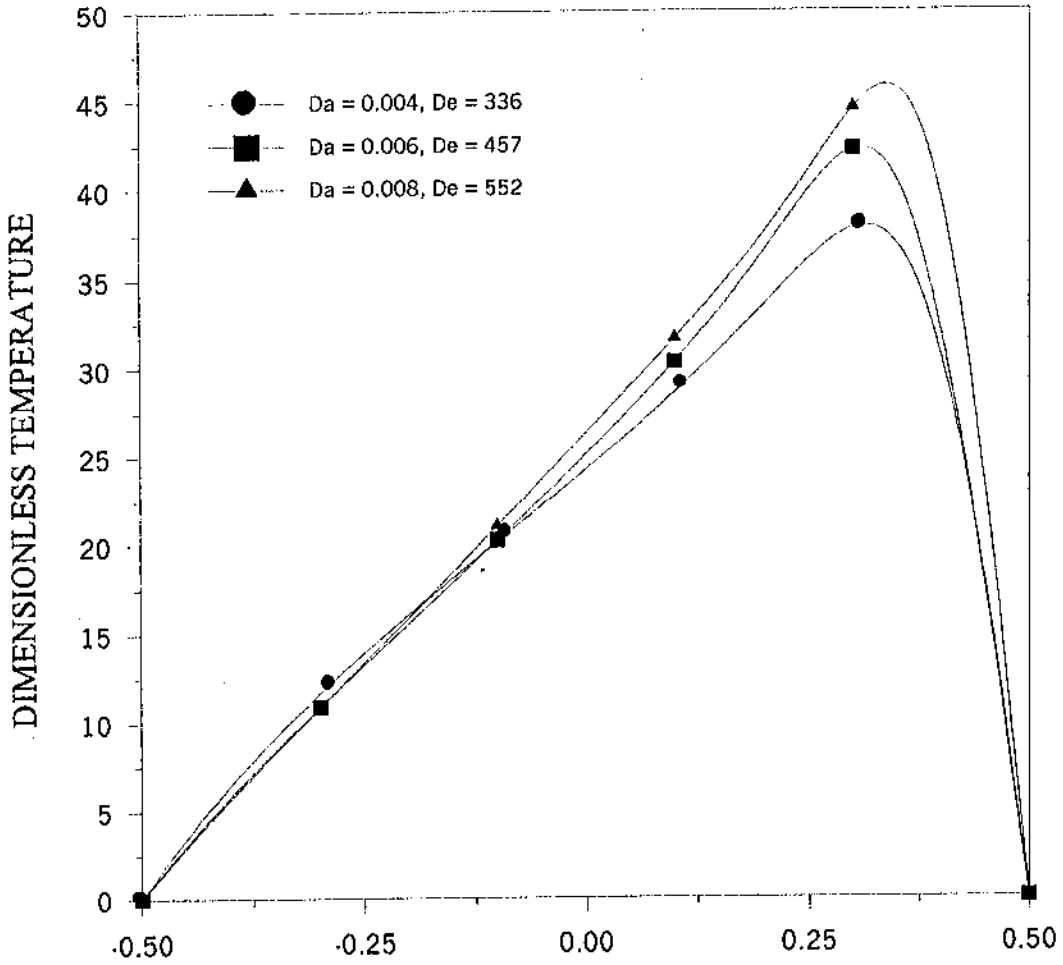

Figure (5.16) Effect of Darcy number on centerline dimensionless temperature, dp/dz = 350000, r = 10.

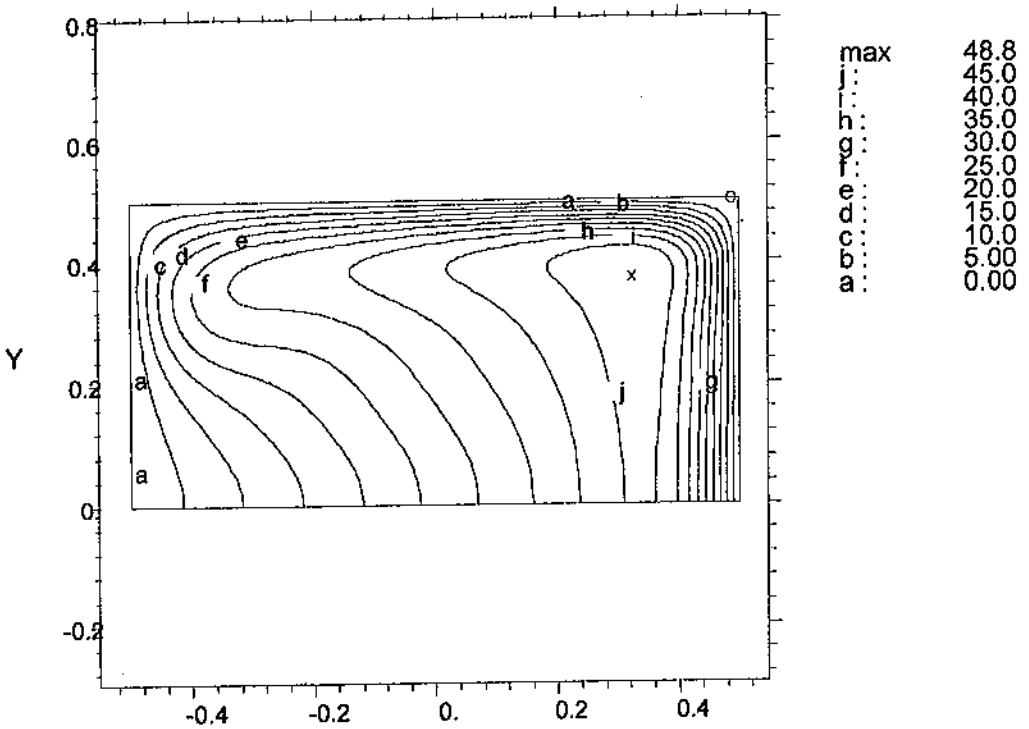

Figure (5.17) Temperature contours, dp/dz = 350000, Da = 0.008, De = 457, r = 10, Pr = 1.

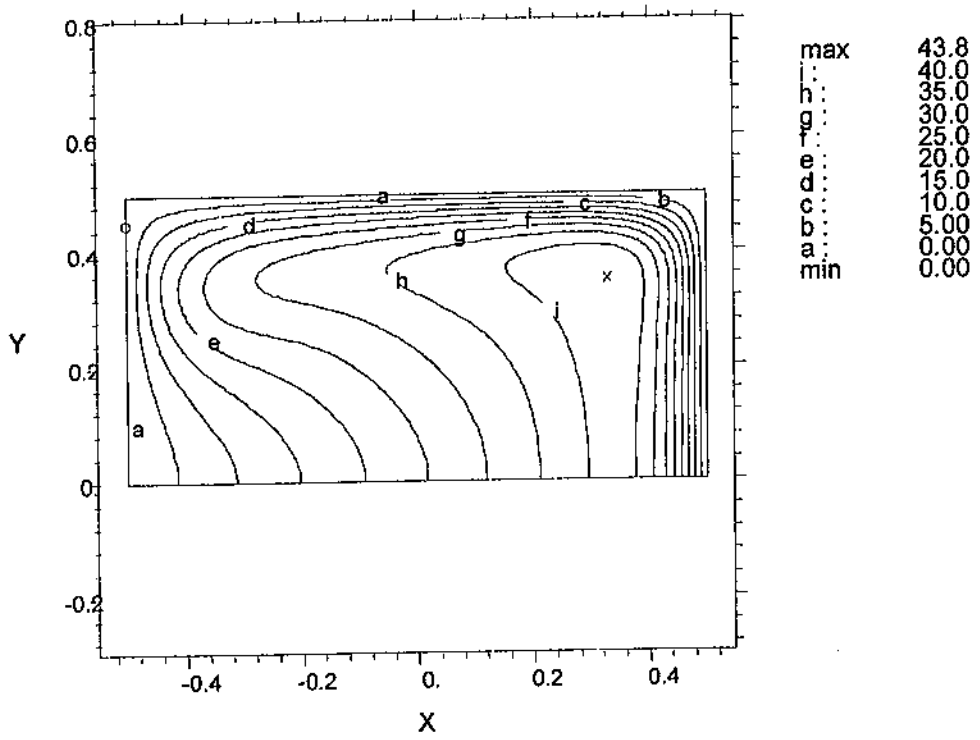

Figure (5.18) Temperature contours, dp/dz = 350000, Da = 0.006, De = 457, pr = 1.

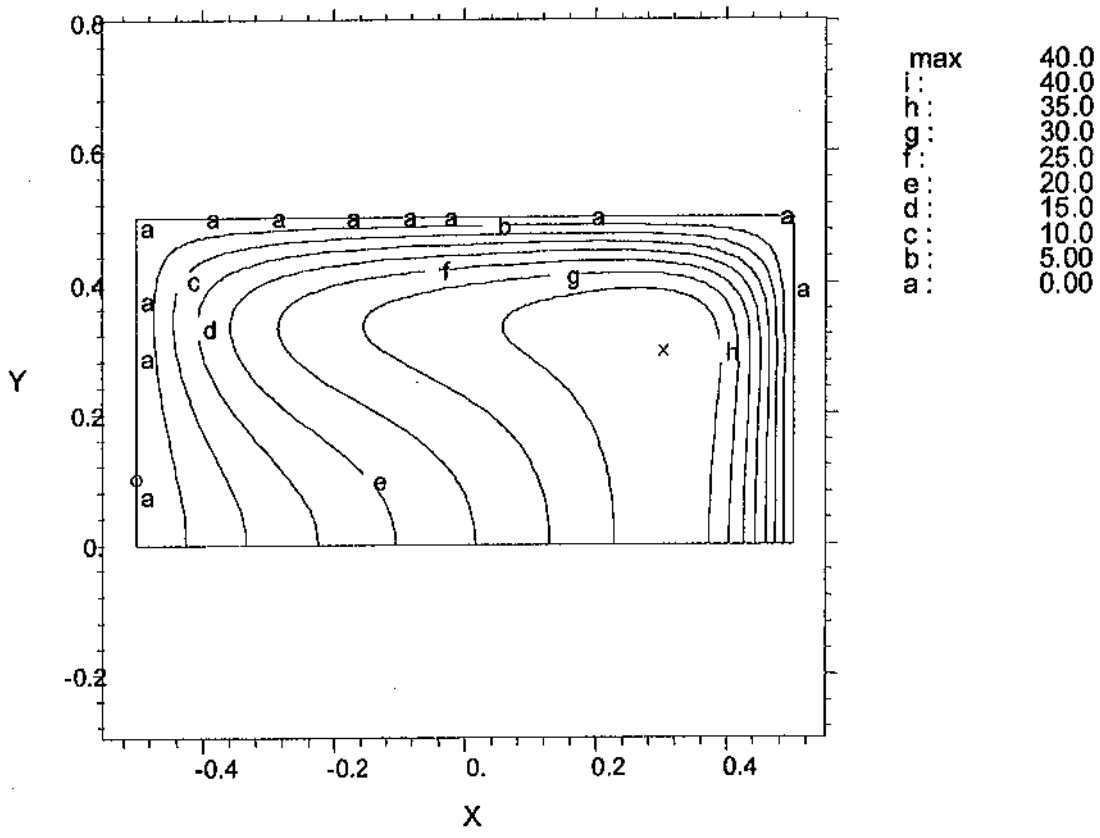

Figure (5.19) Temperature contours, dp/dz = 350000, Da = 0.004, De = 336, Pr = 1, r = 10.

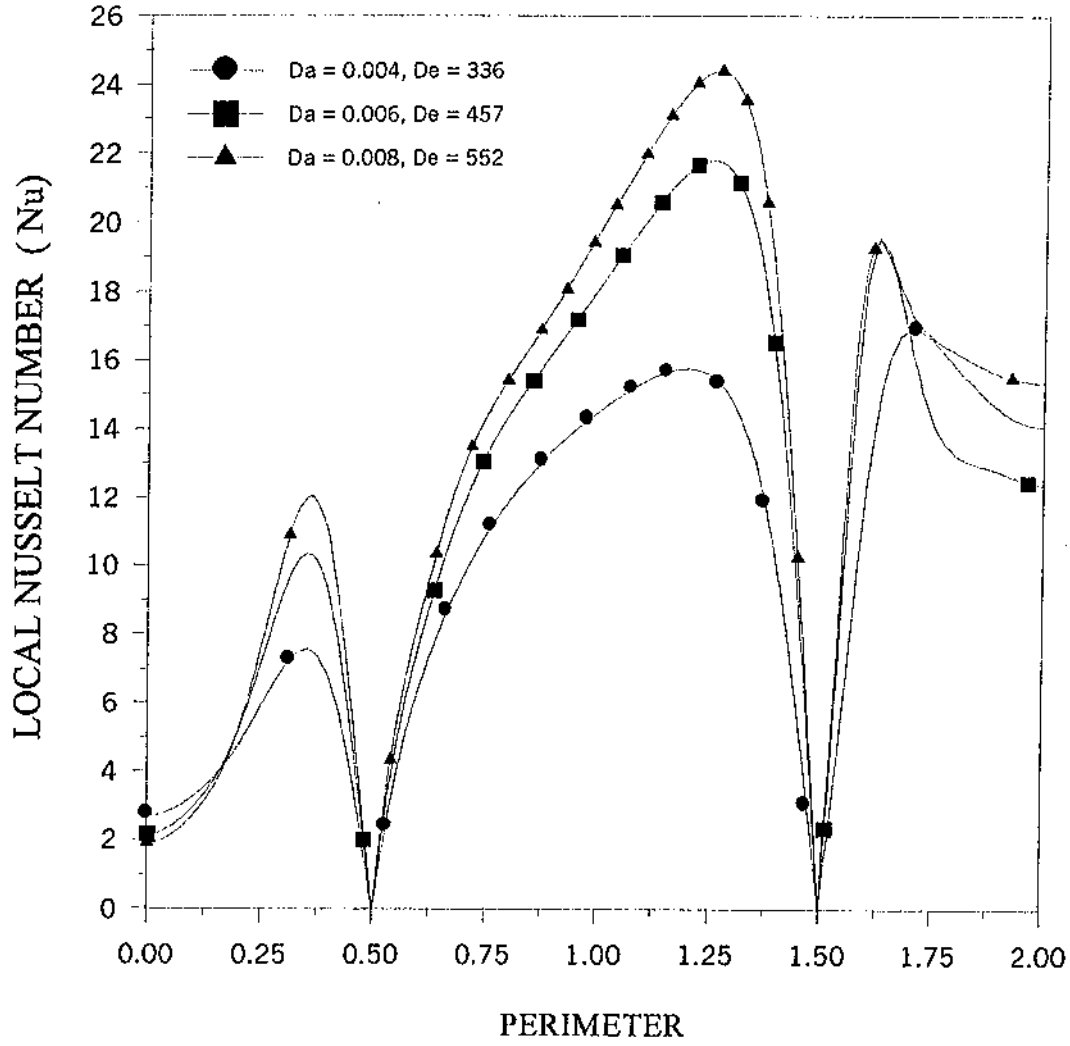

Fig. (5.20) Effect of Darcy number on local Nusselt number, dp/dz = 350000, r = 10.

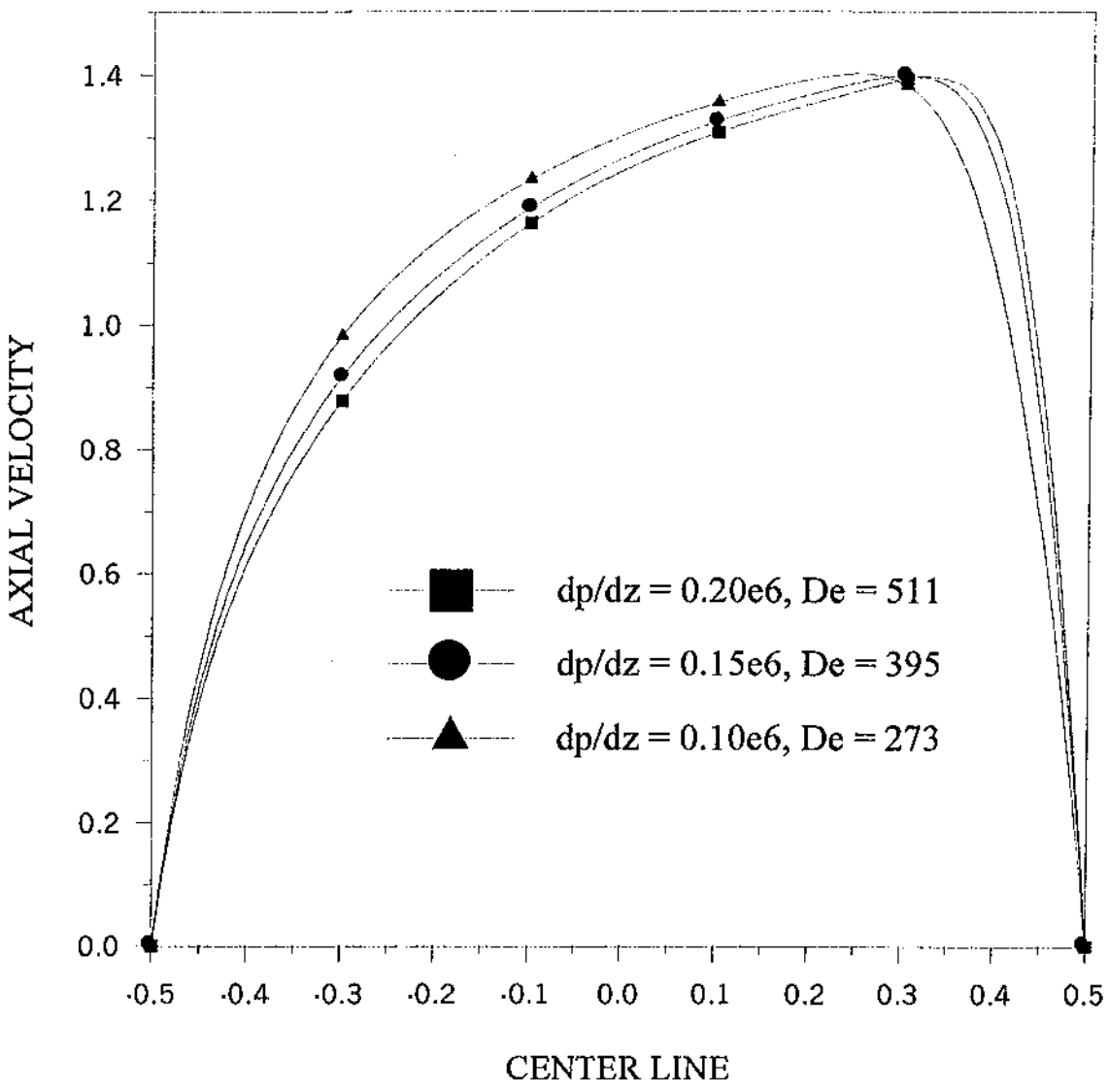

Figure (5.21) Effect of axial pressure drop on centerline velocity profile, Da = 0.01, r = 5.

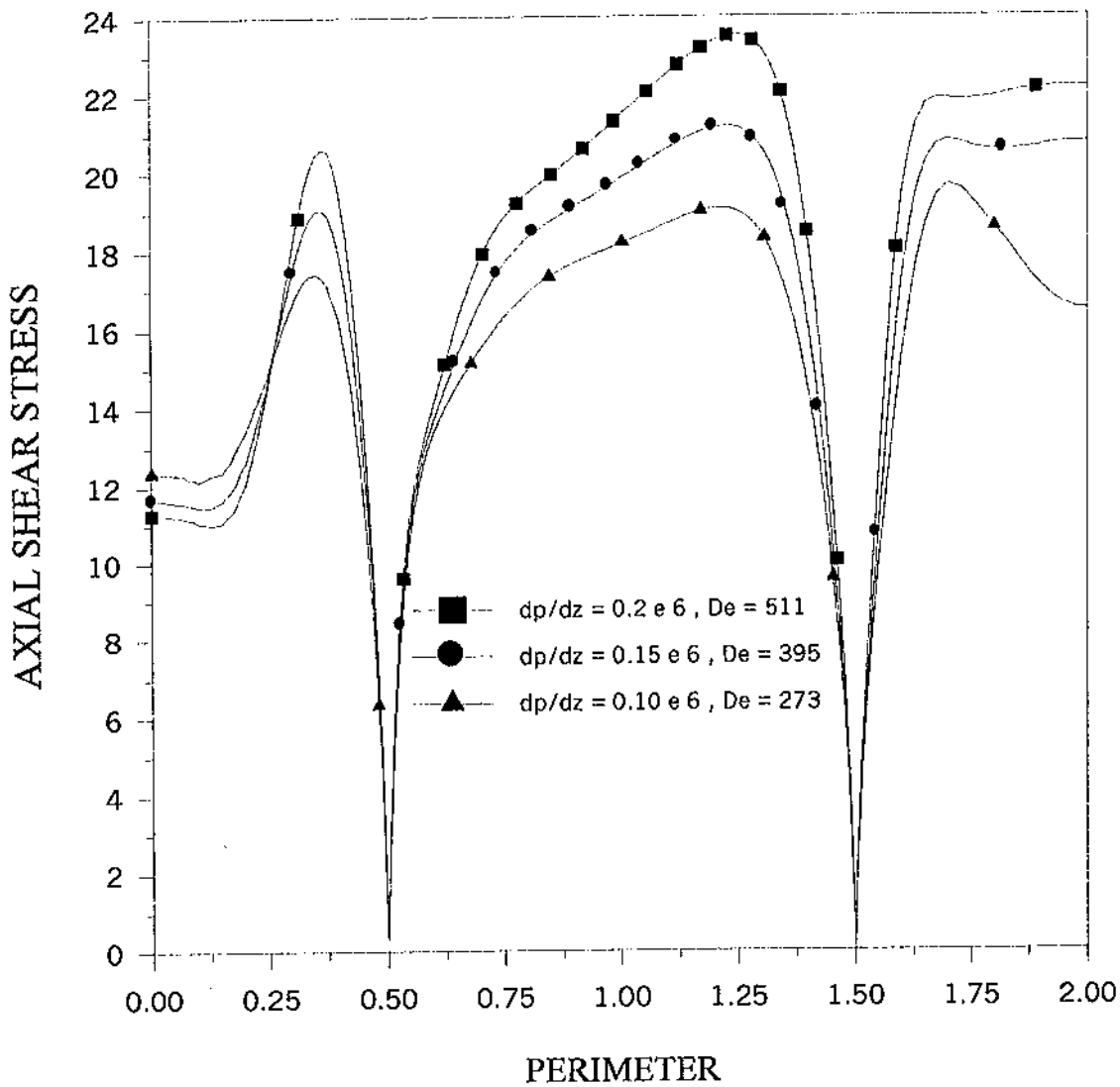

Figure (5.22) Effect of axial pressure drop on axial shear stress, Da = 0.01, r = 5.

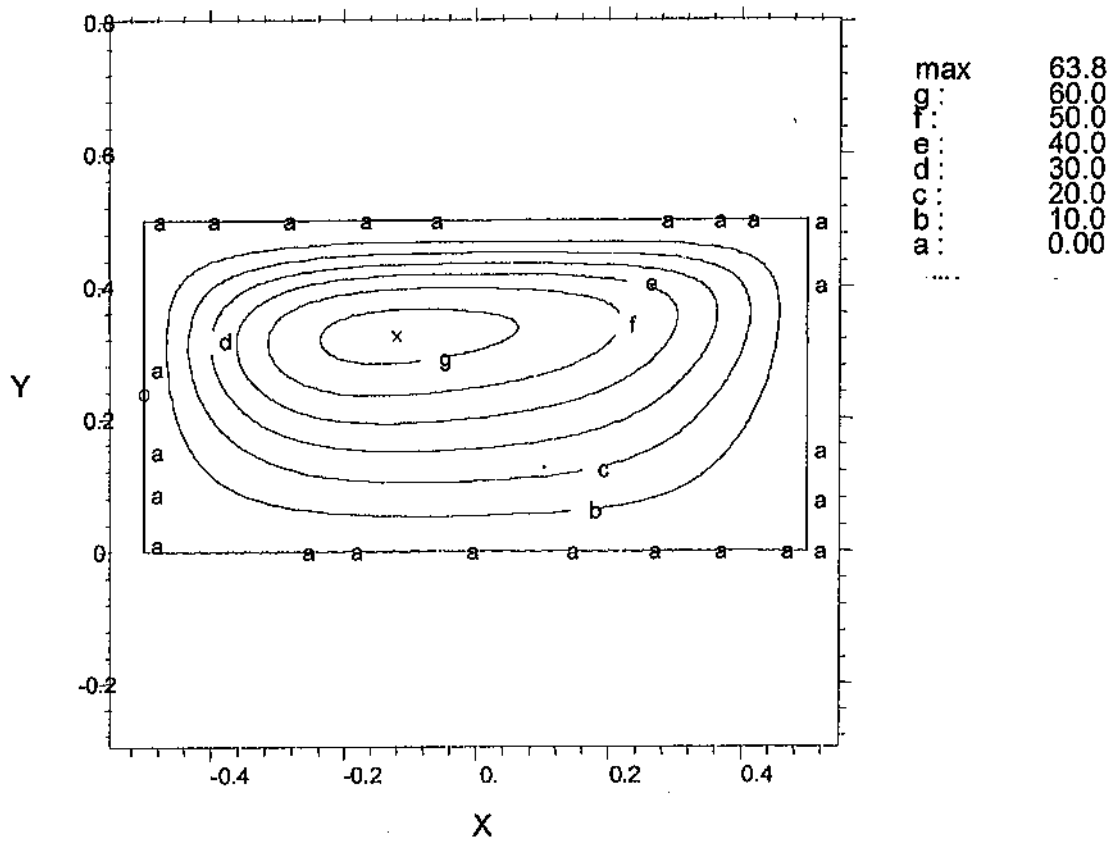

Figure (5.23) Stream function contours (secondary flow), dp/dz = 0.1×10^6, Da = 0.01, De = 273, r = 5.

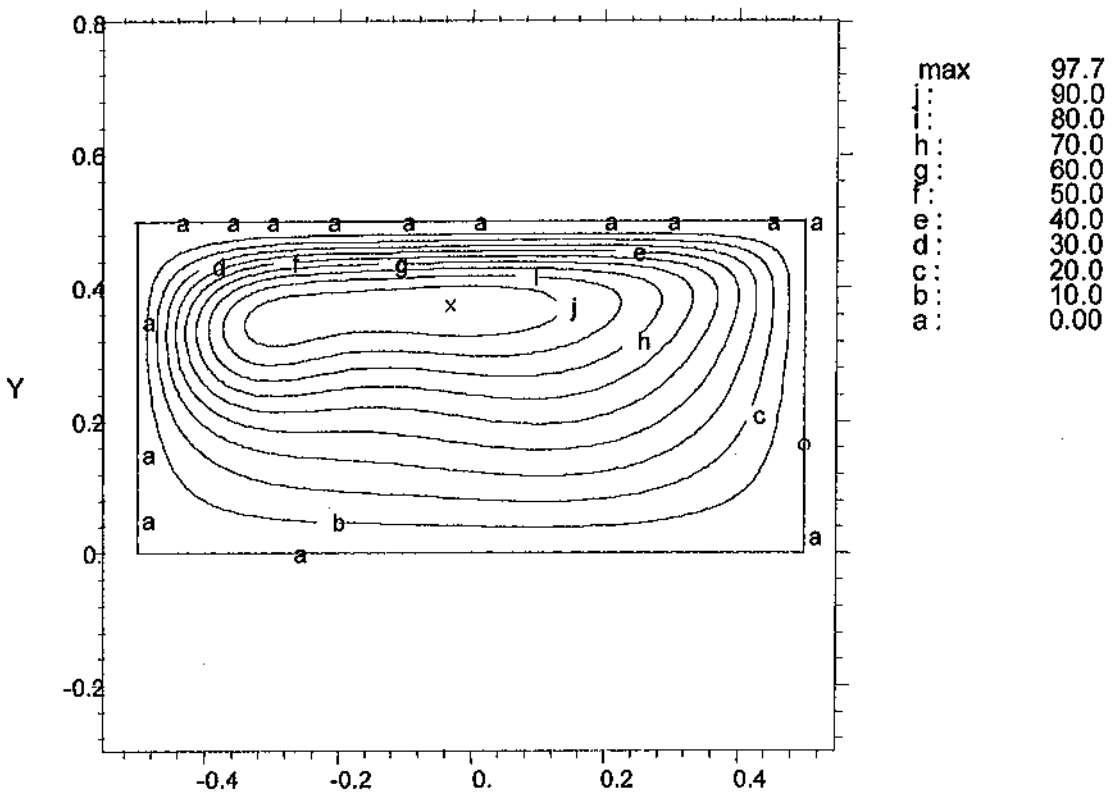

Figure (5.24) Stream function contours (secondary flow), dp/dz = 0.2x10^6, Da = .01, De = 511, r = 5.

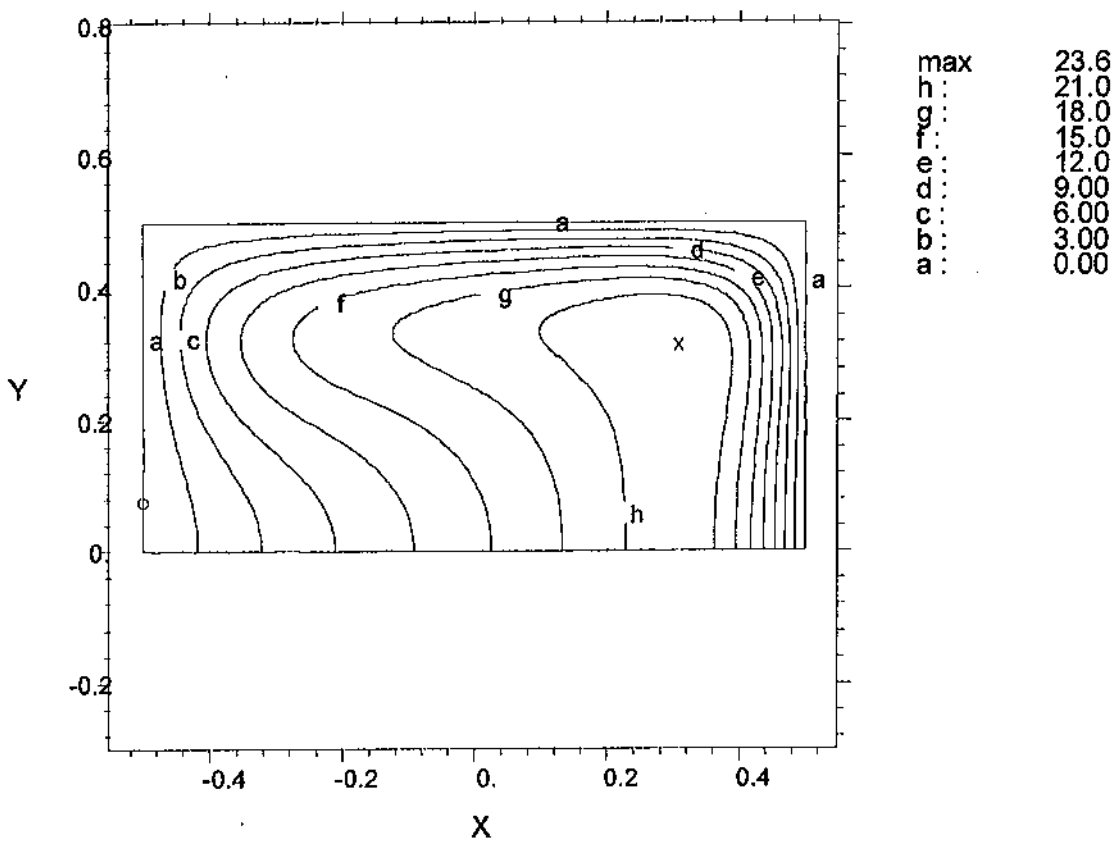

Figure (5.25) Temperature contours, dp/dz = 0.1×10^6, Da = 0.01, De =273, r = 5, Pr = 1.

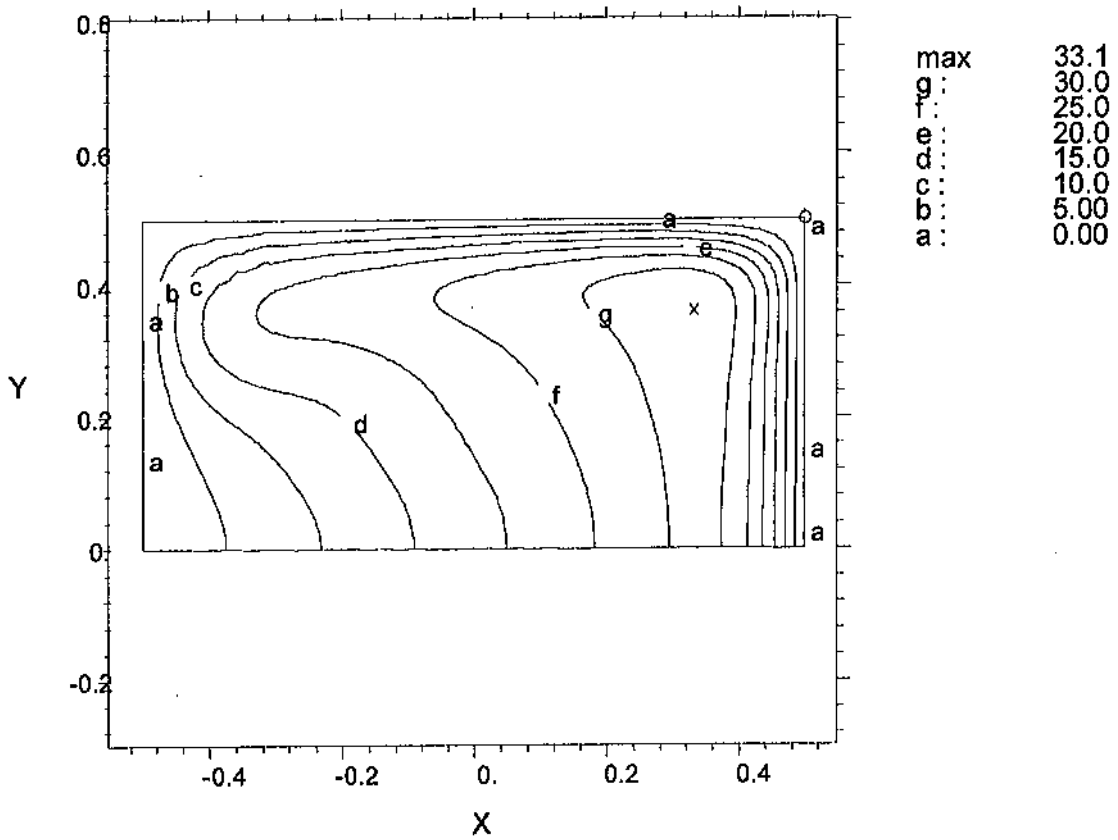

Figure (5.26) Temperature contours, dp/dz = 0.2x10^6, Da = 0.01, De = 511, r = 5, Pr = 1.

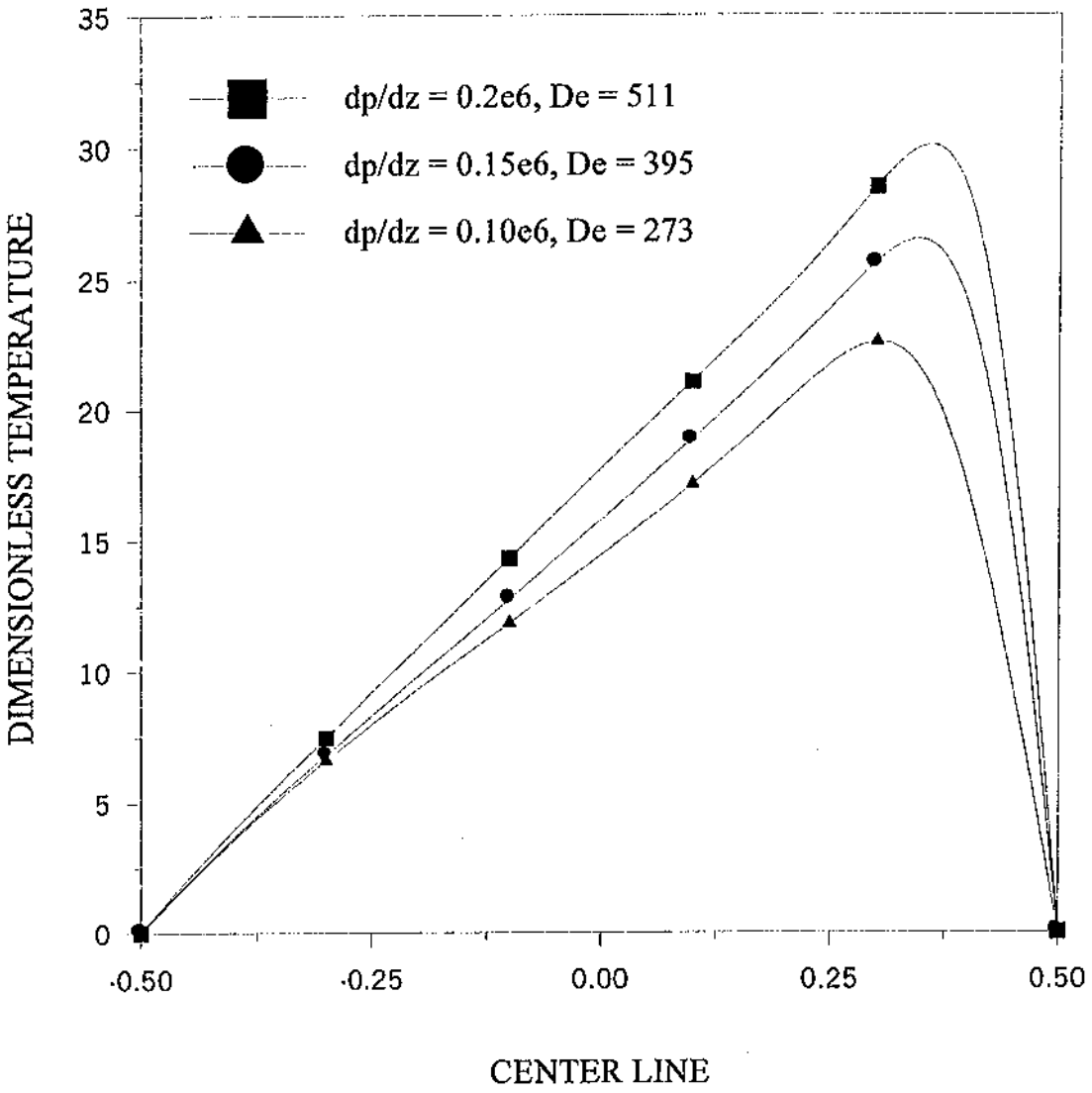

Figure (5.27) Effect of axial pressure drop on centerline temperature profile, Da = 0.01, r =5, Pr = 1.

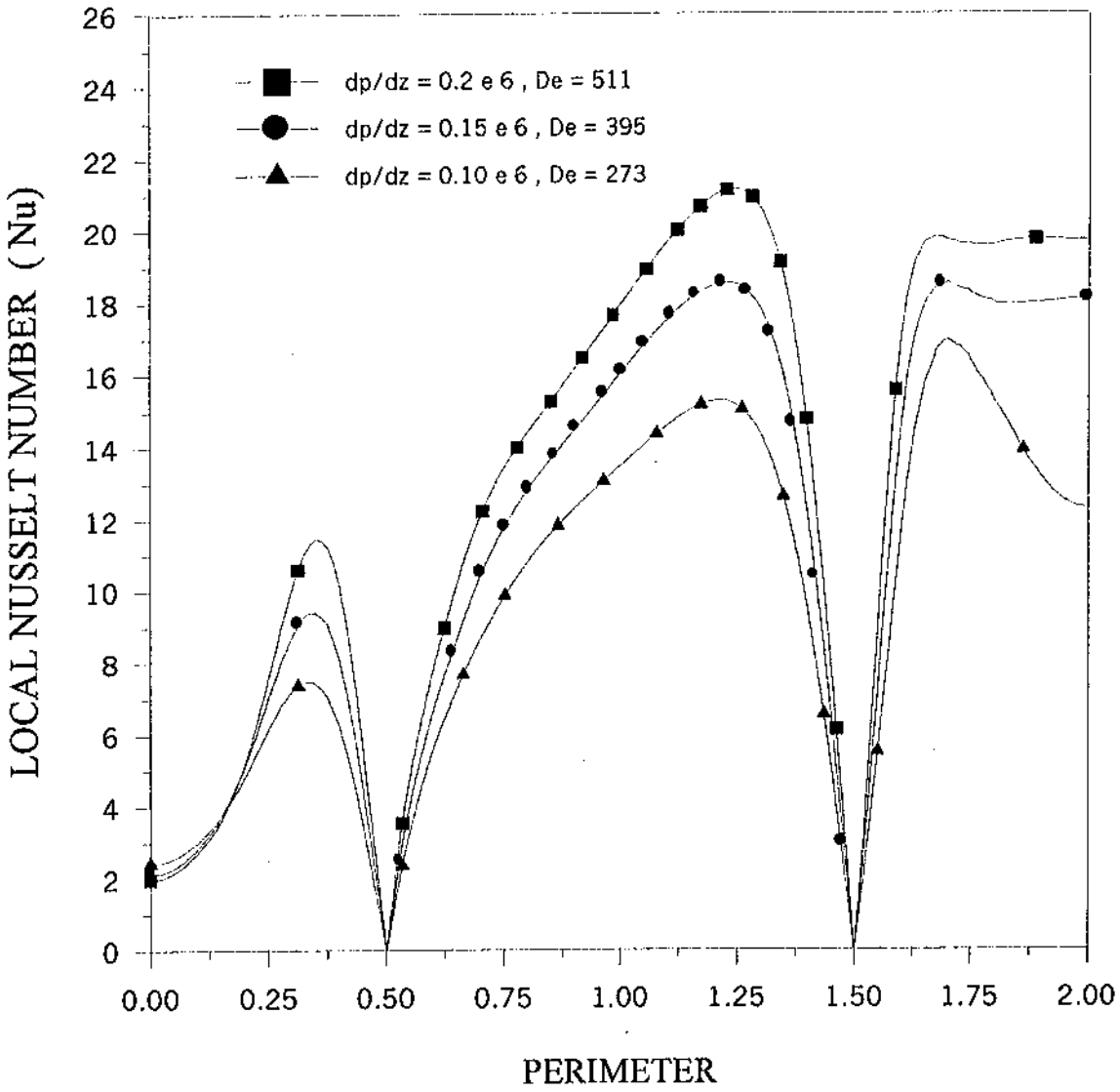

Figure (5.28) Effect of axial pressure drop on local Nusselt number, Da = 0.01, r = 5, Pr = 1.

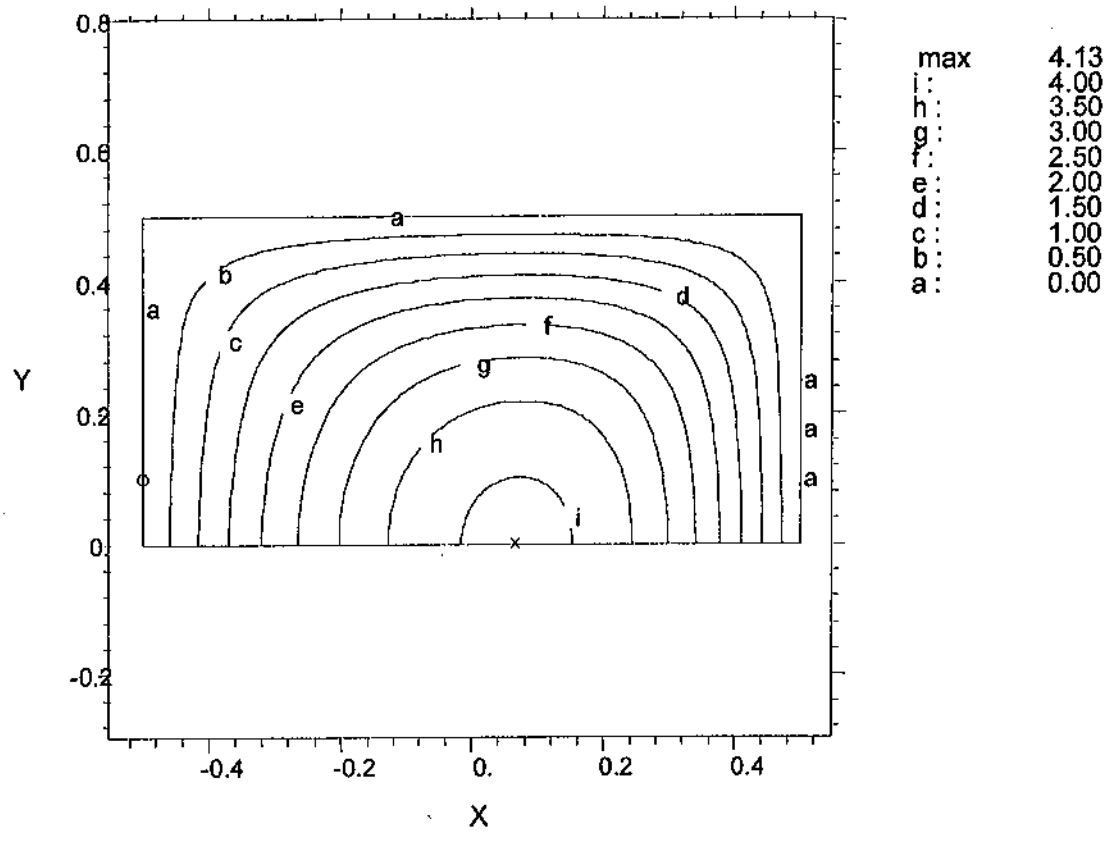

Figure (529) Temperature contours, dp/dz = 150000, Da = 0.01, De = 291, r = 10, Pr = 0.05.

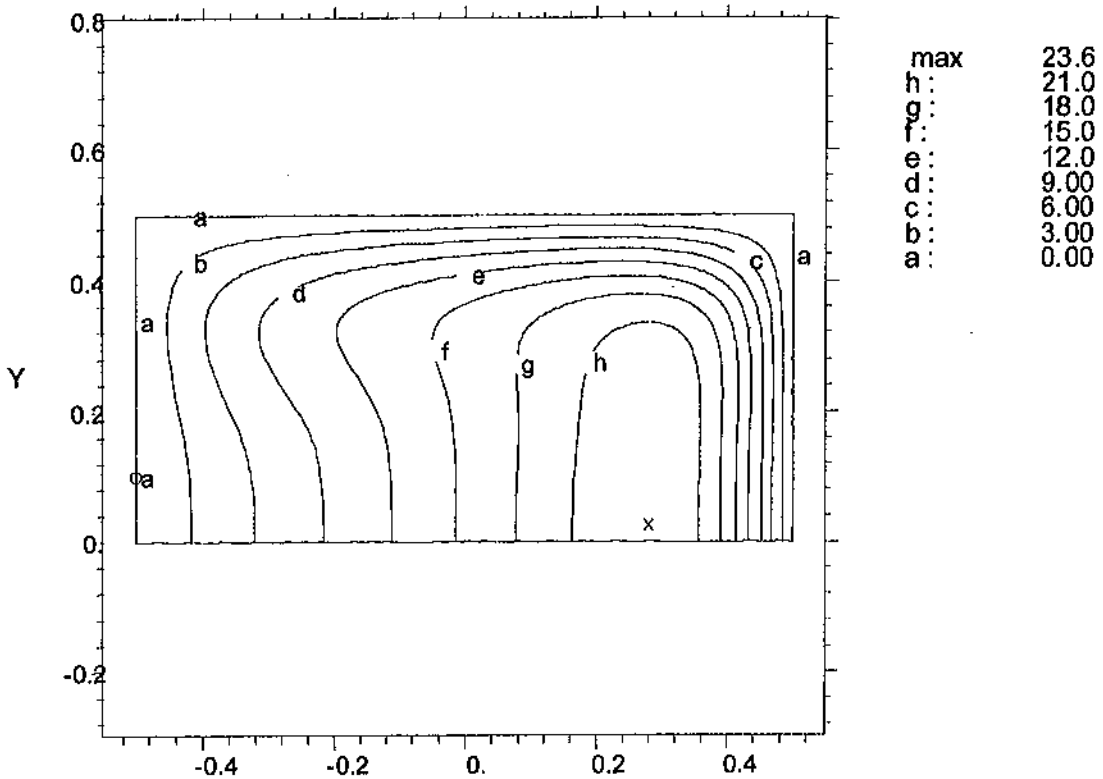

Figure (5.30) Temperature contours, dp/dz = 150000, Da = 0.01, De = 291, r = 10, , Pr = 0.5.

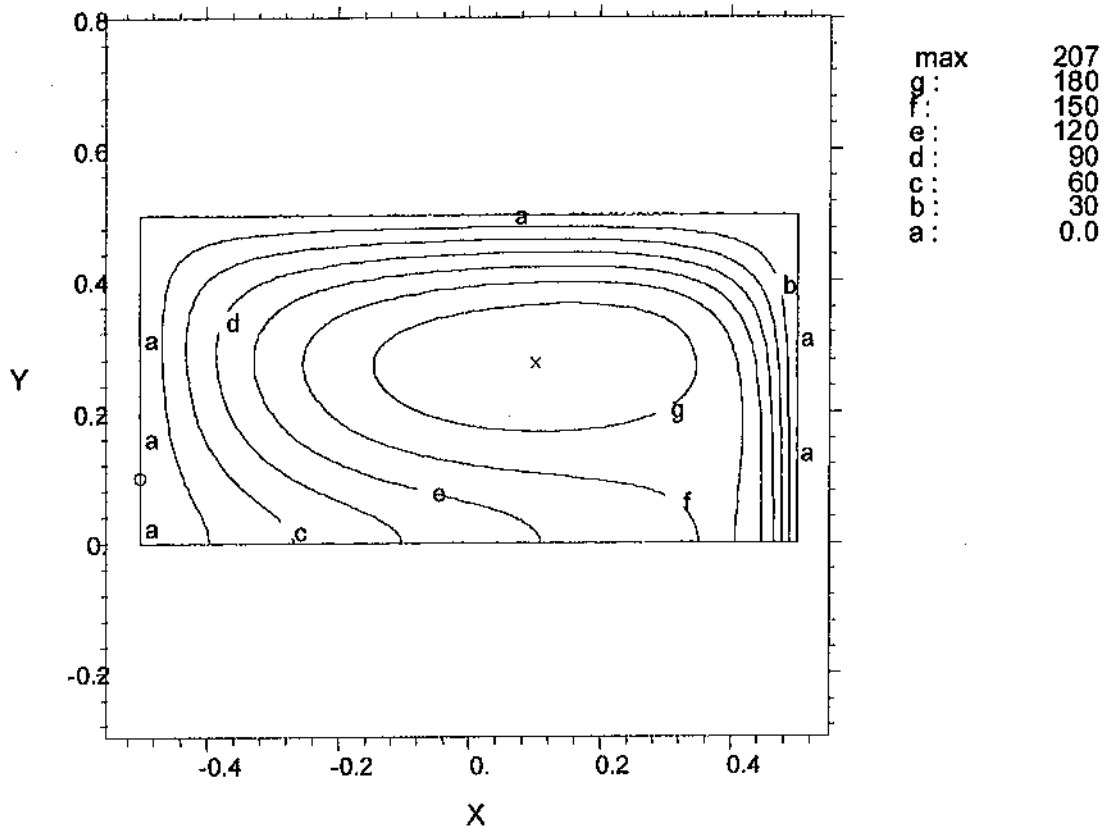

Figure (5.31) Temperature contours, dp/dz = 150000, Da = 0.01, De = 99, r = 100, Pr = 5.

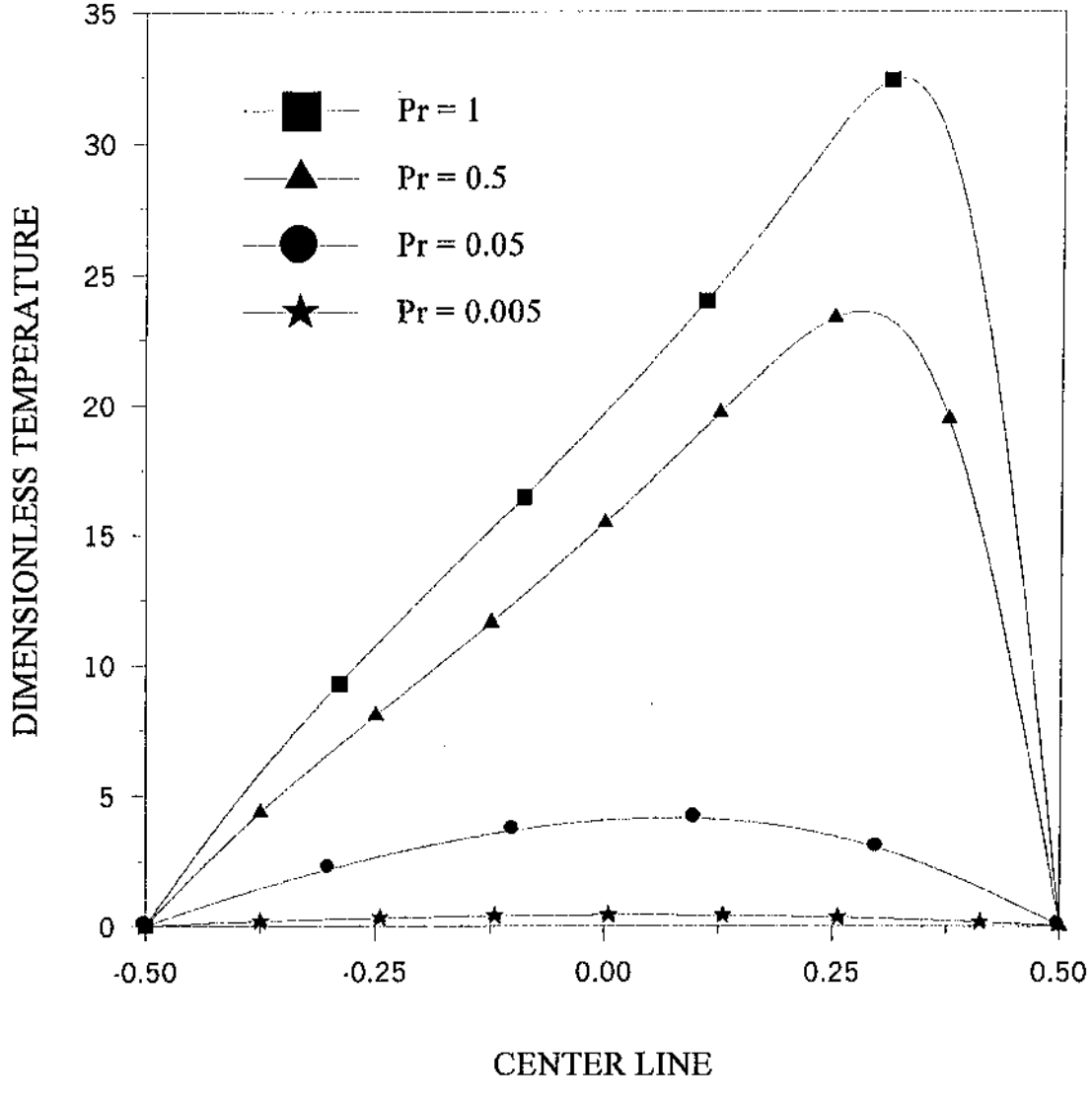

Figure (5.32) Effect of Prandtl number on centerline temperature, dp/dz = 150000, Da = 0.01, De = 291, r = 10.

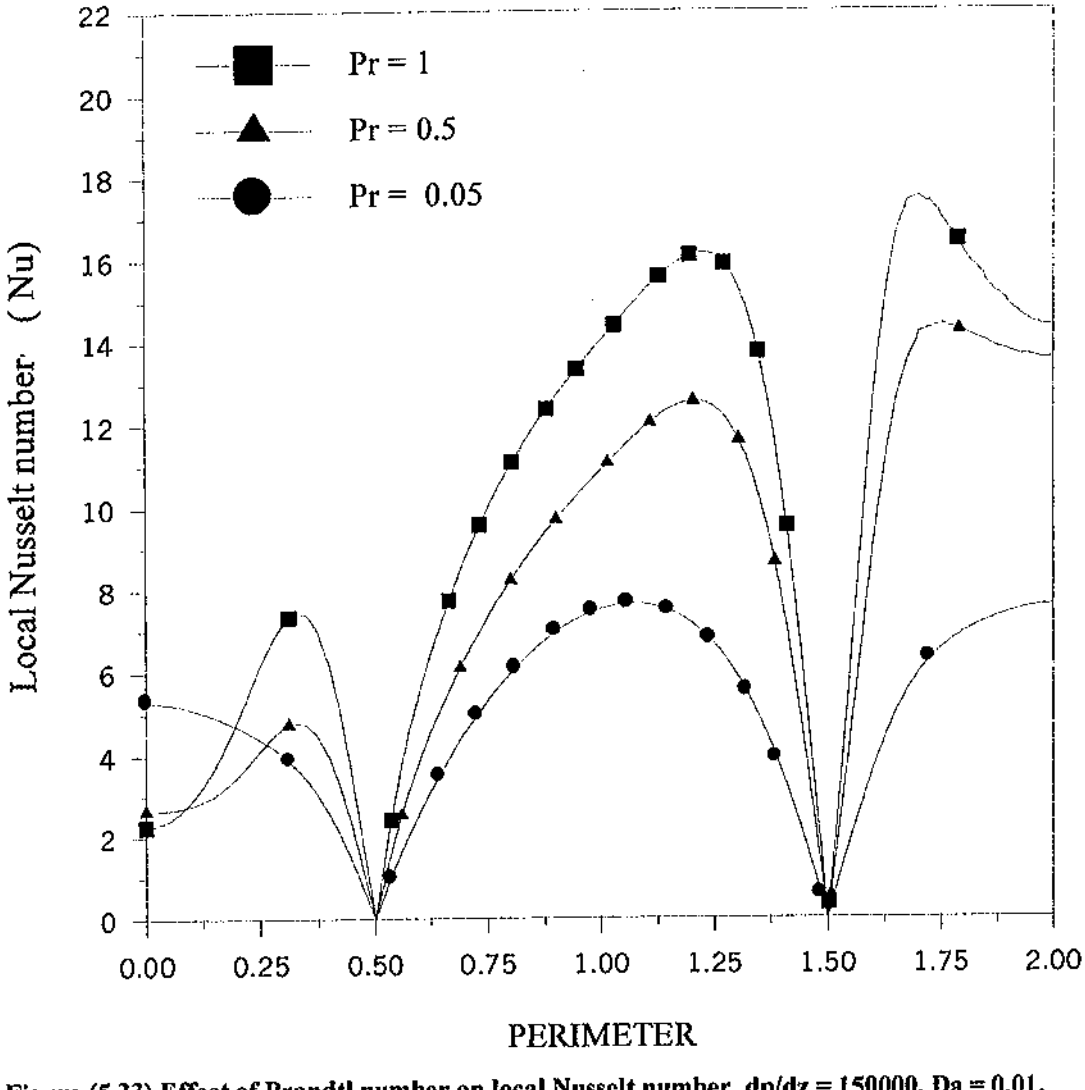

Figure (5.33) Effect of Prandtl number on local Nusselt number, dp/dz = 150000, Da = 0.01, r = 10.

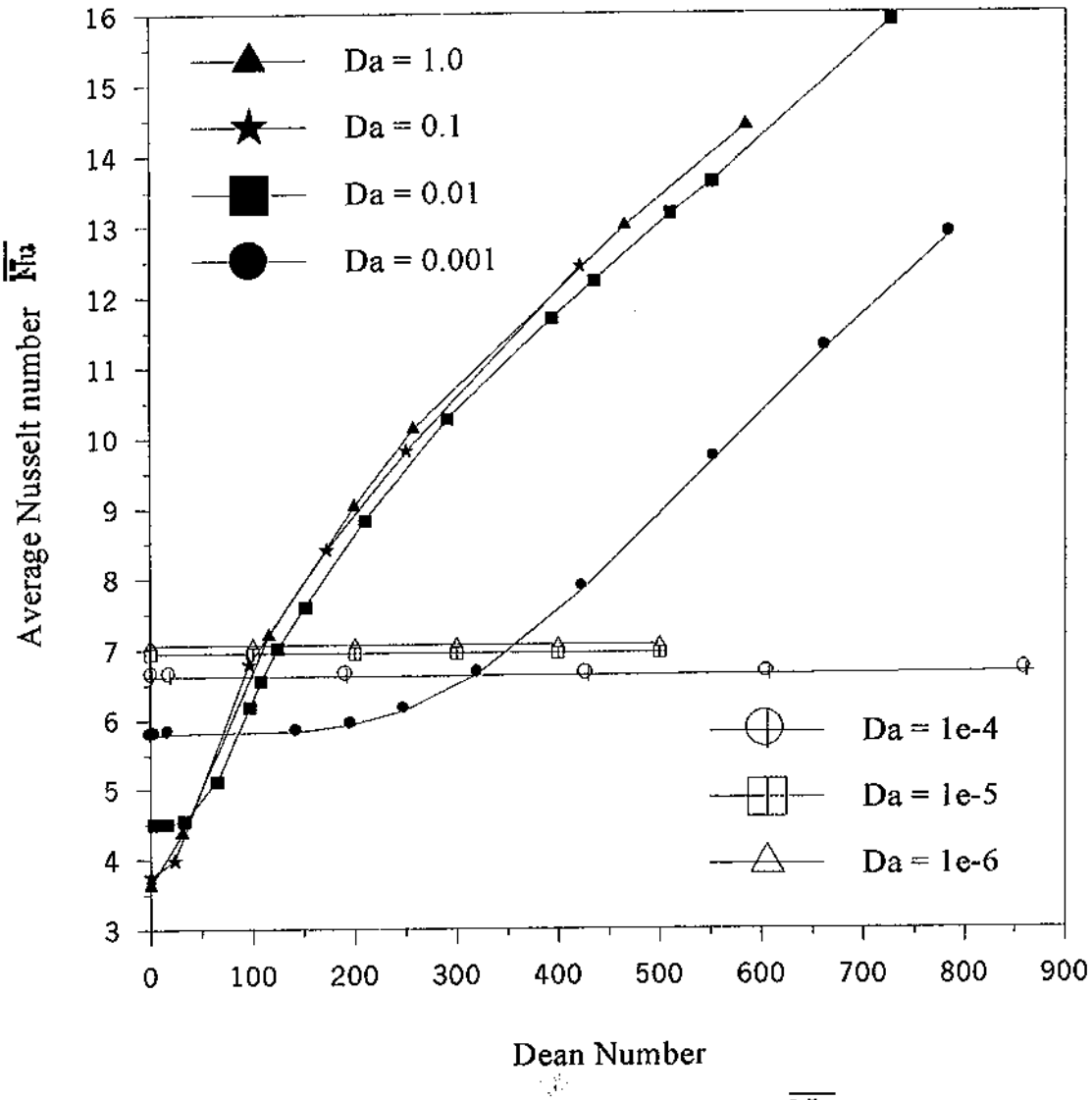

Figure (5.34) Effect of Dean number on average Nusselt number ($\overline{Nu}$), Pr = 1.

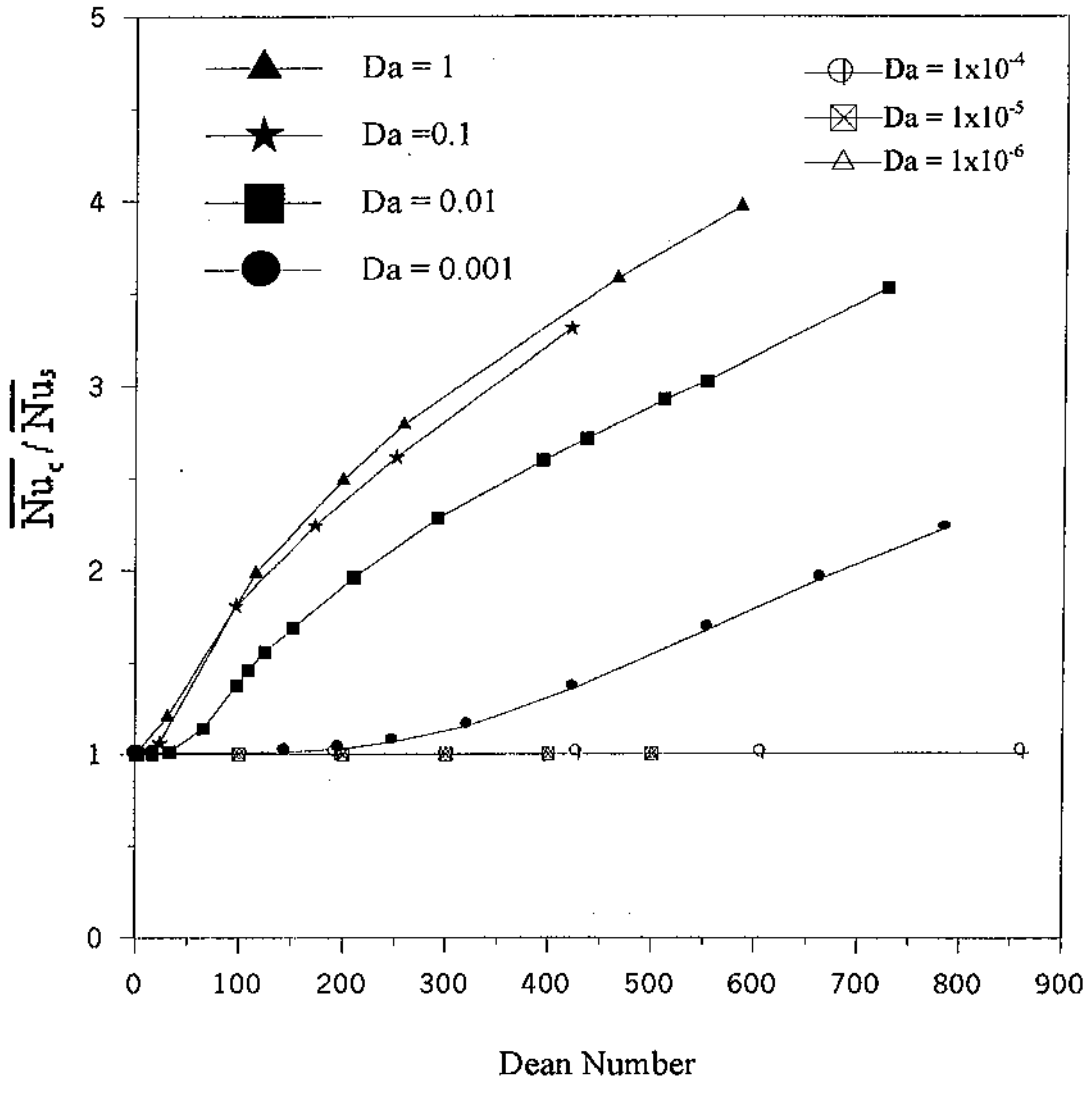

Figure (5.35) Effect of Dean number on average Nusselt number ($\overline{Nu}$), Pr = 1.

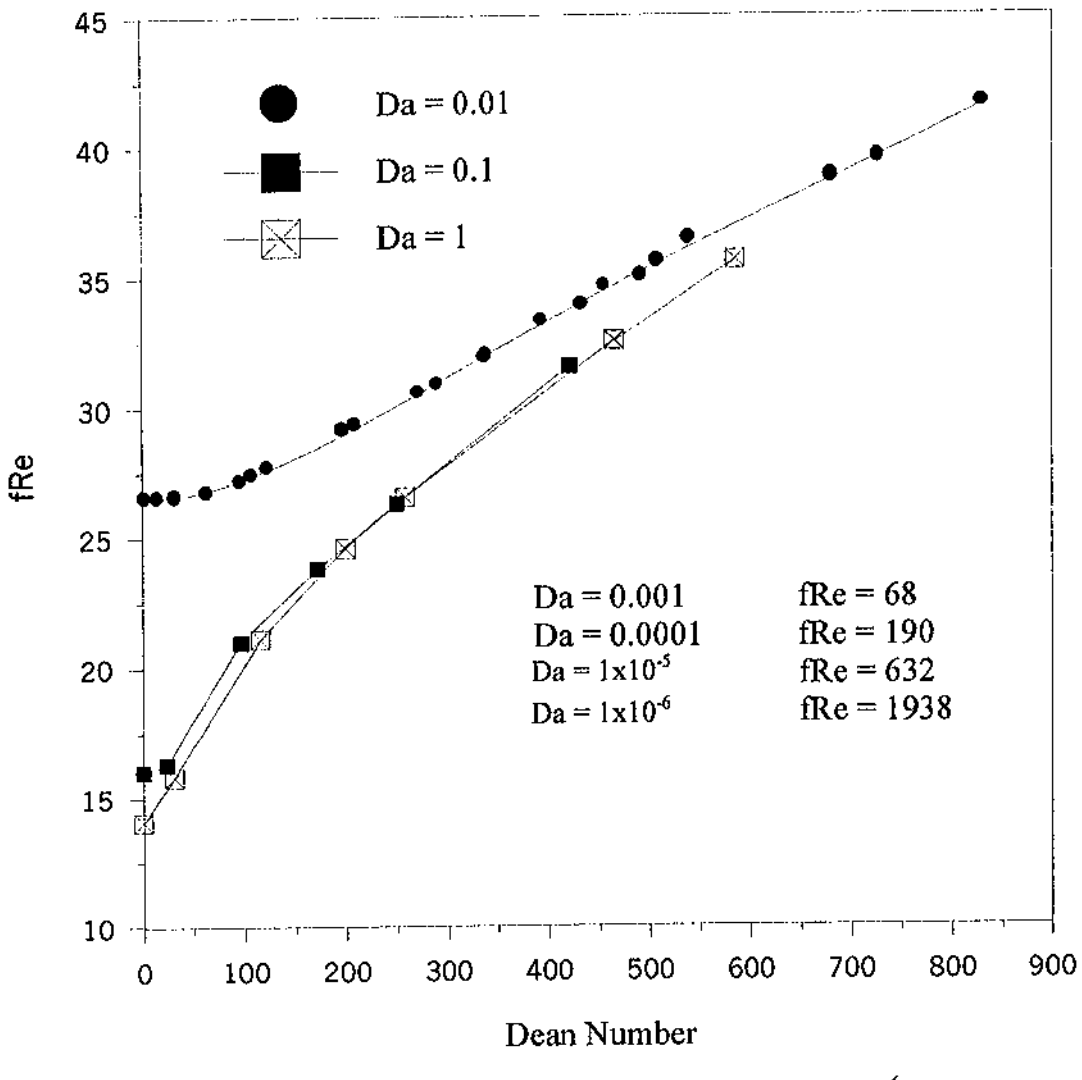

Figure (5.36) Effect of Dean number on average shear stress, Da = 1x 10^{-6} -- 1.

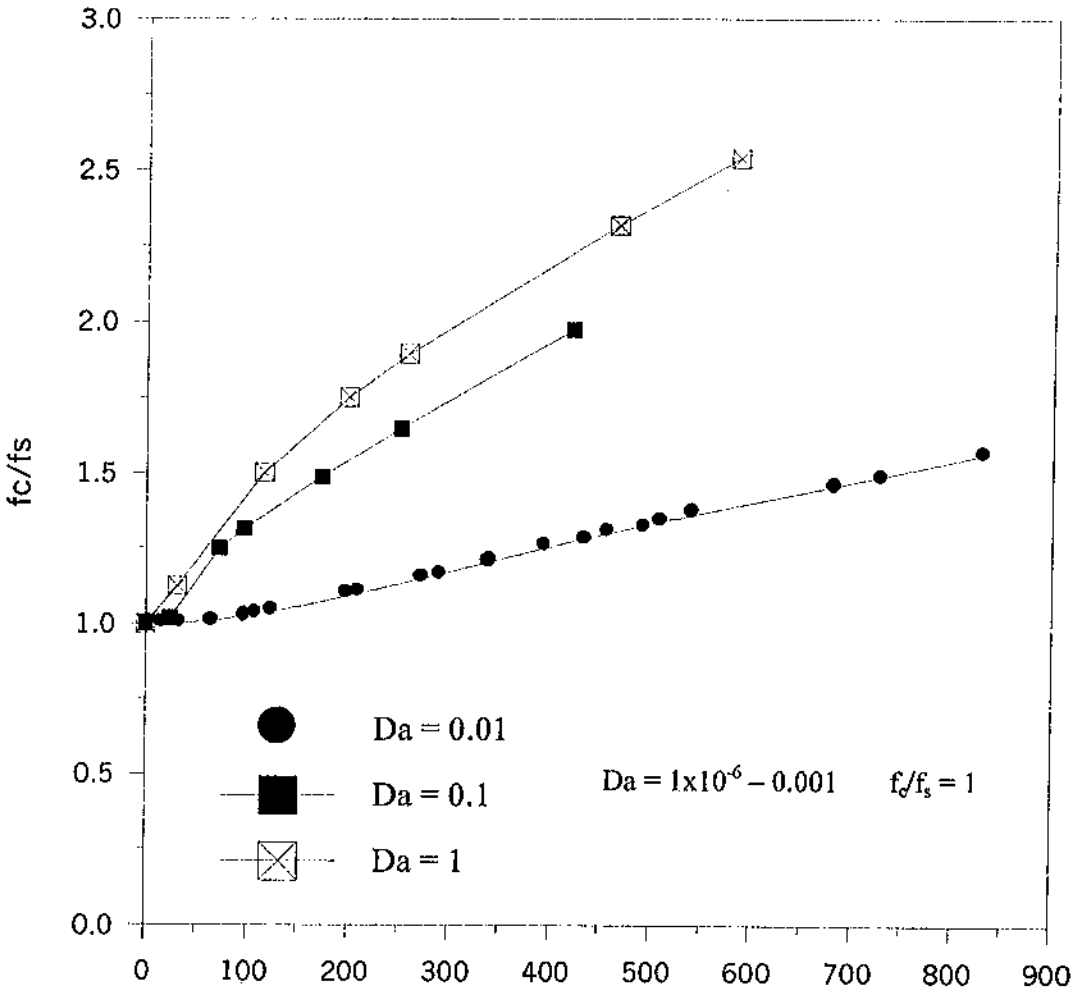

Figure (5.37) Effect of Dean number on average shear stress, Da = $1x10^{-6}$ – 1.

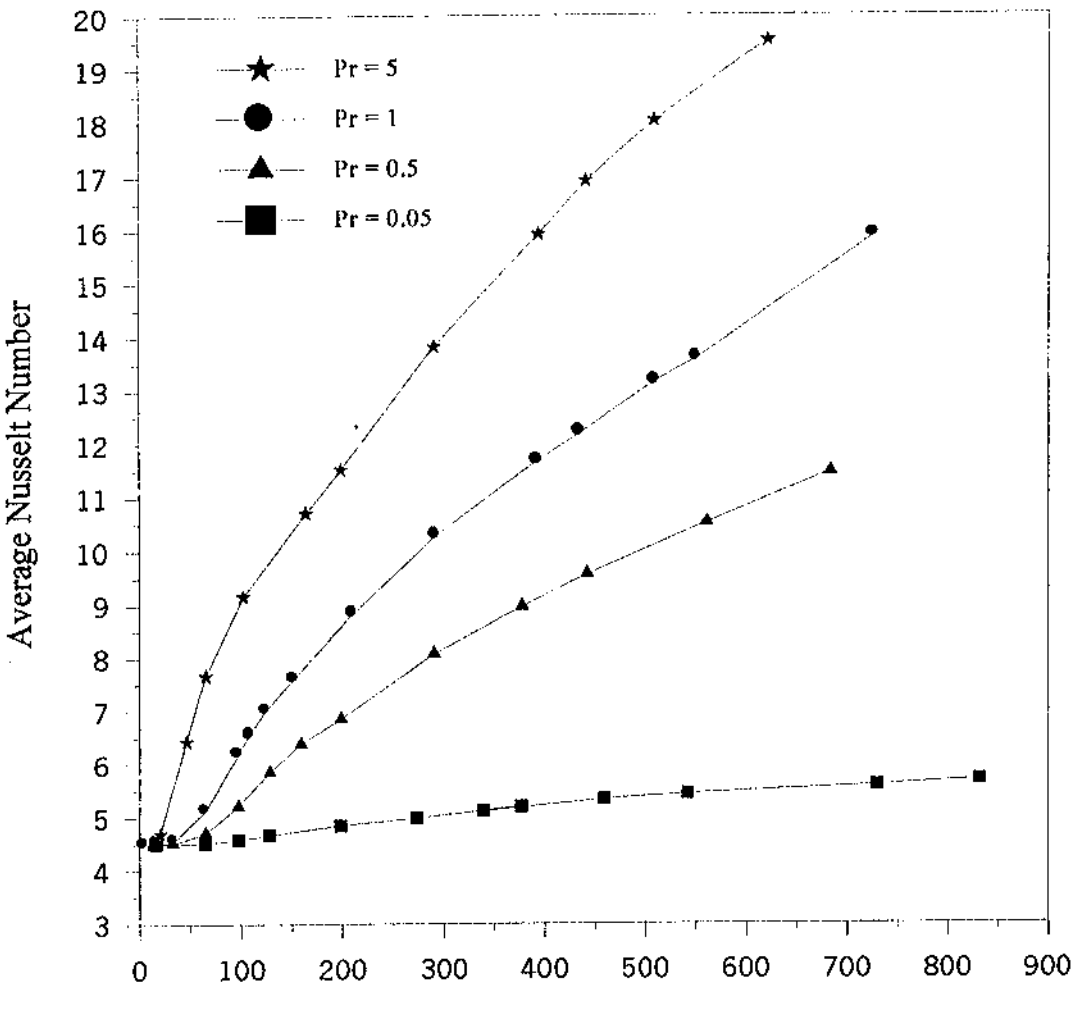

Figure (5.38) Effect of Dean on average Nusselt number ($\overline{Nu}$), Da = 0.01.

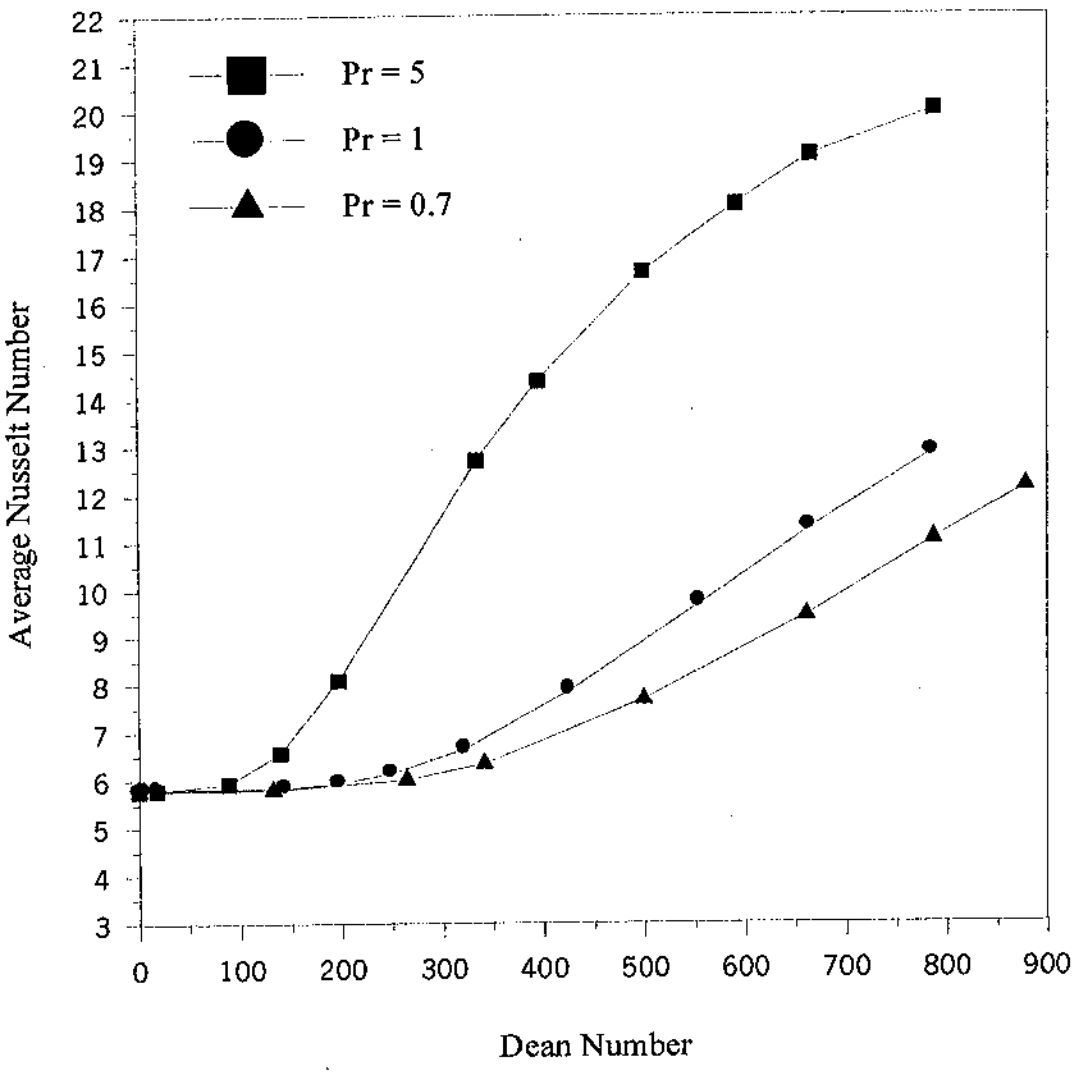

Figure (5.40) Effect of Dean number on average Nusselt number, Da = 0.001.

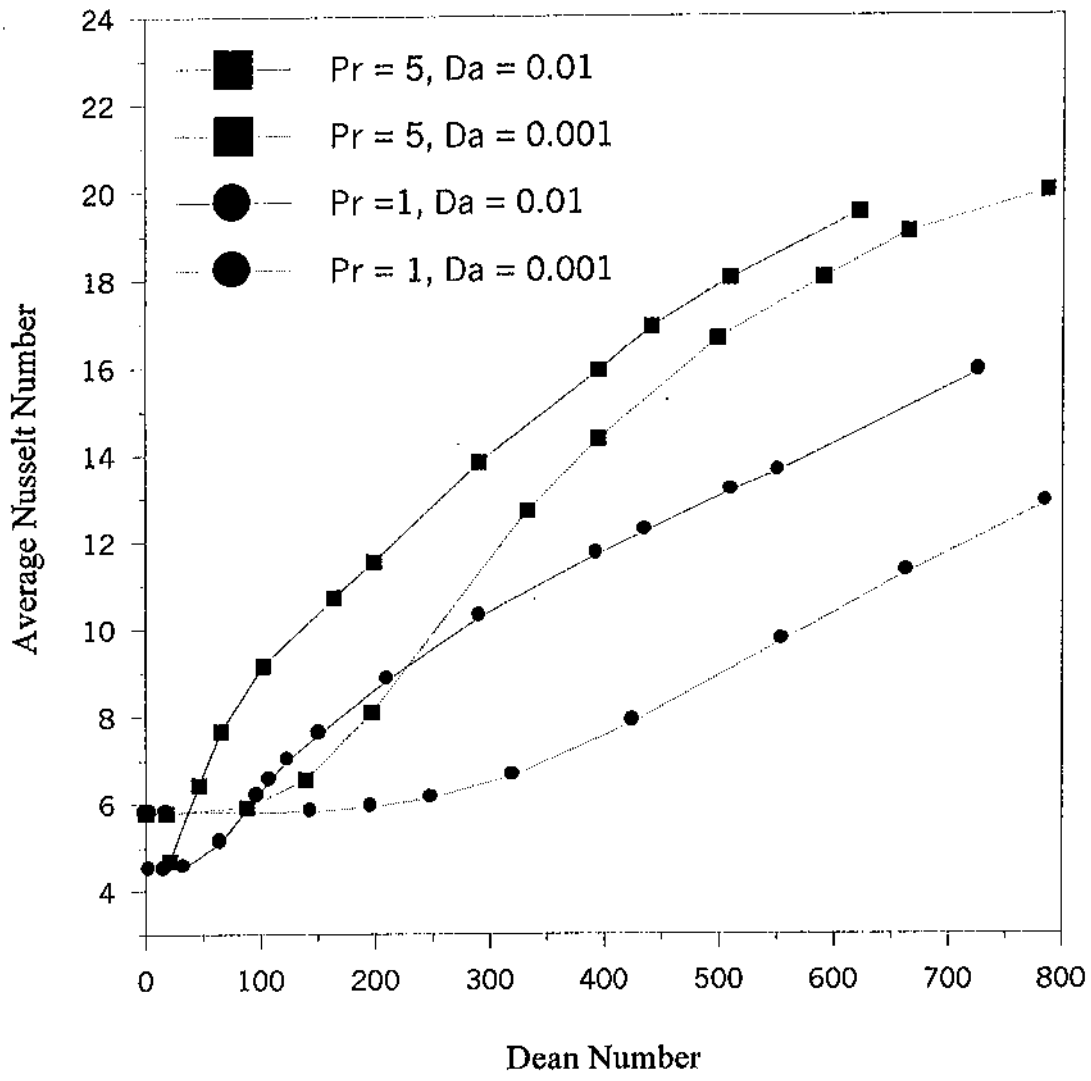

Figure (5.41) Effect of Dean number on average Nusselt number, with Pr and Da are parameters.

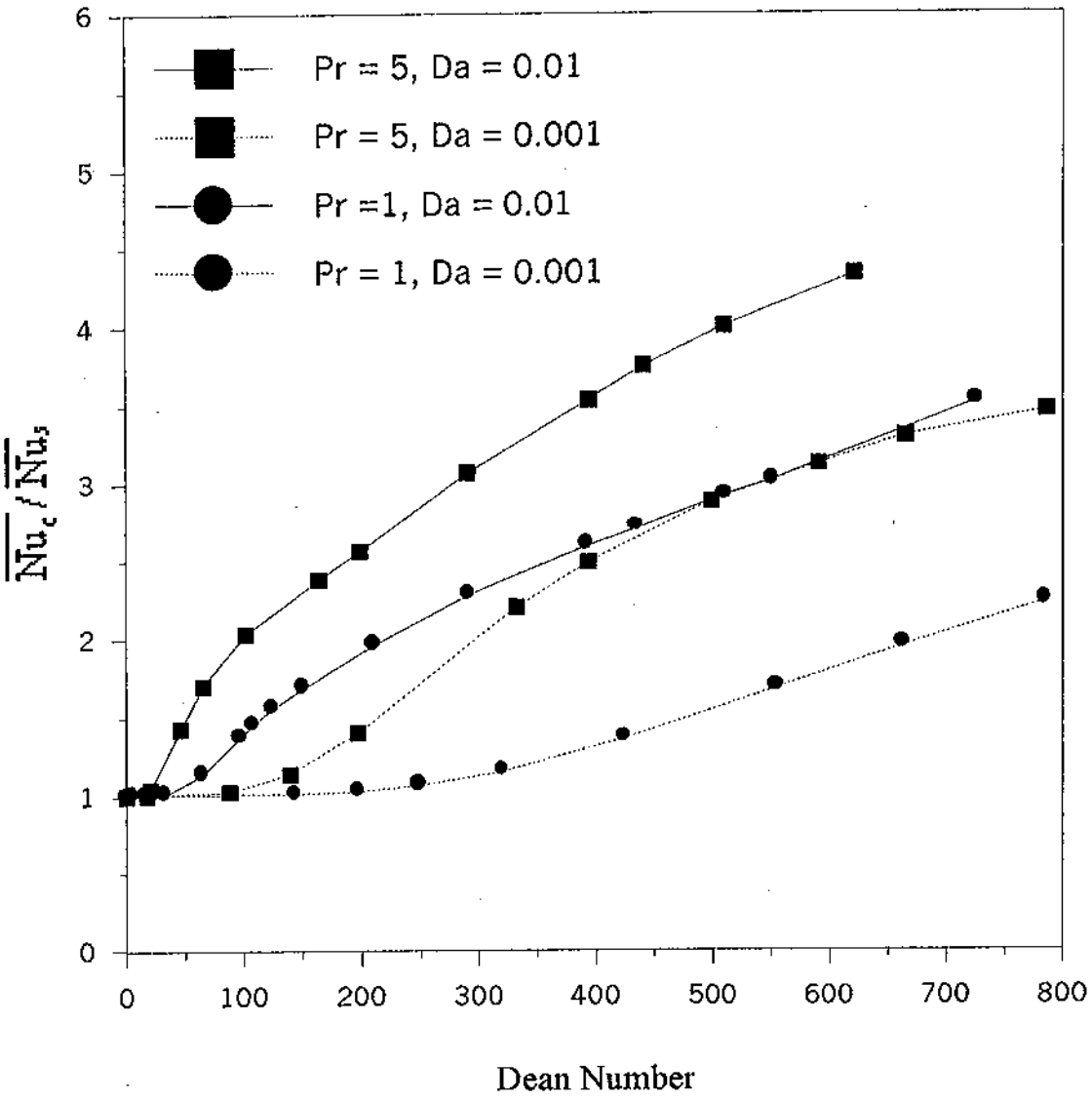

Figure (5.42) Effect of Dean number on average Nusselt number, with Pr and Da are parameters.

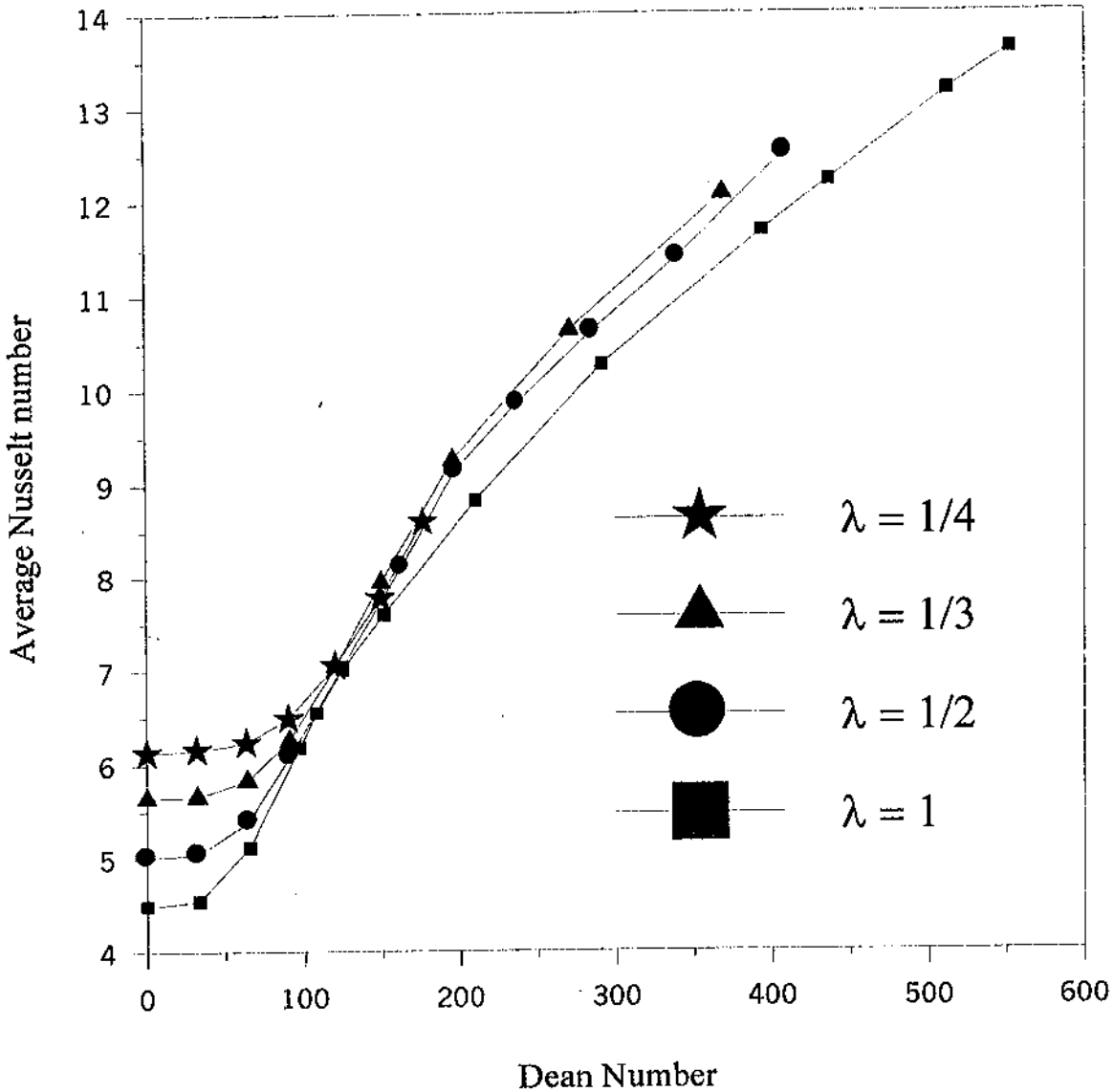

Figure (5.43) Effect of Dean number on average Nusselt number, Da = 0.01, Pr = 1.

7. REFERENCES

Austin, Larry R., and Seader J. D., 1973. Fully developed viscous flow in coiled circular pipes, *AIChE Journal. 19: (1). 85-94.*

Charles, E. Kalb, and Seader, J. D. 1974. Fully developed viscous flow and heat transfer in curved circular tubes with uniform wall temperature. *AIChE Journal.* 20: (2). 340-346.

Chen, Chao-Kuang, Chien-Hsin Chen, Minkowycz, W. J., and Gill, U. S. 1992. Non-Darcian effects on mixed convection about a vertical cylinder embedded in a saturated porous medium. *Int. J. Heat and Mass Transfer.* 35: (11). 3041-3046.

Cheng, K. C., Ran-Chau Lin, and Jenn-Wuu Ou. 1976. Fully developed flow in curved rectangular channels. *Journal of Fluids Engineering.* March: 41-48.

Cheng, P., and Hsu, C. T. 1986. Fully-developed forced convective flow through an annular packed-sphere bed with wall effects. *Int. J. Heat and Mass Transfer.* 29: (12). 1843-1853.

Cheng, P., and Zhu, H. 1987. Effects of radial thermal dispersion on fully developed forced convection in cylindrical packed tubes. *Int. J. Heat Mass Transfer.* 30: (11). 2373-2383.

Futagami, Kozo, and Aoyama, Yoshiyuki. 1988. Laminar heat transfer in a helically coiled tube. *Int. J. Heat and Mass transfer.* 31: (2). 387-396.

Greenspan, D. 1973. Secondary Flow in a Curved Tube. *Journal of Fluid mechanics.* 57: Part 1.177-208.

Gyves, T. W., Irvine Jr., T. F., and Naraghi, M. H. N.1998. Gravitational and centrifugal buoyancy effects in curved square channels with conjugated boundary conditions. *International Journal of Heat and Mass Transfer.* 42: 3954-3964.

Gyves T. W., and Irvine Jr., T. F. 2000. Laminar conjugated forced convection heat transfer in curved rectangular channels. *International Journal of Heat and Mass Transfer.* 43: 3954-3964.

Hadim, A. 1994. Forced convection in a porous channel with localized heat sources. *Journal of Heat Transfer.* 116 (1). 465-472.

Hille, P., Vehrenkamp, R., and Schulz-dubois, E. O. 1985. The development and structure of primary and secondary flow in a curved duct. *Journal of Fluid Mechanics.* 151: 219-241.

Hu, C. T., and Cheng, P. 1990. Thermal dispersion in a porous media. *Int. Journal of heat and mass transfer.* 33: (84). 1587-1597.

Huang, X. Y., and Lu, K. T. 1996. The development flow in a channel filled with porous media. *Int. Comm. Heat mass Transfer.* 23: (1). 123-132.

Humphrey, J. A. C., Taylor, A. K., and Whitelaw, J. H. 1977. Laminar flow in a square duct of strong curvature. *Journal of Fluid Mechanics.* 83: Part 3. 509-527.

Hwang, G. J., and Chao, C. H. 1992. Effects of wall conduction and Darcy number on laminar mixed convection in a horizontal square porous channel. *Journal of Heat Transfer.* 114: August. 614-621.

Jinsuo, Z. Benzhao, and Jianwei J ü . 2001. Fluid flow in a rotating curved rectangular duct. *International Journal of Heat and Fluid Flow.* 22: 583-592.

Joseph, B., Smith, E. P. and Adler, R. J. 1975. Numerical treatment of laminar flow in helically coiled tubes of square cross section. *AIChE Journal.* 21: (5). 965-974.

Kalb, Charles E., and Seader J. D., 1974. Fully developed viscous-flow heat transfer in curved circular tubes with uniform wall temperature. *AIChE Journal.* 20: (2). 340-346.

Kaviany, M. 1985. Laminar flow thorough a porous channel bounded by isothermal parallel plates. *Int. J. Heat Mass transfer.* 25: (4). 851-858.

Kim, S.Y., Kang, B.H., and Hyun, J. M. 1994. Heat transfer from pulsating flow in a channel filled with porous media. *Int. J. Heat Mass transfer.* 37: (14). 2025-2033.

Kou H. S., and Lu, K. T. 1993. Combined boundary and inertia effects for developed mixed convection in a vertical channel embedded in porous media. *Int. Comm. Heat mass Transfer.* 20: 333-347.

Lan, X. K., and Khodadadi, J. M. 1993. Fluid flow and heat transfer through a porous medium channel with permeable walls. *Int. J. Heat Mass transfer.* 36: (8). 2242-2245.

Larry, R. Austin, and Searer, J. D. 1973. Fully developed viscous flow in coiled circular pipes. *AIChE Journal*, 19:(1). 85-94.

Lee J. B., Simon, H. A. and Chow, J. C. F. 1985. Buoyancy in developed laminar curved tube flows. *Journal of Heat and mass transfer.* 28: 631-640.

Nield, D. A., Junqueira, S. L. M. and Lage, J. L. 1996. Forced convection in a fluid-saturated porous medium channel with isothemal or isoflux boundaries. *Journal of Fluid Mechanics.* 322: 201-214.

Nield, Donald A., and Bejan, Adrian 1999. *Convection in porous media.* 2nd edition. Spriger-Verlag. New York.

Patankar, S. V., Pratap, V. S. and Spalding, D. B. 1974. Prediction of laminar flow and heat transfer in helically coiled pipes. *J. of Fluid Mechanics.* 62: 539-551.

Pei-Xue J., and Ren, Z. P. 2000. Numerical investigation of forced convection heat transfer in porous media using a thermal non-equilibrium model. *International Journal of Heat and Fluid Flow.* 22: 102-110.

Poulikakos, D., and Renken, K. 1987. Forced convection in a channel filled with porous medium, including the effects of flow inertia, variable porosity, and Brinkman friction. *Journal of Heat Transfer.* 109: November. 880-888.

Prusa, J. 1982. Numerical solution for fully developed flow in heated curved tubes. *Journal of Fluid Mechanics.* 123: 503-522.

Rabadi, Nasri J., 1980. *Pulsation flow and heat transfer in curved tubes.* Ph.D.Thesis, University of Illinois at Chicago Circle, Chicago, Illinois, USA.

Sadrul I., A. K. M., Chowdhury, A. J. A. Naser, and Quamrul I. Md. 1995. Numerical study of forced convection in a packed channel with asymmetric heating. *Chem. Eng. Comm.* 138: 75-87.

Thangam, S., and Hur, N. 1990. Laminar secondary flows in curved rectangular ducts. *Journal of Fluid Mechanics.* 217: 421-440.

Truesdell, JR., and Adler, R. J. 1970. Numerical treatment of fully developed laminar flow in helically coiled Tubes. *AIChE Journal.* November. 1010-1015.

Vafai, K. 1984. Convective flow and heat transfer in variable porosity media. *Journal of Fluid Mechanics.* 147: 23-259.

Vafai, K., Alkire, R. L. and, Tien, C. L. 1985. An investigation of heat transfer in variable porosity media. *Journal of Heat Transfer.* 107: August. 642-647.

Vafai, K., and Kim, J. 1989. Forced convection in a channel filled with a porous medium: an exact solution. *Journal of Heat Transfer.* 111: November.1103-1106.

Vafai K., and Tien, C. L. 1981.Boundary and inertia effects on flow and heat transfer in porous media. *Int., J. Heat mass Transfer.* 24: 195-203.

Varahasamy, M., and Fand, R. M. 1996. Heat transfer by forced convection in pipes packed with porous media whose matrices are composed of spheres. *Int. J. Heat Mass transfer.* 39: (18). 3931-3947.

Yang R., and Chang, S. F. 1993. A numerical study of fully developed laminar flow and heat transfer in a curved pipe with arbitrary curvature ratio. *Int. J. Heat and Fluid Flow.* 14: (2) June. 138-145.

Yao, L. S, and Berger Stanley A. 1978. Flow in heated cueved pipes. *Journal of Fluid Mehanics.* 88: part 2. 339-354.

White, Frank M. 1991. *Viscous fluid flow.* 2nd Edition. McGraw-Hill. New York.

Zapryanov, Z., Christov, C., and Toshev, E.1980. Fully developed laminar flow and heat transfer in curved tubes. *Int. J. Heat Mass Transfer.* 23: 873-880.

الجريان الانسيابي وانتقال الحرارة في الأنابيب المنحنية المملوءة بوسط مسامي مشبع

اعداد

عمر محمد جديتاوي

المشرف

الأستاذ الدكتور نصري الربضي

ملخـــــــــص

هذه دراسة لجريان الموائع وانتقال الحرارة في الأنابيب المنحنية المملوءة بمادة مسامية مشبعة بالمائع. تم في هذة الدراسة استخدام طريقة العنصر المحدود لحل المعادلات التفاضلية الجزئية لجريان انسيابي متطور ومستقر داخل أنابيب ذات مقطع عرضي متغير.

لقد تبين من النتائج ان رقم Darcy الذي يعتبر مقياس لشدة مسامية الوسط، له تأثير كبير على رقم Nusselt المتوسط وكذلك على معامل الاحتكاك، وتم الحصول على نتائج باستخدام قيم لرقم Darcy تتراوح ما بين(1.0 - $1x\ 10^{-6}$). وتم أيضا دراسة تأثير تغير نسبة ارتفاع الأنبوبة إلى عرضها، فوجد أن نقصان هذه النسبة له تأثير ضعيف على رقم Nusselt المتوسط. أما بالنسبة لرقم Dean الذي يميز شدة انحناء الأنبوبة، فقد تبين أن زيادته لها تأثير ايجابي كبير على رقم Nusselt المتوسط، حيث تم الحصول على نتائج إيجابية الى حد كبير عند استخدام رقم (Dean = 800).

ومن مجمل النتائج التي تم الحصول عليها، تم تطوير معادلات ربط بين رقم Nusselt و معامل الاحتكاك كمتغيرات معتمدة من جهة، وبين الأرقام Darcy، Prandtl و رقم Dean من جهة أجرى، باستخدام طريقة المربعات الصغرى.